EXPERIMENTAL STUDY OF AXIAL COMPRESSIVE BEHAVIOR OF A HYPER-ELASTIC ANNULAR SEAL CONSTRAINED IN A PIPE

By

Rony Chandra Shaha

A Thesis Submitted to the Faculty of Graduate Studies of

The University of Manitoba

In partial fulfillment of the requirements of the degree of

MASTER OF SCIENCE

Department of Mechanical Engineering

University of Manitoba

Winnipeg, Manitoba

ABSTRACT

The compressive behavior of an annular rubber seal constrained in a pipe and the interaction between the pipe and the seal was studied experimentally using a specially designed test fixture that allowed the concentric alignment of the seal within the pipe and its axial compression using an electro-hydraulic Instron load frame. The hoop strain introduced in the pipe wall, due to the constraint of lateral expansion of the seal, displayed a parabolic distribution with a maximum value at the mid-height of the seal similar to the parabolic shape of the lateral expansion of the seal. The magnitude of the pipe strain increased with the friction coefficient of the interface between the seal and the compression rings, strain rate, and shape factor for a constant gap between the seal and the pipe wall. The relationship between the apparent compressive modulus and the shape factor (beyond experimental range) was studied using FEA.

ACKNOWLEDGEMENTS

First and foremost, I would like to express my deepest gratitude to my thesis supervisors, **Dr. Christine Q. Wu and Dr. Raghavan Jayaraman** for their support, guidance and supervision. It was almost impossible for me to complete the thesis without their continuous invaluable guidance, patience and efforts. It was a great honor and privilege to work with them.

I would also like to express my great appreciation to my supervisor, **Dr. Christine Q. Wu** for her generous help in both academic and non-academic area which greatly encouraged me for study in Canada.

I would like to thank ProForma Engineering Ltd. for their cooperation and supports providing technical information in this research.

I would particularly like to thank my research partner Alix Bartel for his help in my research. I would also like to thank Tamrin Tanha, Buddhi Wimarshana and Sharif Ahmed for all the academic discussions and happy time sharing with them. I am grateful to my colleagues and friends of our Nonlinear Dynamics lab for supporting and shearing their knowledge during my research.

Last but not least, I would like to express my gratitude to my parents and wife for their consistent encouragement and unconditional supports during my research.

DEDICATION

This thesis is dedicated to my mother and my beloved wife for their sacrifices, inspirations and supports throughout my entire life to achieve success.

TABLE OF CONTENTS

LIST OF FIGURES

LIST OF TABLES

1 INTRODUCTION

This chapter presents a brief introduction to the subject of the compressive behavior of hyperelastic annular seal constrained in a pipe, the importance of this research and its relevance to the industrial application.

1.1 Background

The hyperelastic materials are those that exhibit elastic behavior over very large strain ranges, 100 - 400%. Polymeric hyperelastic materials known as elastomers or rubber are used primarily in sealing applications in petroleum, automotive, aerospace industries, and civil infrastructures. Over the last few decades, many studies were performed to characterize the elastic behavior of the elastomer used in seismic protection, bridge bearings, and the elastic foundations of machinery and motors.

Seals are used in a wide range of technical applications to prevent the leakage or exchange of gasses and fluids. The geometry of the seals vary from O-rings and gaskets to thick annular seals used in pipeline sealing required for pipeline isolation, maintenance, and repair. Previous research on conventional seals predominantly focused the effect of temperature on the leakage rates of seals and the sealing force [1][2]. Flow isolation of pipes is a pre-requisite to maintenance and modification.

During this sealing process, an annular rubber seal is compressed axially. The lateral expansion of the seal due to Poisson's effect forces the seal against the pipe wall creating the sealing. The stress exerted by the seal on the pipe should be sufficient to prevent any leakage while not

exceeding the yield strength of the pipe material. The magnitude of this stress depends on the magnitude of the lateral expansion and the constraint to this expansion by the pipe.

The magnitude of lateral expansion would depend only on the applied load, the compressive modulus and the Poisson's ratio of the elastomer used in manufacturing the seal. However, the frictional interaction between the seal and the compression plates have been known to limit the lateral expansion. The amount of constraint depends on the size of the seal, which determines the contact area between the seal and the compression plate, and the friction coefficient for the contact surface between the seal and the compression plates. Thus, the apparent compressive modulus of the seal, under such constraints, will be different from that of the compressive modulus of the elastomer used in manufacturing the seal and is a function of compressive modulus and Poisson's ratio of the elastomer, geometry (quantified by shape factor which is defined by the ratio of loaded and unloaded area) and friction coefficient.

There have been a number of studies on the compressive behavior of seals in various forms, solid and annular cylindrical blocks, and square blocks [3]–[5]. The effect of shape factor and the nature of the interface (bonded or frictional) on the compressive behavior of the seal (evaluated using load-displacement curves and apparent compression modulus) have been studied theoretically assuming incompressible behavior and limited experimentation involving a bonded interface between the seal and the compression plates. However, experimental studies involving the frictional interface between the seal, which is not completely incompressible (Poisson's ratio less than 0.5), and the compression plate are rare and is required to understand the behavior in real-life applications.

1.2 Relevant Research and Motivation

Experimentally characterizing the compressive behavior of nonlinear materials like rubber requires proper control of operational input parameters, sensitive equipment and measuring instruments since the rubber behaves differently with chemical composition, temperature, aging, and environmental conditions. Moreover, it is another challenge to generalize relations for rubber in sealing applications.

A research project was conducted by Bartel *et al*. [6] to characterize the compressive behavior of a rubber seal in a pressurized environment. Due to the absence of accurate measuring systems and controlled operational parameters and techniques, the findings of that research were not sufficient to characterize the compressive behavior of the annular seal in a pipe.

Parallel work on the previously mentioned project was performed by Zhao *et al.*[7] to simulate the compressive behavior of the seal in a pipe using finite element analysis. Although the initiation of the FE model was developed to simulate the interaction between the seal and the pipe under compression, the model prediction was not confirmed due to the lack of material properties specific to the rubber seal.

However, the compressive behavior of such seals under constrained conditions encountered during sealing applications has not been clearly studied. Empirical equations such as Roark's formula [8] are available to predict the stresses on the pipe wall assuming it to be thin-wall. However, its use requires the knowledge of the contact area and the contact pressure developed by the constrained lateral expansion of the seal, and no information on predicting this using the lateral expansion of the seal is available. Thus, the effect of the friction coefficient and the seal's

shape factor on pipe wall stress due to constrained lateral expansion of the seal in the pipe is not known.

Currently, there is a lack of research in the experimental characterization of laterally constrained seals in pipes for sealing applications. The aforementioned research publications were inaccurate due a lack of specific material testing, seal testing, and seal behavior characterization. The motivation for this research is to develop a case-specific and controlled experimental methodology with which to explore the compressive behavior of a seal used in pipe sealing. This analysis would help to provide a suitable guideline to the design and testing of sealing applications in pressurized environments.

1.3 Thesis Objective

The overall objective of this thesis is to experimentally study the compressive behavior of a seal constrained in a pipe and the stresses introduced in the pipe wall. The specific tasks that have been completed to realize this objective are:

a) Develop an experimental methodology to carry out uniaxial compression tests of annular rubber seal constrained in pipe and measure the pipe wall strain, contact pressure and the axial compressive force - displacement curve.
b) Study the effect of friction of the contact surface between the seal and the compression plates and seal's shape factor on the pipe wall strain, contact pressure and the axial compressive force - displacement curve.

c) Study the effect of frictional coefficient and seal's shape factor on the apparent compressive modulus of the seal (using experiments and FEM) and use this information to understand the results from (a) and (b).
d) Develop a theoretical approximation to calculate pipe strain and compare the predicted strain distribution with the experimental results.

1.4 Thesis Outline

The investigation of the compressive behavior of the hyperelastic annular seal in a constrained and unconstrained condition is presented in the thesis as following.

Chapter 2: Literature Review

In the second chapter, a literature review has been presented in the area of the compressive behavior of the solid and annular rubber blocks bonded and non-bonded with the steel plates. Previous studies related to this research are also discussed. Finally, the knowledge gap in the literature is also discussed.

Chapter 3: Methodology

In the third chapter, the details methodology has been presented for experimental, theoretical and finite element analysis. The materials, test equipment's, design of the fixture, contact pressure measuring system in between the seal and the steel pipe, hoop strain measuring systems on the outer membrane of the steel pipe and test procedures have been discussed in the experimental analysis section. In the theoretical section, apparent compressive modulus and hoop strain for thin

wall pipe is predicted. A parametric study with the Finite Element Model is also presented for predicting the apparent compressive modulus at various shape factor and friction coefficients.

Chapter 4: Results and discussion

The fourth chapter presents the results obtained from the experimental studies of the annular rubber seal under axial compression at two strain rates, two surface conditions, and different shapes factors. The experimental results, along with the theoretical predictions and FEM results have been discussed in details to understand the compressive behavior in a constrained and unconstrained states.

Chapter 5: Conclusions

This chapter summarizes the results drawn from the experiments, theoretical predictions and FEM analysis for characterizing the compressive behavior of the annular rubber seal in a constrained and unconstrained state.

2 LITERATURE REVIEW

In this chapter, an overview of the literature on the hyperelastic material is presented. A comprehensive discussion of the literature on bonded and non-bonded rubber blocks, rubber blocks of different geometries, material properties, Finite Element Analysis of rubber blocks, rubbers in bridge bearings, analytical models, incompressibility of rubbers, etc. is presented.

Early in the 20th century, very few observations on rubber properties are reported. In 1805 J. Gough [9] found that the stretched rubber contracts reversibly for heating and a rapid stretching of rubber increases temperature. However, the observations from rubber were found unusual and interesting as the stretched bar of metal elongated with heating and a rapid stretching of rubber decreases temperature.

2.1 Behavior of Rubber Material

In general, the behavior of the hyperelastic material is characterized by the elastic moduli, hardness, abrasion, oil resistance, and aging, etc. Hyperelastic materials do not obey the Hooke's law under large strain as the displacement is not proportional to the load. The deformation mechanism of hyperelastic materials differs significantly as a function of stress, strain, strain rate, friction, etc. However, the spring rate or stiffness is another key parameter for engineering design. The incompressibility assumption has been used to predict the deformed shape under loading during the testing of the rubber. Rubbers are essentially an incompressible material which deforms by changing the shape rather than changing volume. It is difficult to compress the rubber block unless the pressures are extremely high. Hyperelastic materials are desired for shock dampening industrial applications because of the viscoelastic nature. Some common phenomena's such as

creep, stress relaxation, compression set, mechanical irreversibility and energy loss for deformation cycle (Hysteresis) are the key manifestations of the viscous properties of rubber [10].

2.1.1 Compression set

The compression set is the deformation that remains after an imposed strain has been removed. The compression set measures the ability of the hyperelastic material to recover its original dimensions. Therefore, the compression set is expressed as,

$$\text{Set} = \left[\frac{\text{to} - \text{tr}}{\text{to} - \text{ts}}\right] \text{X } 100\%$$

Where, t_o: The initial thickness, t_r: The recovered thickness, and t_s: The compressed thickness.

2.1.2 Stress Relaxation

When a hyperelastic material is held at a constant deformation, the stress decreases as a function of time. Therefore, stress relaxation can be of great importance in sealing applications as the material of the seal is required to maintain a constant level of sealing force to prevent the leakage. It can be the dominant factor which limits the effective life of the seal. It is defined as the reduction in stress expressed as a percentage of the initial stress [11]. Therefore,

Stress Relaxation = $[(\sigma_o - \sigma_r)/\sigma_o]$ X 100%

Where, σ_o is the initial stress and σ_r is the stress at time t.

The rate of stress relaxation is then the stress relaxation divided by some function of time.

2.1.3 Creep

When a hyperelastic material is subjected a static preload, then this load causes a progressive increase in deformation as a function of time. This can be important in a wide variety of application from building mounts to automotive suspensions. Creep is usually expressed as a percentage of the initial deflection. Therefore,

$$\text{Creep} = [(x_t - x_o) / x_o] \text{ X } 100\%$$

Where x_o is the initial deflection, and x_t is the deflection at time t.

2.1.4 Important Terms and Definitions

The important terms and definitions related to the compressive behavior of rubber blocks have been stated in this section, for a better understanding of the terms specified in this study.

Shape factor, S: Shape factor is defined as the **r**atio of the loaded area to the force free area available for bulging. The Shape factor significantly influences the stiffness of the rubber upon compression. In the most common cases, the rubber is bonded to metal plates to eliminate the slippage. In this case, the shape factor that is a function of geometry significantly affects the compression modulus in the design of rubber mounts and bearings.

$$\text{Shape Factor, S} = \frac{\text{Loaded Area}}{\text{Force Free Area}}$$

The shape factor of annular rubber seal is given as,

$$S = \frac{(Do - Di)}{4 * t}$$

where, Do & Di are the Outer and the inner diameter of the seal and t is the thickness.

Maximum Bulge Radius: The maximum bulge radius is defined as the maximum radius formed on the midplane at the center of the axially compressed annular cylindrical blocks.

Apparent Compressive Modulus: When a rubber block is compressed with bonded or frictional constraints at the contacting surfaces, the block is prevented from expanding outwards, therefore, the apparent compressive modulus is greater than the materials compressive modulus. Compressive modulus is an intrinsic property which is the amount of an actual change in volume upon compression, not the change in shape such as bulging where the total volume remains the same.

Bulk Modulus: Bulk modulus is defined as a property of materials which defines the resistance to volume change during compression.

Stiffness: Stiffness is the rigidity of the material which resists deformation in response to an applied force.

2.2 Compression of Hyperelastic Material

Simple compression of hyperelastic material is extensively used by lubricating the surfaces that there is no restraints to movement in the contact interfaces and confirms the independence of the geometry by varying the aspect ratios. When the hyperelastic material such as a rubber block is bonded with the steel plates, therefore the subsequent deformed shape is not follows a uniform shape whereas it follows a non- homogeneous deformation in different direction [12].

2.2.1 Bonded Solid Disks

The studies of the compression of rubber disc bonded to rigid surfaces initiated in the early 20th century. As per Pinarbasi *et al.* [13], the compression stiffness was analyzed first in 1937. As the rubber block with bonded or frictional constraints at the contacting surfaces is prevented from expanding outwards upon compression, consequently, the apparent compressive modulus is larger than the actual compressive modulus. It has been also proven that the stiffness of the rubber block during compression test depends on the shape factor. Gent *et al*. stated that the apparent Young's modulus of infinitely long blocks, cylindrical disks, and square prisms in terms of the shape factor was first derived approximately in 1950 [3]. The relations are

- Infinitely long blocks

  $E_a = E(1.33 + 1.10S^2)$

- Cylindrical disks

  $E_a = E(1 + 1.65S^2)$

- Square Prisms

  $E_a = E(1 + 1.65S^2)$

  Where, E: Young's Modulus of Rubber & S: Shape Factor

Further developments of the studies of rubber compression were made by Gent *et al*.[3] They developed an alternative approach for the apparent compressive modulus which is widely used to approximate the stiffness of elastic blocks bonded to rigid supports. This method is based on two assumptions as follows:

1. The shape of lateral deformation is parabolic in the loading configuration.

2. Horizontal planes remain horizontal.

The above-mentioned formulation using the assumptions called the pressure method. Gent and Lindley analyzed the compression load-displacement relations for a different ranges of thicknesses and geometries of bonded rubber blocks by considering the above assumptions. The total displacement for bonded elastic layer is considered as to the combination of two normal displacements which are complete homogeneous compression of the non-bonded layer, as well as the supplementary displacement needed for keeping their original positions on the bonded surfaces. They made an assumption that the pressure distribution along the thickness was constant. They derived an expression for apparent modulus upon compression of infinitely long blocks and bonded circular discs following the incompressibility assumption which are as follows:

- Infinitely long blocks

  $E_a = E(\frac{4}{3} + \frac{4}{3}S^2)$

- Cylindrical disks

  $E_a = E(1 + 2S^2)$

But the equation considering incompressible assumptions overestimates the actual value. Therefore, they proposed a modification for the compression modulus of rubber to consider the bulk compressibility by realizing the effect of material compressibility. Even though the bulk compression modulus of rubber is greater than Young's Modulus and shear modulus with a few orders of magnitude . The modified apparent Young's modulus, E_a' is given by,

$$1/E_a' = (1/E_a + 1/E_\infty)$$

Where E_a is the apparent modulus without considering bulk compressibility and E_∞ is the modulus of bulk compression. They reported that the compression load-deflection relations were fairly linear under very small compressions which are about 5 percent or less from the original thickness [3].

In 1970, Gent *et al*. [14] modified their previous work on the bonded rubber blocks subjected to compression, bending and shear for layers of various shape. Gent and Meinecke, deduced an approximate analytical treatment with three modes of deflections for small compression of bonded elastic layers. The considered modes of deflections are:

1. Compression or extension where the bonded surface moves towards or away from the other.
2. Bending where the bonded surface rotates about an axis of symmetry and its own plane.
3. Apparent shear where one bonded surface is moved parallel to other in its own plane.

In 1972, Holownia performed an analytical analysis for bonded rubber with circular section based on finite difference approach [15]. He mentioned that the stress profile of the circular rubber block is varied significantly with the value of Poisson's ratio and the block's geometry. The maximum height of parabolic stress distribution is reduced with the reduction Poisson's ratio. It has been reported that when a thin block of material bonded with end plates at the Poisson's ratio of 0.499, the stress within the rubber block is high and almost equal in all the three directions. Therefore, a hydrostatic type of stress distribution is generated whereas the hydrostatic stress distribution was not found for thick blocks and the value of the stress turns into minor sensitive to Poisson's ratio. Another observation was found from their analysis that if there were no lateral constraint on the contact surfaces of the circular rubber blocks which means the end faces were lubricated, then the

stress distribution was found to be uniform. However, their numerical analysis was valid for limited values of Poisson's ratio and aspect ratio. In 1979, Lindley was believed to be the first researcher who developed an analytical expression for bonded rubber blocks with a large range of the Poisson's ratio as well as aspect ratio's. He compared the predicted theoretical solutions with FE analysis for materials with Poisson's ratios in from 0.125 to 0.49983 and blocks having diameter-to-thickness ratios from 0.25 to 128**.** In his analytical solution, he added one consideration with the pressure method that the strain distribution across the rubber block is parabolic. [16].

Considering a straight procedure, in 1990, Chalhoub *et al*. [17] derived an analytical expression which emphasizes the importance of the bulk compression effects for the layers of thin rubber. This theoretical approach was developed for circular shaped layers and later this method was extended for other shapes. Koh *et al*. derived analytical solutions of square and rectangular layers for the compressive modulus following the assumption that the horizontal sections of the elastic layer remain plane on the other hand vertical sections become parabolic [18] [19].

In 2002, Horton *et al*. derived an analytical expressions which is convenient for calculations of apparent modulus, stress distributions and the deformed profiles of their lateral surfaces of the bonded rubber blocks for thin rectangular and circular sections [20]. Their formulation satisfy the exact governing equations which followed the classical theory of elasticity. They used the pressure method assumptions except the assumption of parabolic bulging shape during loading as they found that the bulging shape of the blocks was not parabolic for lower shape factors (0.1 or 0.2). However, they reported that the shape of the lateral bulging of the rubber block is parabolic for higher shape factor during loading. Their analytical results compared well with the

experimental results performed by Mott *et al*. [12] who analyzed the uniaxial characteristics of the slender circular blocks with 0.11 to 0.27 shape factors.

As per the modification of the analytical formulation for bonded rubber blocks, Yeoh *et al*. (2002) investigated the previous developed theory which assumes that the rubber is incompressible [21]. He mentioned that the rubber is not truly incompressible as the bulk modulus is not infinite even though the values are greater than the shear modulus is of the order of 10^3 times. Using the incompressible assumption of rubber, the theoretical prediction overestimates the stiffness from actual. Gent *et al*. proposed an empirical correction which brings into better agreement for smaller shape factor ($S < 10$). In the earlier studies [3], [17] on the rubber layers bonded to rigid surfaces was for average solutions which was based on the displacement and stress distributions. These assumptions are not applicable for stress distribution and displacement over the entire layer. Earlier, it has been clearly shown that the top and bottom faces of the bonded elastic layer showed significant changed on the layers behavior. The modulus for compression and bending of a bonded layer is greater than that of the corresponding unbonded layer because of the restraint imposed on the lateral expansion for the bonded cases. Moreover, the effect of bonded surfaces on the elastic layers highly dependent on the material properties and the geometry with nearly incompressible assumptions [19], [22]. In 2006, Pinarbasi *et al*. deduced analytical solutions to predict the displacement and stress distributions of an infinite strip shaped layer at any section following deformation modes which were uniform compression, apparent shear and pure bending and also under their combinations [23]. They also investigated the significance of the shape factor and the Poisson's ratio for the elastic layer behaviors. They reported that the shape factor and Poisson’s ratio had significant effect not only on the stiffness’s but also on the stress distributions and displacement.

2.2.2 Bonded Annular Disks

In the earlier, most of the research was done on the bonded rubber blocks, very few attention has been given to the analysis of bonded annular blocks. In 1959, Gent et al. investigated the bonded rectangular and annular rubber blocks with different sizes circular hole in the center. In their experimental study, they measured the apparent compressive modulus of annular rubber disks for different shape factors. They concluded that the determined apparent compressive modulus of annular blocks for large holes in the center compared well with the predicted apparent compressive modulus for infinite rectangular blocks whereas that of the annular blocks of rubber with small holes closest to the analytical results for the circular rubber blocks [3].

Though the experimental study of annular rubber blocks was performed in 1959 by Gent *et al*. [3] whereas the first analytical studies on bonded annular disc were found in 1990 by chalhoub *et al*. [17] [20]. Particularly, the study of bonded annular disc came to the attention of the researchers when the popularity of the uses of the elastomeric bearings for seismic isolators widespread in all over the world [24].

In 1992, Constantinou *et al* [25] presented analytical formulations for predicting the compression modulus and the maximum shear strain at the bonded interface due to compression of annular circular bearings. They investigated the compressive characteristics of annular layers with bonded cases by using the theoretical approach developed by Chalhoub *et al*. [17]. Constantinou *et al*. came to a conclusion based on their analytical study that the circular block with a circular hole not only decreased the apparent modulus but also increased the maximum shear strain substantially. Now it is established that most of the elastomeric bearings as seismic isolators are designed and manufactured with a circular hole.

In 1994, Gent [4] derived a formulation for the compression of a cylindrical disc containing a center hole. Here, he assumed the material is incompressible in bulk employing zero pressure at both internal and external radius. He concluded that even when the inner radius is extremely small such as 1% of the external radius, the effective modulus is reduced substantially to about 78% of that for an equivalent solid disc.

$$E_a/E = 1 + [(a_1^2 + a_2^2) - (a_1^2 - a_2^2)/\ln(a_1/a_2)]\ /2.h^2$$

Where,

E: Young's Modulus of Rubber,

E_a: The apparent Young's Modulus,

h: Thickness,

a_1 : External radius,

a_2: Internal radius.

In 2002, Yeoh *et al*. [21] verified the theoretical prediction relaxing the incompressibility assumption to near compressibility by using the linear FE analysis. They compared the theoretical predictions with the FE analysis for the long strip, rectangular, cylindrical and annular disks and found good agreement with linear FEA. In 2003, Horton *et al.* [26] derived closed form expressions by using a superposition approach based on the classical theory of elasticity upon axially loaded annular bonded rubber blocks.

In 2008, Pinarbasi *et al*. [13] presented the compressive characteristics of the bonded annular circular blocks using their analytical formulation. Mainly, they gave the emphasizes to the effect of the center hole in the circular rubber disk on the modulus, stress distribution and the maximum state of stress for radius ratio of the inner circle and the blocks, aspect ratio and Poisson's ratio.

2.2.3 Non-Bonded Solid Disks

A number of theoretical approximate solutions were published for the apparent compressive modulus and stress distributions for bonded blocks with the plates but very few attention was given to the compression of the rigid frictional surfaces. Most of the published researches were related to the bonded rubber blocks in different shapes like rectangular, cylindrical and annular etc. There are many industrial applications in all over the world where rubber blocks are used in between the rigid frictional surfaces under compression. In the case of sealing purpose, rigid frictional surfaces were used instead of perfectly bonded blocks. It is really challenging and interesting topic to investigate that in what degrees of the extent the friction at the loading surfaces differs from perfect bonding. In 1994, Gent deduced an analytical solution for the apparent compressive modulus of the rubber blocks in between rigid frictional surfaces considering incompressibility assumption [4]. Remarkably large effect in the apparent compressive modulus of rubber block was predicted at various shape factor due to the use of frictional restraints instead of perfect bonding at loaded surfaces. He investigated the size of slip zone, pressure distribution, and apparent compressive modulus considering a circular block of incompressible material. There was a strong tendency for arising slip at the edges of the block as there was a minimum value of normal stresses and the maximum value of shear stresses. In his analytical analysis, he calculated the maximum frictional stress at the interfaces between the frictional surfaces and the rubber block

by coulomb's law. Based on his theoretical analysis, it was reported that the slip zone was varied with the shape factor and the co-efficient of friction. The slip zone is restrained up to the outer edge of the contact circle for higher shape factor. Slip zone is also affected by the coefficient of friction such as the slip zone was very small for the high values of the friction coefficient. It is reported that when the coefficient of friction is small and the slip zone is large, the distribution of contact pressure is radically different from the parabolic distribution obtained for bonded blocks. He concluded that radical drops in compressive modulus happen due to the relatively small amounts of slipping although the load and deflection relation remains linear. There was no significant difference of the apparent compressive modulus of the rubber block in between the fully bonded and rigid frictional surfaces for very low shape factor and high friction coefficient.

Following the above theoretical analysis, in 2008, Gent *et al*. conducted a theoretical analysis of axial compression and retraction of rubber block with rigid frictional surfaces. They evaluated the interfacial slipping, overall stiffness, normal and shear stress distributions with a wide range of aspect ratios and frictional coefficients. They also performed a FE analysis of a rubber block with rigid frictional surfaces and compared with the analytical results for different aspect ratios and coefficient of friction. A substantial amount of contact area was slipped outwards corresponding to the lubricated surfaces with a small coefficient of friction. It was reported that the slip zone size was highest with the aspect ratios of 2 to 3 even for moderately higher friction coefficients. They compared the shear and normal stress distributions with finite element analysis results with the aspect ratios of 2 and 12 using friction coefficients of 0.2, 0.5 and 1.0. The stress distribution was predicted from the center of the disk up to the edge of the disk. It was reported that the compressive stress followed a parabolic decay curve up to the point where the slip started. However, the compressive stress then followed an exponential decay beyond the point where the

slipping start. It was also found that the compressive stress was increased rapidly towards the edge of the disk for low aspect ratios whereas this effect was not significant for higher aspect ratios [5].

Back in 1972, Holownia [15] performed an analytical analysis with circular rubber blocks by axial compression using the dynamic – relaxation solutions of classical theory of elastic stress-strain. He reported that if there were no lateral restraint on the contact interfaces rubber blocks such as the interfaces were lubricated then the apparent Young`s modulus would be uniform.

2.2.4 Rubber Disks under Large Strain

Most of the theoretical approximation is based on the small compression strain and linear solution. In 1959, Gent *et al*. [3] performed an experimental study for the load – deflection relations under moderately large compressions up to 40 percent of its initial height. They reported that the compressive load – displacement relations were non–linear and an increasing slope was found with the increasing of the compression. They compared the experimental results with the analytical results based on the simple kinetic theory of rubber for a pure homogeneous compression. The analytical results were in good agreement with the measured values of stress for compression of the square and circular bonded rubber blocks under relatively large compressions. In 2005, Patenaude *et al*. [27] investigated the behavior of elastomeric blocks under large compressive strain. They analyzed the scanned images of the axial pressure distribution of the materials compressive response. Actual contact area and the nonlinear stress distribution across the sample surface were measured by using pressure indicating films at eight strain levels ranging from 17 to 74 percent. A non-linear stress distribution was reported at higher strain due to the singularity at the edge of the sample. They also measured quantitatively the nonlinear

characteristics of two rubber compounds for strain between 17 to 74 percent. They modified the Gent model to account for the area enhancement at large compression strain. They concluded that the contact area increases substantially during large strain as the consequence of a rolling flow phenomenon.

In 2013, Sridharan *et al*. [28] investigated the deformation behavior of rubber blocks at higher strain with a recently developed image processing tool based on machine vision. They tested the rubber tread block with same contact area but varied geometry. They concluded that the rubber for constant area of contact but various geometry showed a distinguished behavior under large compression strain. In 2014, Sridharan *et al*. [29] extended their research for analyzing the compression behavior experimentally at higher strain rate. They used their developed imaging tool to measure the maximum bulge radius and compared the experimental results with the established model. Though the established model is based on the assumptions that the deformed shape of the rubber block is parabolic under small strain. They reported from the evident of the images that the deformed profile of the lateral surfaces at higher compressive strain was not parabolic in shape whereas it looked to be flatter. In the stress – strain analysis, non-linear stress distribution was confirmed from their experimental results at the large compressive strain.

2.3 Rate Dependency Behavior of Rubber

The stress – strain characteristics of hyperplastic materials are dependent on the rate and it showed hysteresis under cyclical loading. Bergstrom *et al*. [30] inspected the rate dependent stress relaxation and hysteresis under compressive loading. They concluded with few key observations through their experimental analysis which was stated as follows:

1. Hyperelastic materials are dependent on strain rate and higher rate dependency is found during loading than unloading.
2. Hysteresis was found during cyclical loading.

They developed a constitutive model based on the experimental data for the rate dependency and relaxation behavior and compared well with the experimental results. In 2012, an experimental study was conducted by Hossain *et al*. [31] to investigate the deformation behavior at the strain rates. They conducted the experiments with cyclical loading for various extent of deformations at various strain rates. It has been reported that the experimental results showed a rate dependency on the rubber behavior. In agreement with the previous study, they found significantly less rate-dependency behavior during unloading. In 2013, a comprehensive experimental study was performed by Sahu *et al*. [32] to investigate the rate dependency of deformation, hysteresis loss, and relaxation of elastomer material. They revealed the strain rate dependency on the properties of the hyperelastic material such as stress, relaxation, stress softening, hysteresis, and residual strain. From the literature survey, it has been found that the rubber material is sensitive to the strain rate.

2.4 Friction

The frictional behavior of rubber does not follow the conventional frictional behavior of metal. The frictional characteristics of rubber sliding against the frictional contact surfaces have great importance in the sealing application. Many factors such as the properties of rubber and contact materials, contact geometry and the interaction of rubber-lubricant influences the frictional behavior of rubber. Many significant researches already focused the characteristics of the elastomer to vehicle tire in dry condition, very few research has focused on the frictional behavior

of elastomers in conjunction with seal and sealing systems under the lubricated state. Some recent work has investigated the frictional behavior of elastomers in lubricated contact with the steel [33], [34]. The coefficient of friction of rubber sliding against rigid frictional contact surfaces decreases for the application of lubricating oil which reduces the contact area between the rubber and the contact surfaces [35], [36]. The influence of lubrication in the interaction of rubber and rigid surfaces plays an important role on the frictional behavior of sealing purpose. Mofidi *et al*. investigated the frictional behavior of four different types of rubber samples which are commonly used in the sealing applications. They came to a conclusion that the coefficient of friction of rubber not only dependent on the contact geometry, lubricant properties and the modulus of rubber but also on the viscoelastic properties.

2.5 Finite Element Analysis

The finite element method is the most important developed method for numerical analysis of the hyperelastic material. Over the last few decades, hyperelastic materials were simulated especially by finite element method for numerical analysis. Hyperelastic materials were modeled considering the assumptions of incompressibility. Since the use of rubber or rubber-like materials was growing considerably in the automotive, aerospace, petroleum industry, and in the many engineering applications, the finite element analysis was performed for the development of the products taking the benefits of prompt decision making. Several hyperelastic models, e.g. Mooney-Rivlin model, Yeoh model, Ogden model were established for stress – strain relations.

Several analytical approximations were developed for the compression of bonded solid and annular rubber blocks. Therefore, several hyperelastic material models were formed for the compression analysis of bonded solid and annular rubber blocks. In 1995, Ling *et al*. developed

a finite element model and compared the load-deflection relation and stress distribution with their approximate analytical solutions for bonded annular blocks [37]. In 2002, Yeoh *et al*. carried out a linear finite element analysis and compared more accurately with their modified approximate solutions by relaxing the incompressibility assumptions to near incompressibility for bonded rubber blocks [21].

Later, in 2009, Gent *et al*. derived an analytical approximate analysis for the compression and retraction of a rubber disks in between frictional surfaces. Further, they carried out the finite element analysis using ABAQUS for rubber disks at different aspect ratios and coefficient of frictions [5] . The analytical force-displacement relations and stress distributions are compared with that of the finite element results. The overall agreement is found to be good in between the analytical and numerical results.

2.6 Related Research

An experimental study was conducted by Bartel *et al.* [6] in 2014 to study the stress analysis of an axially compressed annular rubber seal in a pressurized environment. He performed the compression test by controlling the parameters including axial displacement and contact surface friction with 30KN MTS Insight compressive tester. In his experiment, he used 4inch NPS schedule STD (Intermediate wall) steel pipe and used an annular old seal with 102.5 mm outer diameter, 47 mm inner diameter and 31.5 mm thickness. Pressure indicating films and rectangular strain rosettes were used for measuring the contact pressure and strain, respectively. Contact pressure was then measured approximately by comparing the colored film with the color chart visually. In his experiment, rectangular strain rosettes were attached along the sealing area of pipe to determine hoop, 45°, and longitudinal strain. He found that the seals exhibited a linear elastic

properties up to 18.2% of axial strain. He concluded that the seal stiffness was dependent on friction and the pipe strain was inversely proportional to the seal stiffness. Since the contact pressure measurement used in his study was the visual comparison of pressure indicating film with the color chart, it was difficult to measure the maximum contact pressure and contact pressure distribution. Moreover, rectangular strain rosettes used in the previous study need more space to mount on the pipe wall along the sealing area. It is important to mention that strain on the pipe's membrane varies significantly with a very small interval of length along the sealing area. Therefore, it was difficult to measure the maximum strain on the pipe's membrane by using rectangular strain rosettes. Previously, he used 500mm length of steel pipe for his experiment but it was really difficult to align the pipe concentrically with the seal. Furthermore, 30 KN load frame was not sufficient for the compression test of the seal with pipe for confirming proper sealing. The properties of rubber seal material were unknown as the used rubber seal was old and was being used for a long time. Since the properties of rubber depend on the contact surface friction, strain rate, aging, chemical compositions, hardness, etc., it is not possible to develop a numerical model which can compare the experimental results. As a consequence, by considering the above constraints it was difficult to explore the compressive behavior of the annular seal and to establish a relation between the seal properties (stiffness, apparent compressive modulus, and shape factors) and the pipe strain under compression for sealing applications. This research is the continuation of the previous studies conducted by Bartel *et al.* to modify the experimental methodology and improve the results by controlling different parameters.

2.7 Knowledge gap in the previous research

Published studies related to the compressive behavior of annular rubber seal which was constrained in a pipe was not sufficient to characterize the compressive behavior of annular rubber seal. Hence, an improved and modified experimental analysis is required to characterize the compressive behavior of an axially compressed annular rubber seal constrained in a pipe.

Different sizes annular rubber seals have been used in different sizes pipes for sealing in the industry. No research has been done to explore the effect of shape factors (geometries) of uniaxial compressed annular rubber seals on the apparent compressive modulus for different frictional contact surfaces. Since the pipe strain depends on the annular rubber seal stiffness and apparent compressive modulus resulting from the sealing application. It is necessary to find out the relation between the apparent compressive modulus and the shape factor of the annular rubber seal at various frictional coefficients.

3 METHODOLOGY

This research was mainly focused on the experimental study that was designed and developed for the analysis of compressive behavior constrained in a pipe. In addition to the experimental study, theoretical predictions and finite element analysis were performed. The methodology of this research is organized by three sections, e.g. experimental analysis, theoretical predictions and finite element analysis. This chapter presents the details methodology of the experimental, theoretical and finite element analysis. The work flow of this research methodology is shown in Figure 1 consisted of three sections. The methodology of the experimental analysis was covered with the design and manufacturing of the customized fixtures, testing procedures, measurement systems, testing conditions, operational input and output parameters for unconstrained and constrained conditions. In the theoretical section, strain distribution and apparent compressive modulus were predicted by using the exact dimensions of the annular rubber seal and the pipe and the material properties for specific strain rates. A parametric study was performed to analyze the effect of shape factor on the apparent compressive modulus by using the finite element model developed by Bartel *et al*. [38].

The experimental analysis was performed to characterize the compressive behavior of the seal constrained in a pipe. The effect of friction of the contact surface between the seal and the compression platens and seal's shape factor on the pipe strain were analyzed through experimentally. Then, the analysis was extended to study the effect of frictions of the contact surface and seal's shape factors on the apparent compressive modulus of the seal using experiments and FEM. This information was used to realize the results of the seal compression test. Theoretical analysis was performed to compare the experimental and FEM results.

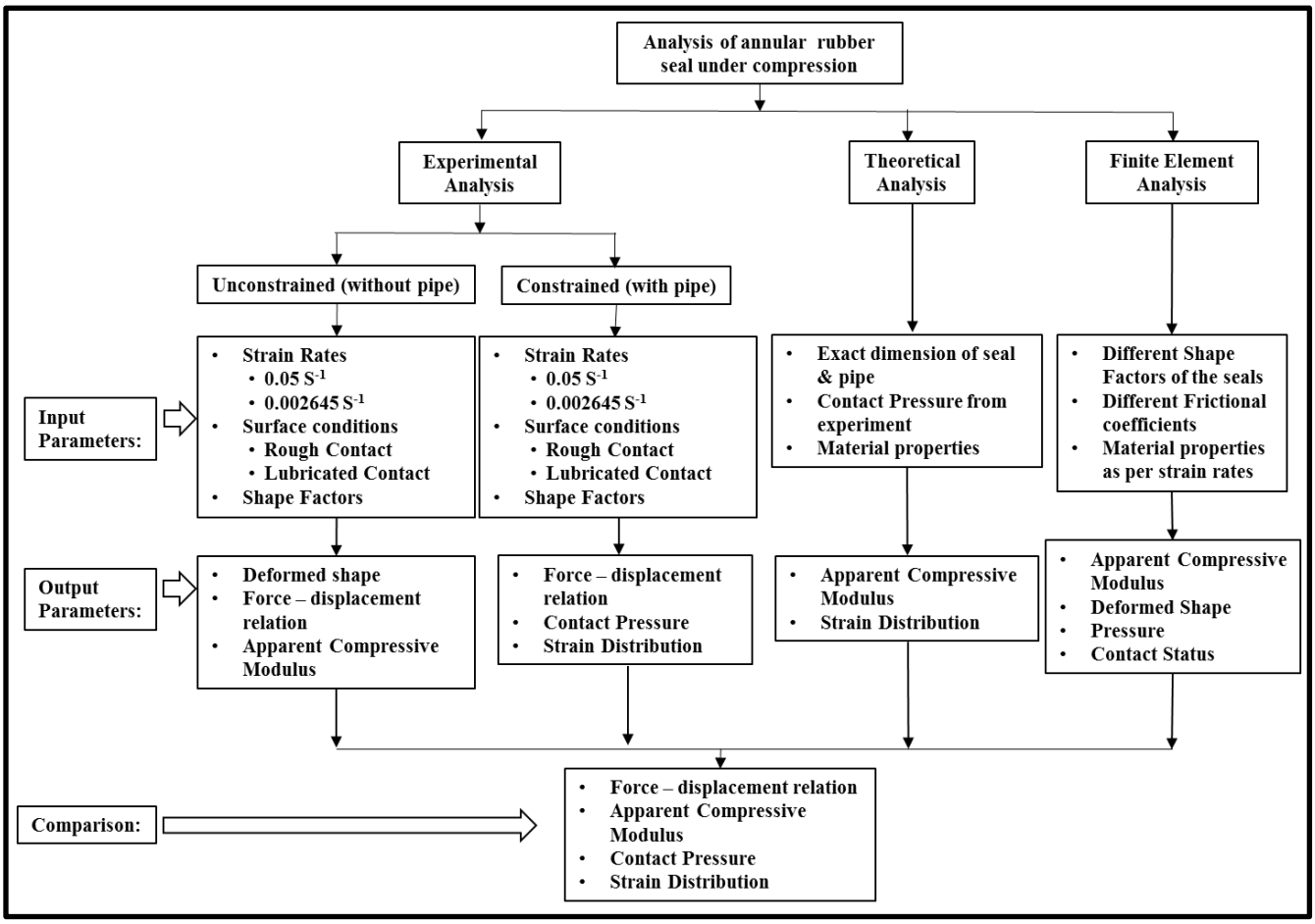

Figure 1: Work Flow of Research Methodology

3.1 Experimental Analysis

The concept of this experimental study was developed according to the scenario of the real world pipeline sealing application. According to the literature review, the properties of rubber material is dependent on the frictional contact surface conditions, strain rates, shape factors, strain, temperature, etc. This experimental study was designed with a modified methodology to characterize the compressive behavior of the annular rubber seal in both constrained and unconstrained states by controlling three operational parameters, e.g. strain rate, surface conditions and shape factor. For the experimental result analysis, force-displacement relations, stiffness, hysteresis, apparent compressive modulus, radial displacement, contact pressure in between the seal and the pipe wall, strain distribution on the pipe wall were investigated.

3.1.1 Materials

3.1.1.1 Steel Pipe

The steel pipe was selected as per ASME B36.10M with specific nominal pipe size and schedules. The pipe is recognized with the nominal pipe size and its schedule which refers the diameter and the wall thickness respectively. The length of the steel pipe was selected to 200 mm is shown in Figure 2. The outer surface of the pipe was polished with recommended sizes sand papers to prepare the surface for strain gauge mounting. The material properties of the steel pipe is assumed as follows:

Young’s Modulus: 210 GPa

Poisson’s Ratio: 0.3

The dimensions of the steel pipe are listed in Table 1

The measurement of the contact pressure inside the pipe wall was affected by the inner surface roughness of the pipe. The inner surface of the pipe was ground by using a honing tool to have a consistence surface roughness. The honing tool was used to ground the pipe’s inner surface is shown in Figure 3.

3.1.1.2 Rubber Seal

Annular rubber seal, made from nitrile butadiene rubber (NBR) and manufactured by Spareage Seals Ltd., Bombay, India, was used in this study. Three different sizes annular rubber seals were used with a different batch of production. Seals were tested in both constrained and unconstrained conditions. The material properties of the rubber were tested with uniaxial tension, equal-biaxial extension and volumetric compression from Axel Products Inc.[40]. The actual axial compressive modulus is influenced with the friction between the steel plates and the rubber. Therefore, the actual compressive modulus was measured from the test data of equal-biaxial extension by using the conversion equation without the influence of friction. In the equal-biaxial extension test, a disc sample was pulled equally in the radial direction. The conversion equation from the equal-biaxial extension to compression is defined as follows:

Table 1: Dimensions of the steel pipes

Nominal Pipe Size	**Schedule**	**Outer Diameter (mm)**	**Inner Diameter (mm)**	**Wall Thickness (mm)**
4 inch	10	114.3	108.8	2.75
4 inch	40	114.3	102.4	5.95

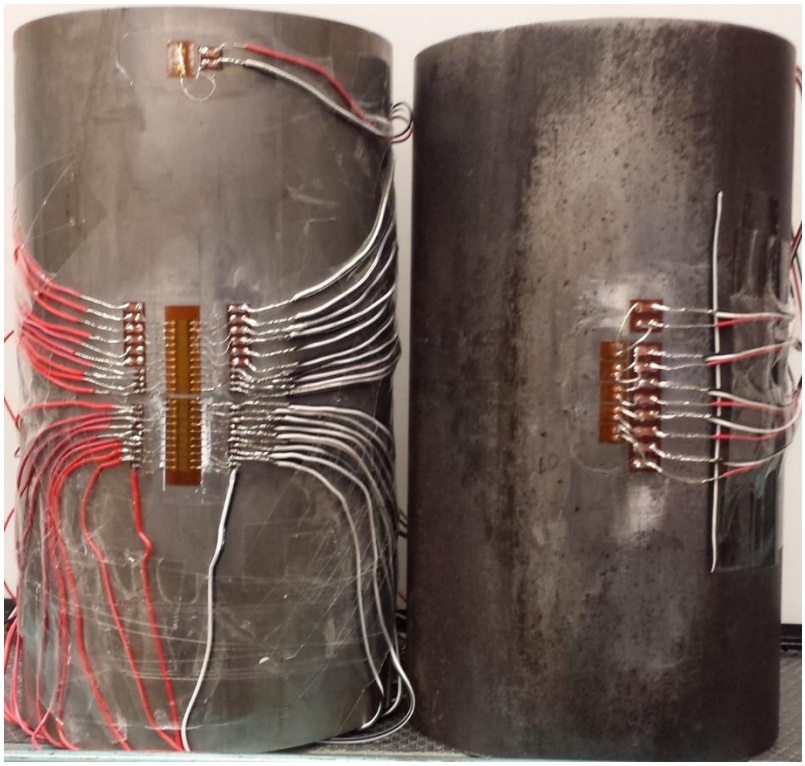

Figure 2: Low carbon steel pipe

Figure 3: Honing Tool[39]

$$\sigma_c=\sigma_b(1+\varepsilon_b)^3 \quad (1)$$

$$\varepsilon_c=1/(1+\varepsilon_b)^2-1 \quad (2)$$

$$E=\sigma_c/\varepsilon_c \quad (3)$$

Where,

σ_c : Nominal Engineering Compression Stress

σ_b : Nominal Biaxial Extension Stress

ε_b : Nominal Biaxial Extension Strain

ε_c: Nominal Engineering Compression Strain

However, one new seal manufactured from the same materials which were tested in Axel Products Inc. was used for this experiment. The materials for testing was selected from the same batch of production of the new seal with same chemical properties, surface conditions, and aging. The dimensions of the three different sizes seals are listed in Table 2.

Inner diameter and thickness of all the seals were same whereas the outer diameter of the seals was different. The new seal was selected with the outer diameter of 102.5 mm. Three different sizes annular seals are shown in Figure 4.

Table 2: Dimension of the Seal

Type of Seal	**Outer Diameter (mm)**	**Inner Diameter (mm)**	**Thickness (mm)**
Annular	102.5	47	31.5
Annular	96.3	47	31.5
Annular	73	47	31.5

Figure 4: Annular Rubber Seal

3.1.1.3 Lubricant

Lubriplate no. 105 is a zinc-oxide based light – bodied grease manufactured by Lubriplate Lubricant Company, Newark, USA. Lubriplate grease was used to reduce the friction of contact surface between the seal and the steel rings. The lubricant allows the seal to move in a lateral direction with a minimum amount of constraint imposed by the steel rings.

3.1.2 Fixture and Test Equipment

The customized fixture was designed and manufactured for simulating the compressive behavior of the annular seal constrained in a pipe. The test fixture, shown in Figure 5 consists of the following sections:

- Top Section
- Bottom Section
- Annular Rubber Seal
- Annular Steel Rings (Upper and Lower)
- Steel Plate
- Steel Pipe

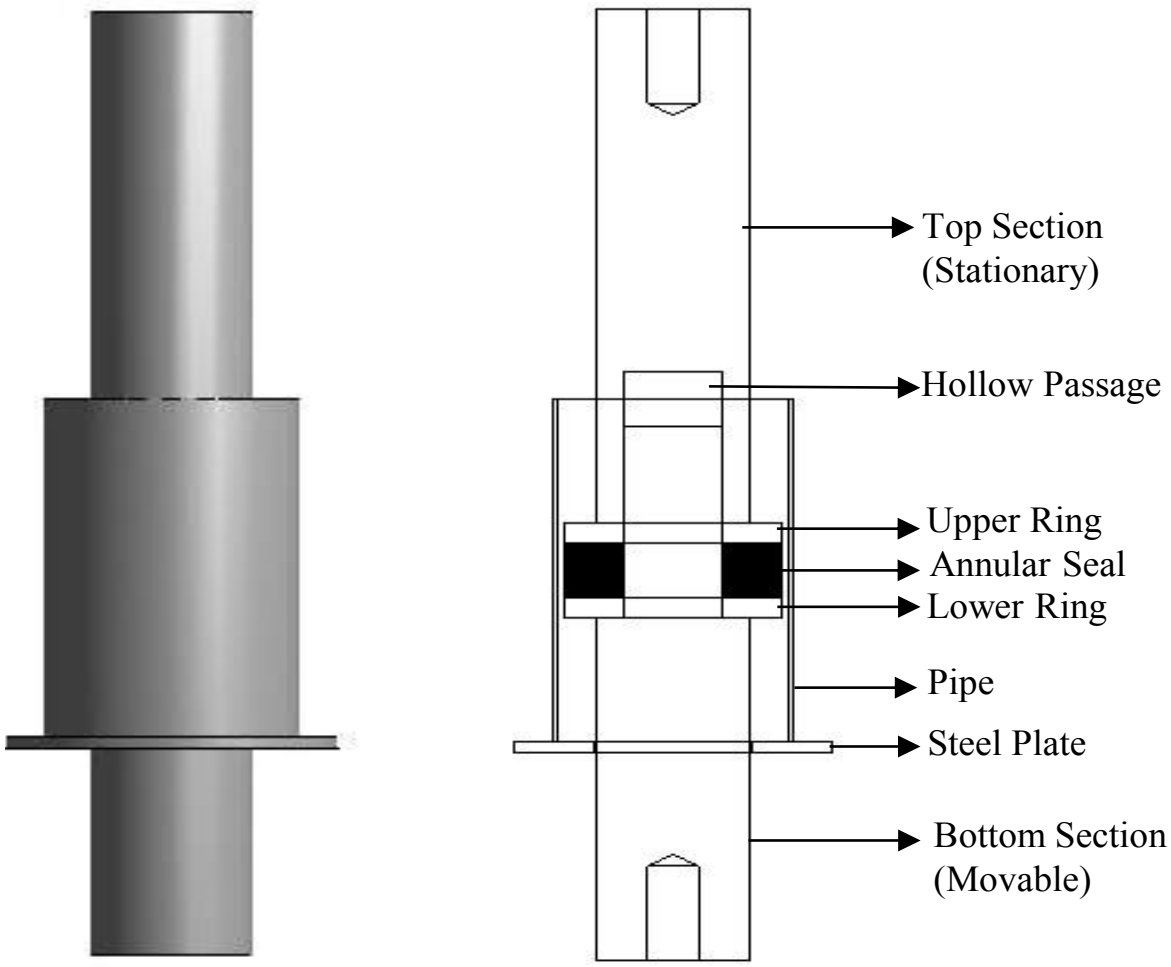

Figure 5: Customized Test Fixture

All the materials of the customized fixture were made from AISI 1018 cold drawn steel. The annular seal sandwiched between two annular steel rings was fitted into the top end of the bottom section. The pipe was kept on a steel plate which was attached to the bottom section. The mandrel of the bottom section passed through the hollow passage of the top section. The seal and the rings were concentric to the pipe. The mid-height of the seal was positioned to be at the mid-height of the steel pipe with a radial clearance. The top section was fitted onto the top end of the bottom portion and compressed against the top annular steel ring. The details of the customized test fixture are described below.

Top section:

The top section of length 250 mm consisted with 112.5 mm depth and 47 mm diameter hollow passage. The mandrel of the bottom section passes through the hollow passage of the top sections. The upper part of the top section was screwed on to the load cell of the Universal testing machine and the lower part of the top section was brought into contact with the upper ring. The top section of the test fixture is shown in Figure 6.

Bottom section:

The bottom section of the fixture of length 300 mm was equipped with a mandrel on the upper part of length 112.5 mm is shown in Figure **7**. The lower part of the bottom section was screw threaded with the moving cross head. The diameter of the mandrel was same as the inner diameter of the annular seal and the steel rings. The steel rings and the annular seal sat on the top part of the bottom section through the mandrel. A steel plate with three circular marks was attached on the circumference of the bottom section.

A steel plate:

A steel plate was fabricated with three circular marks for three different sizes pipes for the center alignment of the pipe with the annular seal is shown in Figure 8. The steel plate was attached to the circumference of the bottom section in a way that the mid-height of the pipe was placed in the mid-height of the annular seal.

Annular rings:

Three different pairs of annular steel rings were fabricated as the same inner and outer diameter of the three different sizes seals. Inner diameters and thicknesses of all the rings were 47 mm and 12.7 mm, respectively. The outer diameters of the rings were 73 mm, 96.3 mm and 102.5 mm. Each pair of the rings were used for the respective size of the seal with the same inner and outer diameter. Two types of frictional surface conditions were maintained for this experiment which was rough and lubricated. The rough surface of the steel rings shown in Figure 9 was prepared by abrading the steel rings surface using 400 grit SiC sand paper to maintain the same surface roughness during the material testing at Axel Products Inc. The lubricated surfaces shown in Figure 10 were prepared by using the lubriplate No.105.

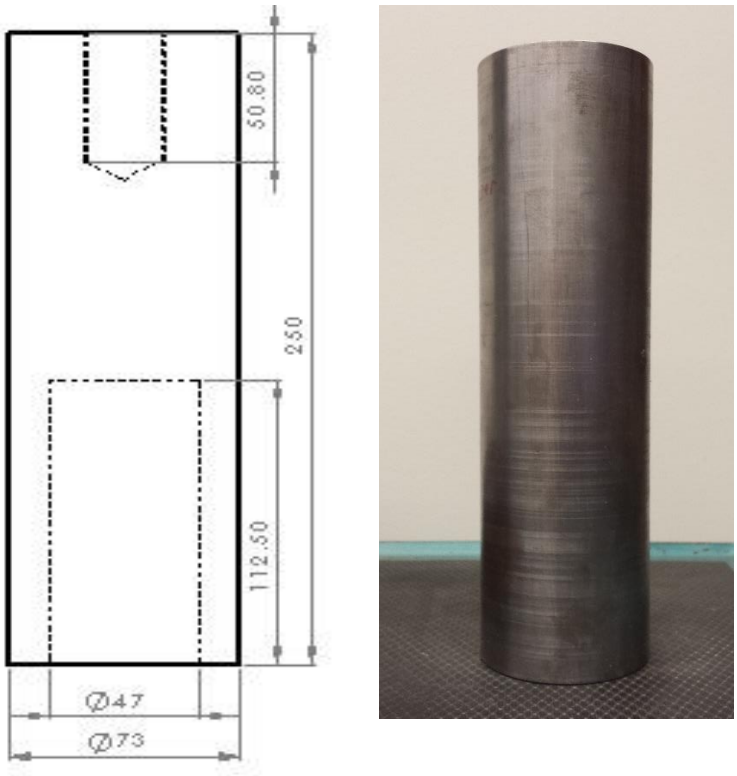

Figure 6: Top Section of the fixture

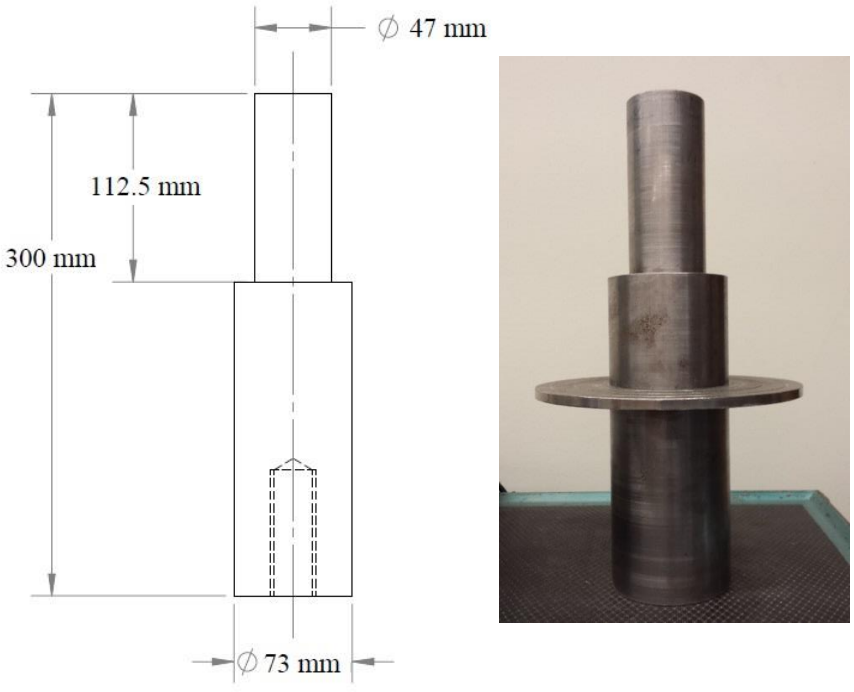

Figure 7: Bottom Section of the fixture

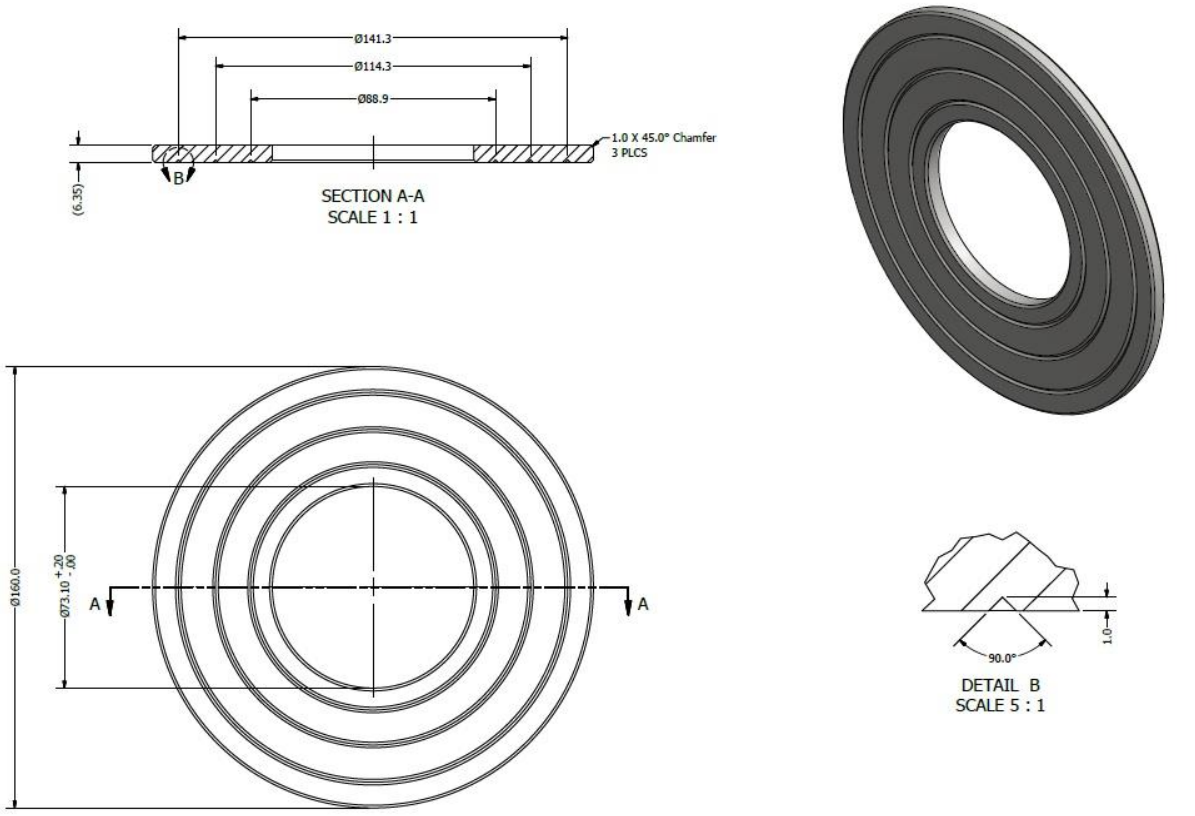

Figure 8: Steel Plate

Figure 9: Rough Surface

Figure 10: Lubricated Surface

All the experiment was conducted in two universal testing machine. The complete fixture was fitted, as shown in Figure 11 between the cross-heads of electro-servo Instron 8562 universal test frame fitted with 250 KN load cell and controlled by the wave matrix software. The bottom section of the fixture was connected to the moving cross-head and top section was connected to the stationary cross-head screwed on to the load cell. The wave matrix software with Instron universal test frame allowed both displacement and force control for the force - displacement measurement. It also stored the loading and unloading data at 10 Hz for force, displacement and time measurement.

The other universal testing machine, MTS Insight electromechanical test frame, as shown in Figure 12 was fitted with 30KN load cell and controlled by the test works 4 software. Here, the upper cross-head was movable fitted with 30 KN load cell and the lower cross-head was stationary. The data was stored automatically at 10Hz in both machines were then plotted for a continuous force-displacement curve. Different sizes seals were tested without pipe for measuring the apparent compressive modulus in MTS insight electromechanical test frame.

(a) (b)

Figure 11: (a) Complete set-up without pipe (b) Complete set-up with pipe

Figure 12: Complete Set-up without pipe and mandrel

3.1.3 Pressure Measuring System

The measurement of contact pressure that was incurred inside the pipe wall by the sealing action of the annular rubber seal was a challenging part in this experimental study. However, the contact pressure was measured by the pressure distribution mapping system with pressure indicating film. Though the accuracy of the contact pressure measurement varies within 10%, the contact pressure measurement system was stated as follows:

- Pressure Indicating Film

The structure of pressure indicating film, as shown in Figure 13 was consisted of A-film coated with micro encapsulated color forming material and C-film coated with a color developing material. When the pressure was applied to the indicating film, then the tiny micro bubbles burst and red color distribution was formed in varying density. The color density of the pressure indicating the film is directly related to the amount of pressure applied on it [41].

In this experimental study, the range of the contact pressure measurement was chosen from 0.5 MPa to 10 MPa by varying the pressure indicating film. This range of pressure was measured by two types of film: Super Low and Low. The ranges of super low and low pressure indicating films were 0.5 MPa to 2.5 MPa and 2.5 MPa to 10 MPa, respectively.

- Pressure Distribution Mapping System

The pressure distribution mapping system (FPD 8010E) analyze the pressure indicating film to quantify the pressure data in numerical format. The pressure distribution mapping system combined with a dedicated software, a scanner, a scanner cover for the precision of data reading and a calibration sheet from Sensor Products Inc., Madison, USA. The distribution software

converts the color density values to pressure values. The calibration sheets, as shown in Figure 14 made a correlation between the color density and the absolute pressure. The contact pressure distribution inside the pipe wall can be measured along the longitudinal and hoop direction.

The strip of pressure indicating film was inserted into the radial clearance between the annular seal and the pipe. When the annular seal deformed laterally due to the axial compression, the contact pressure was applied to the pressure indicating film to form a red color of varying density in proportion to the contact pressures, as shown in Figure 15. Subsequently, the pressure indicating film was scanned and analyzed using pressure distribution mapping system to yield the maximum pressure, average pressure, and pressure distribution along the axial and hoop directions of the pipe. The temperature and humidity were recorded to analyze the pressure indicating film for better accuracy.

3.1.4 Strain measuring system

The strain was imposed on the pipe wall due to the contact of the seal during axial compression. It was a real challenge to get the exact strain distribution for the stress – strain analysis of pipe in this specific sealing application as the imposed strain was changed significantly even at every 1mm interval. Maximum axial displacement of the seal was selected in such a way that the maximum hoop strain imposed on the pipe's wall should not exceed the yield strain of the pipe. It was another challenging to measure the strain gradient on the pipe wall along the sealing area as the strain distribution was varied significantly over the small sealing area on the pipe's membrane.

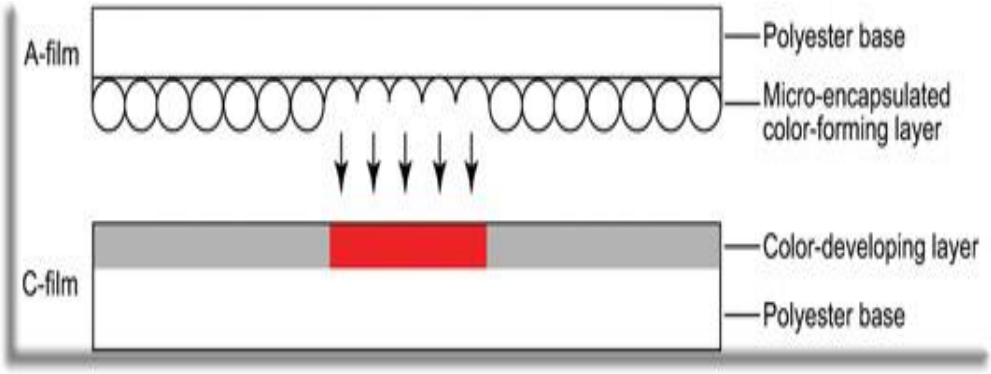

Figure 13: Pressure Indicating Film (Two Layer Type) [41]

Figure 14: Calibration Sheet

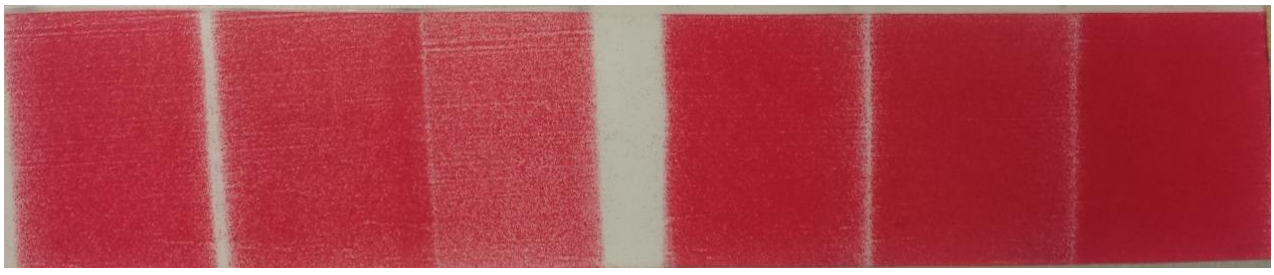

Figure 15: Pressure Indicating Film with varying color density

3.1.4.1 Strain Gauge

There are different types of strain gauges available for measuring the strain. In this experiment, uniaxial strain gauge and strain gauge chain were used to measure the strain on the pipe in the hoop direction. Strain gauge chain is a very special type of measuring instruments which can measure the strain gradients in the confined space. Two strain gauge chains (KY21-2/120) from HBM test and measurement, were used for measuring the hoop strain gradient on the outer surface of the pipe. Each chain consisted of 10 strain gauges which are perpendicular to the chain axis, uniformly spaced on a common backing. The resistance of each gauge was 120 ohm and the gauges were arranged in a quarter bridge configuration. The size of the measuring grid of each strain gauge was 1.7 mm in length and 1.7 mm in width, allowing measurement of strain at every 2.0 mm along the length of the pipe. These chains were bonded to the pipe as shown in Figure 16 using M-Bond 200 adhesive kit. The strain gauge chain was bonded on the pipe's wall in a way that it can measure the strain in the hoop direction. One uniaxial strain gauge was used in the stress-free region for temperature compensation of the strain gauge chain.

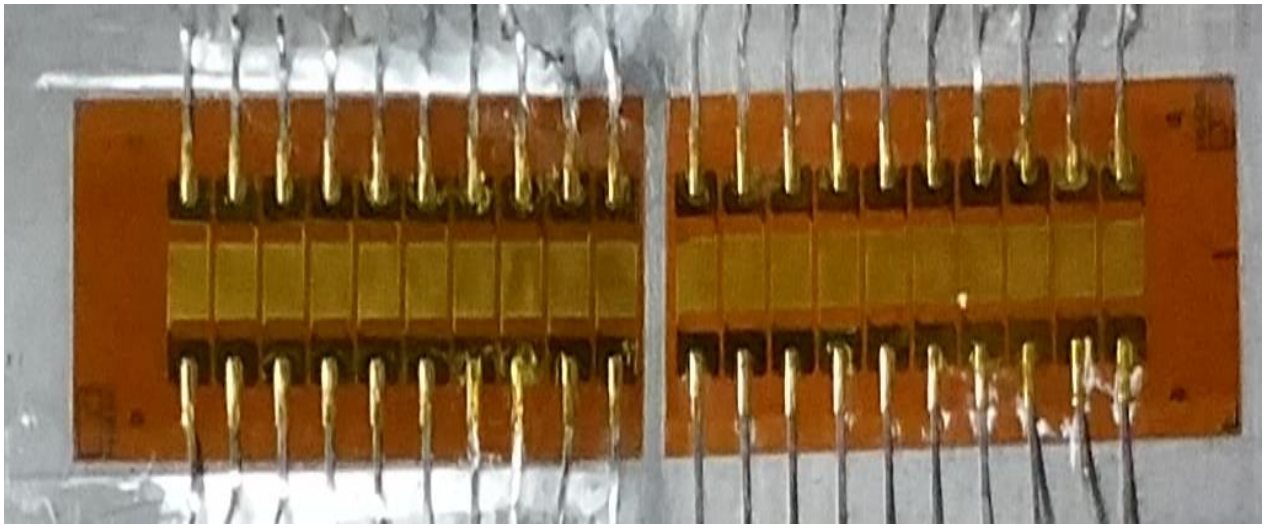

(a)

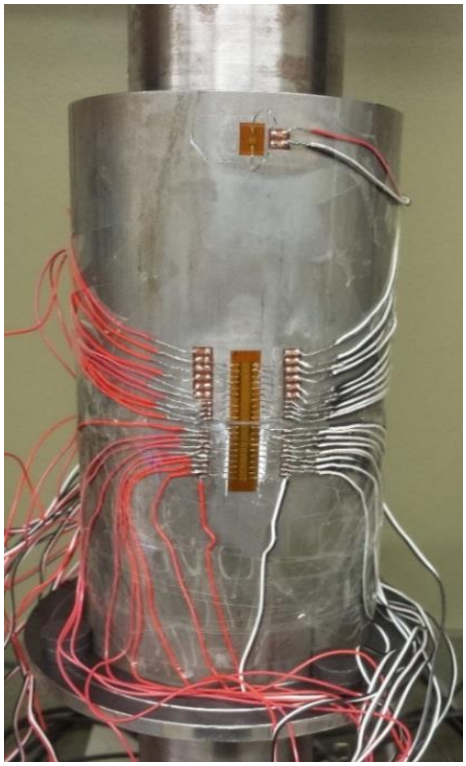

(b)

Figure 16: (a) Strain Gauge Chain (b) Strain Gauge chain mounted on the Pipe

Figure 17: Data Acquisition System

3.1.4.2 Data Acquisition System

Vishay's micro measurement system 7000 as shown in Figure 17 was used to measure the strain of the pipe's outer wall. Vishay 7000 micro measurement system is a versatile data acquisition system intended for static and dynamic test measurement applications. The model of the data acquisition system is 7000-32-SM which supports up to 32 channels. The Vishay's micro measurement system 7000 was coupled with Strain Smart software. Strain Smart is a ready-to-use, Windows® based software system for acquiring, reducing, presenting, and storing data from strain gauges. This software was capable of operating either 120 ohm or 350-ohm resistance strain gauges at various excitation voltage. Furthermore, zero calibration, shunt calibration, and temperature compensation were performed for each set of trials.

3.1.5 Test procedure

Testing of rubber is so sensitive as the properties of the rubber materials is dependent on various operational parameters. In this study, uniaxial compressive testing was conducted to explore the compressive behavior of the seal in the unconstrained state (without pipe) and constrained state (with pipe). The details of the test procedures were stated below by describing the input parameters, output parameters and loading conditions.

Input parameters:

The experimental analysis was performed by controlling the three input parameters that are stated below:

- Surface conditions

It was found from the literature that the apparent compressive modulus of solid rubber disk upon uniaxial compression is dependent on the frictional coefficients at the contact surfaces between the rubber and the steel platens. Therefore, this experimental analysis under uniaxial compression was performed on the annular rubber seal at two frictional coefficients at the contact surfaces between the rubber and the steel platens to observe the compressive behavior of annular seal. The frictional contact surfaces were considered as rough and lubricated. The rough surfaces were prepared by abrading the steel platens with 400 grit SiC sand paper and the lubricated surfaces were prepared using lubriplate No.105. The co-efficient of friction was measured for this two specific surface conditions by Bartel *et al.* from Axel Products Inc.[40] The surface conditions were maintained in every trial during testing with 400 grit SiC paper or grease lubriplate No. 105.

- Strain rates

The characteristic of the annular rubber seal under compression was observed at two strain rates in both constrained and unconstrained state. The rate sensitivity of the annular rubber seal was observed using a lower (0.05 S^{-1}) and higher strain rate (and 0.002645 S^{-1}). The maximum strain rate (0.05 S^{-1}) was selected as it was the maximum available test speed of Axel Products performed during the material testing of rubber. The displacement rates tested were 95 mm/min and 5 mm/min for 31.5 mm thick rubber seal which corresponds to the strain rates of 0.05 S^{-1} and

0.002645 S^{-1}, respectively. However, the displacement rates were also changed due to the changes of the rubber thickness for maintaining the same strain rates.

- Geometry

In this study, the compression tests were performed for the different geometry of the annular rubber seal with two frictional surface conditions. The apparent compressive modulus of the annular rubber seal was measured for various geometry which corresponds to various shape factor. The effect of shape factor on the apparent compressive modulus was investigated at the two frictional surface conditions, e.g. rough and lubricated surface conditions. The tests were conducted with the following shape factors as shown in Table **3**:

Single seal and stack seal were shown in Figure 18 and Figure 19, respectively. The shape factor decreases with the increasing of the initial height by stacking the single seal.

Table 3: Different seal configuration and its shape factor

Seal Configuration	**Outer Diameter (mm)**	**Inner Diameter (mm)**	**Thickness (mm)**	**Shape Factor**
Single Seal	102.5	47	31.5	0.440
Single Seal	96.3	47	31.5	0.3913
Stack Seal	102.5	47	63	0.220
Single Seal	73	47	31.5	0.206
Stack Seal	96.3	47	63	0.1956
Stack Seal	102.5	47	94.5	0.147
Stack Seal	73	47	63	0.103

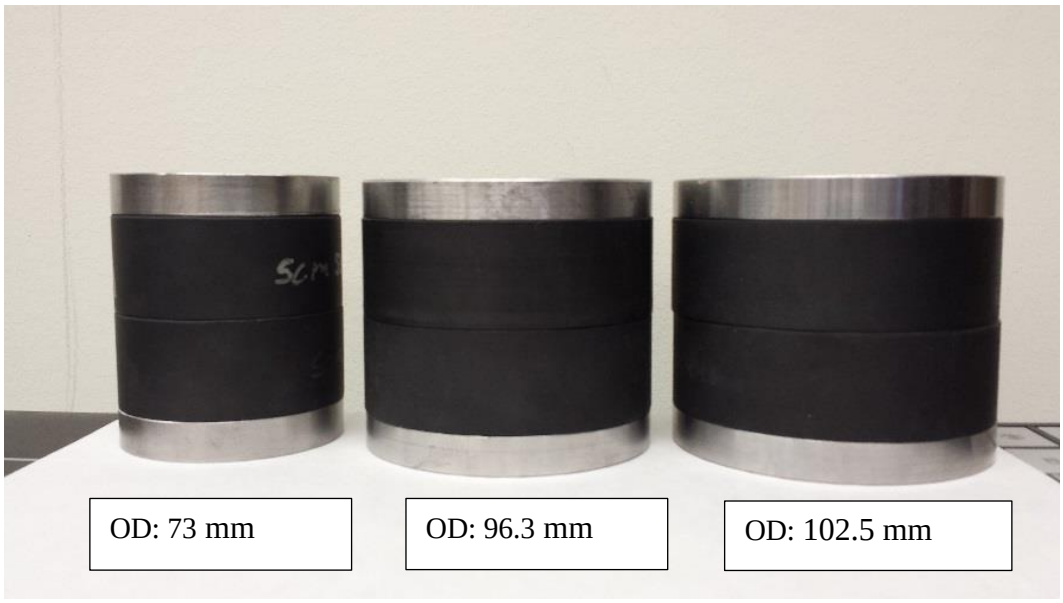

Figure 18: Stack Seal

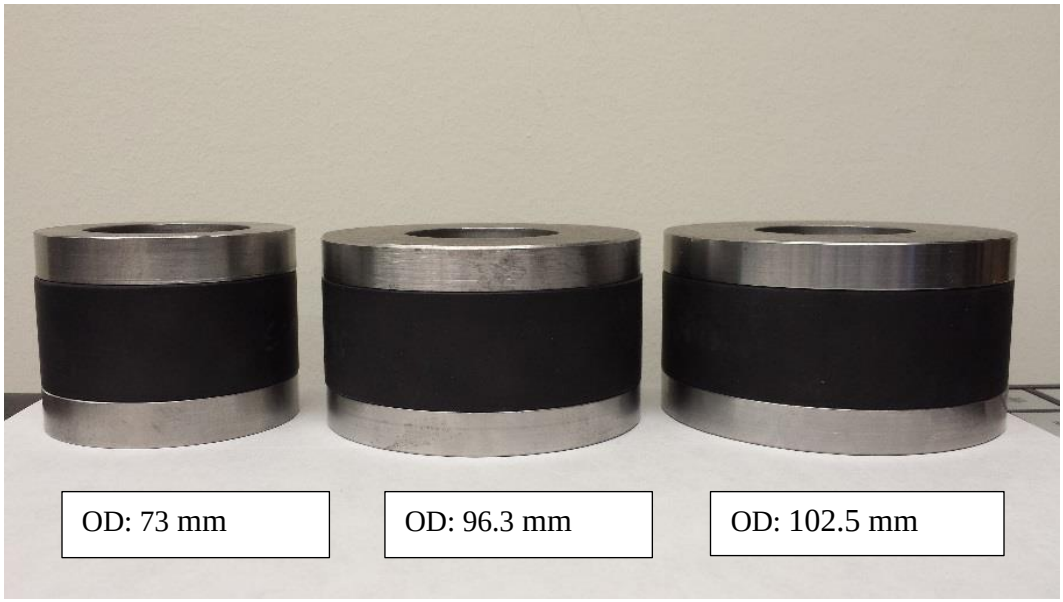

Figure 19: Single Seal

Output parameters:

The output parameters of these tests were focused in two states: constrained state (with pipe) and unconstrained state (without pipe). In unconstrained state (without pipe), the results were analyzed for the deformed shape, radial deformation, force-displacement relation, apparent compressive modulus, stiffness, and hysteresis. On the other hand, the contact pressure distribution in between the annular seal and the steel pipe, the strain gradients on the pipe wall, force-displacement relation and hysteresis were analyzed in constrained state (with pipe). All the test were performed at ambient laboratory conditions (22^{o}C).

Loading Condition:

The properties of the elastic material changes significantly, therefore, it is a real challenge to create a consistence results for each test. The reasons behind the inconsistency of the test results were different chemical compositions, aging, and Mullin's effect, etc. Due to Mullin's effect, the stress-strain curve never shows repetition for the first cycle of loading. The stress- strain curves generally stabilizes after 5 or more loading cycles. When the stress –strain function of the rubber is no longer changes then the material is considered as stable. The consistence test data can be produced by using the samples with same chemical composition, same ages, and cyclical loading. In this study, the compression tests were performed using monotonic and cyclical loading. At least three trials were conducted for each type of test to observe the repeatability. Adequate time was given between trials to allow the seals to recover to its original shape after unloading.

The testing procedure was described in two different states: unconstrained state (without pipe) and constrained state (with pipe). Testing of the annular seal in unconstrained state (without pipe) was followed as stated below:

- Preparation of the contact surfaces between the annular seal and the steel rings with the required surface treatment.
- Set up the experimental fixture with the Universal testing machine.
- Move the cross-head to get the contact with the steel ring.
- Balance the load and displacement to zero using the software of the Universal testing machine.
- Input the operational parameters such as strain rates, strain or displacement, no. of cycles.

The following procedure was used to test the annular seal in constrained state (with pipe).

- Preparation of the contact surfaces between the annular seal and the steel rings with the required surface treatment.
- Set up the experimental fixture with the pipe in the Universal testing machine.
- Move the cross-head to get the contact with the steel ring.
- Balance the load and displacement to zero using the software of the Universal testing machine.
- Insert the pressure indicating film into the radial clearance between the annular seal and the steel pipe.
- Align the pipe concentrically with the seal and the steel rings.
- Input the operational parameters such as test speed, strain or displacement, no. of cycles.

- Set up the data acquisition system with the strain gauges and calibrate the gauges.

3.2 Theoretical Analysis

Theoretical calculations were performed to measure the apparent compressive modulus of the solid and annular rubber disc without pipe and hoop strain distribution on the pipe wall. Later, the theoretical predictions were compared with the experimental and finite element results.

3.2.1 Apparent Compressive Modulus

Apparent compressive modulus of the solid and annular rubber blocks was predicted by using the equation developed by Gent *et al.* [4], [3], [5]in bonded condition. The apparent compressive modulus of bonded solid rubber block, E_a is predicted by using the equation given below:

$$\mathbf{E}_a / E = [\mathbf{1} + 2*S^2] \quad (4)$$

$$\mathbf{S} = \frac{\mathbf{D}}{\mathbf{4}*\mathbf{T}} \quad (5)$$

$$\mathbf{K}_m = \mathbf{3} * \mathbf{e} * \mathbf{r} \quad (6)$$

Where,

E: Actual Compressive Modulus

E_a: The Apparent Compressive Modulus

T: Thickness of the Solid Rubber Block

D: Diameter of the Solid Rubber Block

S: Shape factor of the Solid Rubber Block

e: Applied strain

r: Radius of the rubber block

K_m**:** Maximum Radial displacement

The apparent compressive modulus of bonded annular rubber block, Ea is predicted using the equation given below,

$$E_a/E = 1 + [(D_O{}^2 + D_I{}^2)/4 - (D_O{}^2 - D_I{}^2)/4 * \ln(D_O/D)] /2*T^2 \quad (7)$$

Where,

T: Thickness of the Annular Seal

D_O: Outer Diameter of the Annular Seal

D_I: Inner Diameter of the Annular Seal

The Apparent compressive modulus of solid rubber block between rigid frictional surfaces were also predicted using the equations stated below:

$$r1/(\mu * T) = \exp[2 * \mu \frac{a-r1}{T}] \quad (8)$$

$$\mathbf{E}_a / E = 2*S^2*R_1{}^4+(2*S*R_1{}^3)/\mu+(R_1{}^2/\mu^2)+R_1/(4*\mu^3*S)-1/(2*\mu*S)-1/(8*\mu^2*S^2) \quad (9)$$

$$R_1=r1/a \quad (10)$$

Where,

A: Radius of the solid rubber block,

r1: Radial distance at which slipping starts,

μ: Coefficient of friction,

The apparent compressive modulus was modified by realizing the effect of bulk compressibility on compression modulus. The modified apparent compressive modulus, E_a' is given by,

$$1/E_a' = (1/E_a + 1/E_\infty) \quad (11)$$

Where,

E: Actual Compressive Modulus

E_a: The Apparent Compressive Modulus

E_a': The Modified Apparent Compressive Modulus

3.2.2 Hoop Strain on the Pipe wall

It is another challenging to predict the stress distribution in the localized area of the steel pipe. Strain distribution on the pipe wall was predicted by using the Roark's formula for the stress and strain, table 13.2, and case 12 [8]. According to the Roark's formula, the uniform wall pressure over the thickness of the seal produces the membrane stress distribution on the pipe. A theoretical approximation was developed to calculate the pipe's strain based on seal contact pressure. Roark's formula was used to develop the approximation by considering the assumptions applied to the pipe where one end was free and the other end was sufficiently far enough from the closest load. Here, the Roark's formula was used for the sealing cases where the uniform pressure was applied inside the steel pipe. The experimental contact pressure was used in this theoretical approximation for predicting the hoop strain on the pipe's wall.

Roark's empirical Eqs. (12) - (25) were used to predict the hoop strain on the pipe's outer wall due to localized uniform pressure [8]. Measuring variables of Roark's empirical formula are shown in Figure 20.

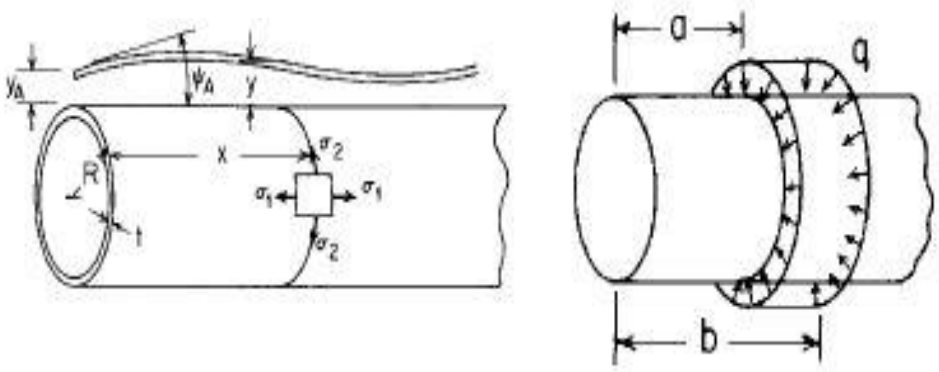

Figure 20: Measuring variables of Roark's empirical formula [8]

$$\lambda = \left(\frac{3*(1-\nu^2)}{R^2*t^2}\right)^{\frac{1}{4}} \quad (12)$$

$$D = \left(\frac{E*t^3}{12*(1-\nu^2)}\right) \quad (13)$$

$$A_2 = 0.5 * e^{-\lambda a} * (\sin \lambda a - \cos \lambda a) \quad (14)$$

$$A_3 = -0.5 * e^{-\lambda a} * \sin \lambda a \quad (15)$$

$$B_2 = 0.5 * e^{-\lambda b} * (\sin \lambda b - \cos \lambda b) \quad (16)$$

$$B_3 = -0.5 * e^{-\lambda b} * \sin \lambda b \quad (17)$$

$$\Psi_A = -q * (B_3 - A_3)/(D*\lambda^3) \quad (18)$$

$$Y_A = -q * (B_2 - A_2)/(2*D*\lambda^4) \quad (19)$$

$$F_1 = \cosh(\lambda x) * \cos(\lambda x) \quad (20)$$

$$F_2 = \cosh(\lambda x) * \sin(\lambda x) + \sinh(\lambda x) * \cos(\lambda x) \quad (21)$$

$$F_{a5} = -\cosh \lambda(x - a) * \cos \lambda(x - a) \quad (22)$$

$$F_{b5} = -\cosh \lambda(x - b) * \cos \lambda(x - b) \quad (23)$$

$$LT = -q * (F_{a5} - F_{b5})/(4*D*\lambda^4) \quad (24)$$

$$Y = Y_A * F_1 + (\Psi_A * F_2)/(2*\lambda) + LT \quad (25)$$

where – Y is the radial deflection, q is the pressure, λ,D, LT, A_2, A_3, B_2, B_3, F_1, F_2, F_{a5}, F_{b5} are the constants and functions, Ψ_A is the meridional slope, R is the mean radius, t is the wall thickness, E is the Young's modulus of pipe, ν is the Poisson's ratio, a and b are the distances from the free end of the pipe.

3.3 Finite Element Analysis

The finite element method is one of the most vital technique in numerical analysis. Though much numerical techniques is used for solving engineering related problems, finite element model is the most versatile, reliable and comprehensive numerical tool for analyzing critical and complex design problems. The finite element model, developed by Bartel *et al*.[38] was used to characterize the compressive behavior of rubber in the unconstrained state by simulating the geometry, materials and boundary conditions correspondence to the experiment. For this analysis, FEM code was written with APDL (ANSYS Parametric Design Language) and used into ANSYS classic for taking overall control of geometry, element, boundary conditions, strain, and other settings. All the dimensions of the annular rubber seal and the steel rings were measured by using slide calipers with ±0.03 mm accuracy and used for finite element analysis. Bartel *et al*.[38] developed the finite element model using a 2D axisymmetric geometry. This finite element model with the 3rd order hyperelastic Yeoh model was developed by using the curve fitting co-efficient from the test results of uniaxial tension, planar tension, equibiaxial extension, and volumetric compression. The hyperelastic tests data conducted at 0.002645 S^{-1} strain rate was used to develop the finite element model as the experimental analysis for different shape factor was performed at this strain rate. The coefficient of friction was measured from the axial compression – torsion test results for rough and lubricated surfaces which were used to incorporate friction into the finite

element model. For simplicity of the model, plane 182 type elements with 4 nodes were chosen which was capable of axisymmetric analysis.

However, a parametric study was performed for a wide range of geometry (shape factor) of the annular rubber seal using the finite element model. The finite element model was developed by validating the simulation results with the experimental results for the annular rubber seal in both rough and lubricated frictional contact surfaces. Later, the finite element model was extended for solid rubber block and compared the simulation results with the established theoretical prediction for a solid block in both bonded and frictional contact surfaces. The intension of this parametric study was to explore the effect of geometry or shape factor on the apparent compressive modulus of the annular seal for different frictional contact surfaces in between the rubber and the steel platens. The range of the shape factor was covered in this finite element analysis was 0.1 to 100. The shape factor of the annular rubber seal geometry was changed by changing the outer diameter of the annular rubber seal while the inside diameter and thickness were kept constant. The force – displacement data were collected from the simulation results in a text format which then converted to excel format. Subsequently, the force –displacement data were processed for calculating the apparent compressive modulus. The range of the friction coefficients of this analysis was selected from 0.05 to 0.8.

4 RESULTS AND DISCUSSION

The results from experimental study of compressive behavior of the unconstrained annular rubber seal is presented first, followed by experimental results on the compressive behavior of constrained annular seal.

Finally, the results from FEM study on compressive behavior of unconstrained annular seal with shape factors beyond those used in the experiments are presented to extend the conclusions from experimental study to shape factors beyond those used in the experiments.

4.1 Effect of Contact Surface Condition

Here, radial deformation, force-displacement relations, apparent modulus (note that stiffness is load/displacement whereas modulus is stress/strain), stress-strain relations, and are discussed in both rough and lubricated contact surfaces in between the seal and the annular steel rings.

4.1.1 Deformed Shape

Axial deformation and its associated radial deformation were observed in rough and lubricated contact surfaces. When the uniaxial compressive force was applied to the non-bonded annular seal, the seal started to bulge in the lateral direction. The maximum bulge radius increased proportionally with the applied compressive force. In agreement with the literature survey [4] for the solid block under compression, it was observed from the experiment that the deformed shape of the annular seal in lateral direction was parabolic. The annular seal was prevented from expanding outwards because of the frictional constraint at the surfaces of the annular seal and the steel rings in contact. The lower friction in lubricated contact exhibits less constraint for the

lateral movement of the rubber seal. This was confirmed by the shape of the deformed seal as observed in Figure 21, wherein the shape in rough contact is more parabolic than that in lubricated contact.

4.1.2 Force-Displacement Relations

The raw data from the Universal testing machine (250 KN Instron load frame) was collected and the compressive force - displacement curve was plotted for analyzing the effect of surface conditions on the compressive behavior of the seal in both constrained and unconstrained state. The compressive force - displacement curve for unconstrained seal in rough contact tested at 95 mm/min is compared in Figure 22 with the curve for lubricated contact. In the force - displacement relation, all the curves were linear and repeatable at all trials within the maximum applied strain of 15%. Repeatability of the force-displacement curve was found when sufficient time was given between the trials to restore the seal to its original shape. Similar repeatability was observed for constrained seal as shown Figure 23.

In unconstrained condition, the seal in rough contact with the steel rings showed higher stiffness than the seal with lubricated contact. The higher stiffness (2778 N/mm) for the rough contact surface at 95 mm/min when compared to 2084 N/mm for lubricated contact surface is due to constraint, applied by the annular steel compression ring.

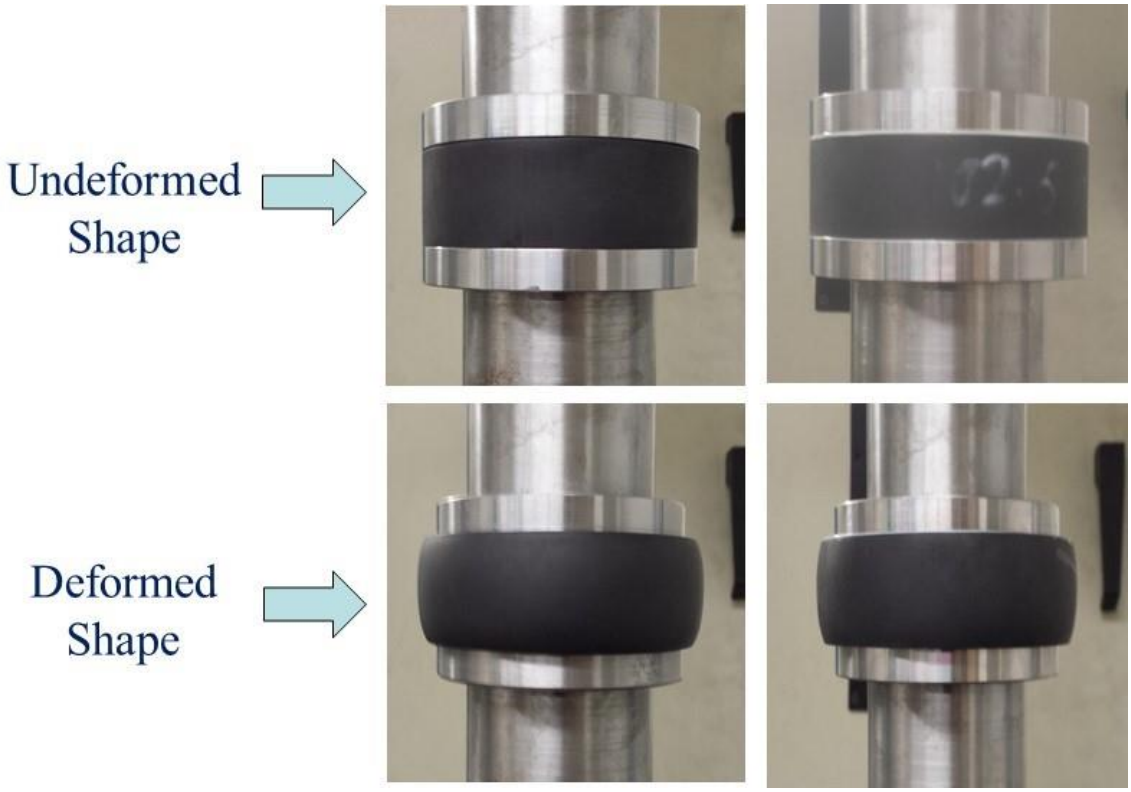

Figure 21: Undeformed and Deformed shape for (a) Rough contact surface (b) Lubricated contact surface

On the other hand, in constrained condition, the seal's compressive behavior was same as that for the unconstrained seal until the seal made contact with the pipe wall due to lateral expansion, as shown Figure 24. When this lateral expansion was restrained by the pipe, the slope of the force - displacement curve increased significantly, as indicated by the deviation of the curve for constrained seal from that for the unconstrained seal in Figure 24. The rapid increase in the compressive force in the curve is due to the constraint applied by the pipe to the radial expansion of the seal. The onset of this increase corresponds to the initiation of the contact between the radially expanding seal and the inner wall of the pipe. It should be noted that the inner wall of the pipe was not lubricated. This rapid increase occurred beyond 4 mm axial displacement (~ 9000N) for the lubricated contact surface, whereas it occurred beyond 4.5 mm axial displacement (~12000N) for rough contact. A rough contact surface reduces the lateral expansion of the seal at an applied axial displacement and hence, higher axial displacement and force is required when compared to the lubricated case, to reach the same lateral expansion.

The seal with lubricated contact surface made contact earlier than the seal with rough contact at the same level of strain and strain rate. The lubricated surface allowed more lateral movement of the seal during axial compression due to its lower friction coefficient whereas the rough contact surface restrained the lateral movement of the seal because of its higher friction coefficient. Though the seal with lubricated contact surface made contact with the pipe first, the maximum compressive force is imposed on the seal in rough contact surface as it exhibited higher stiffness.

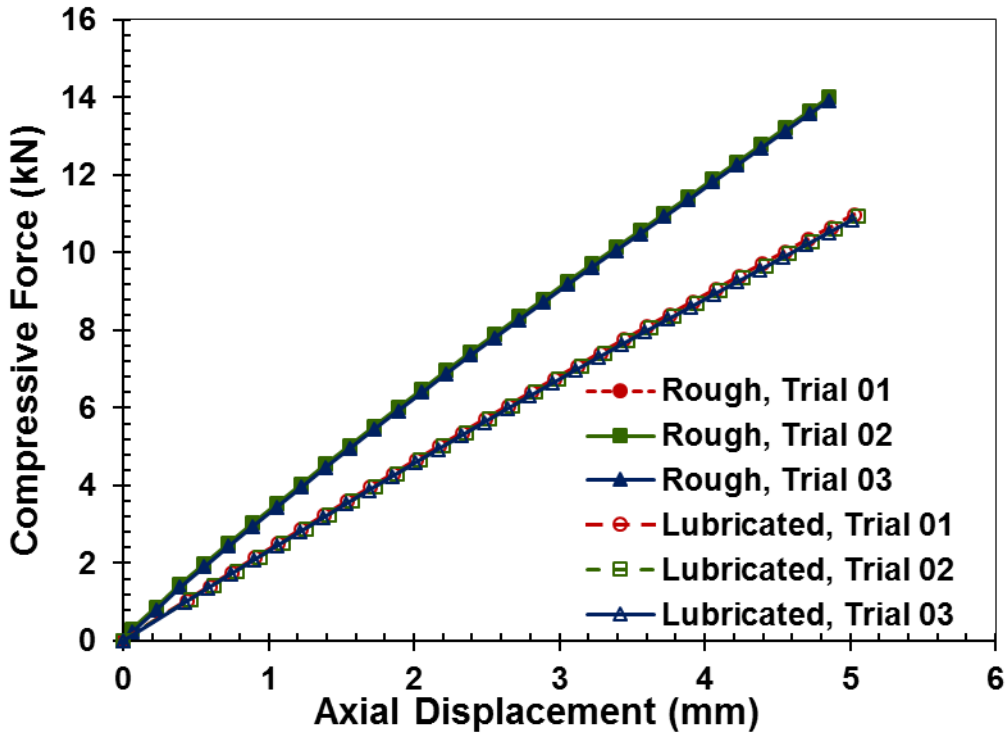

Figure 22**:** Unconstrained compressive force – Displacement curve in contact with rough and lubricated surfaces between the seal and the steel ring at 95 mm/min

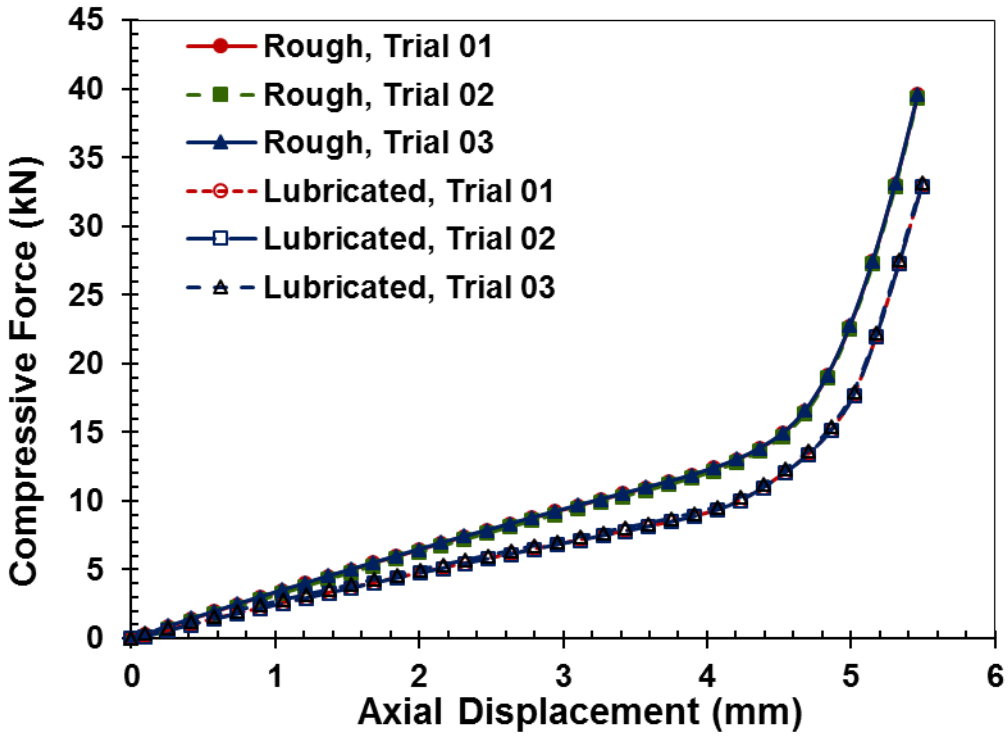

Figure 23: Comparison of Constrained Compressive Force – Displacement curve for rough and lubricated contact surface between the seal and the steel ring at 95 mm/min

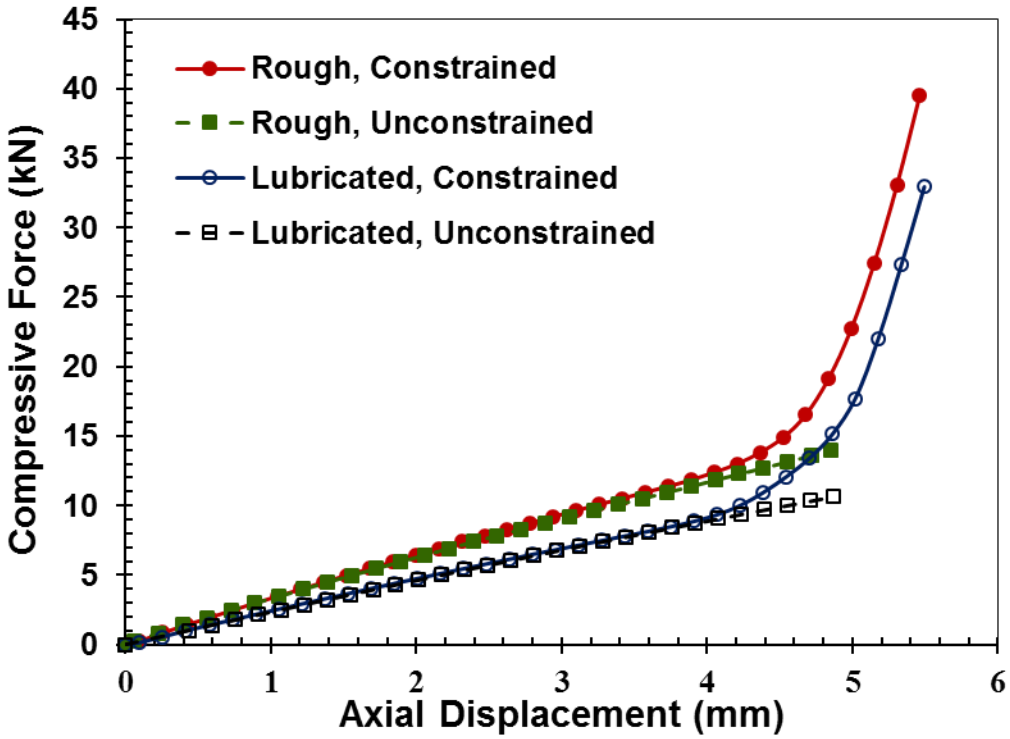

Figure 24: Comparison of Constrained and Unconstrained Compressive Force – Displacement curve for rough and lubricated contact surface between the seal and the steel ring

4.1.3 Stress-Strain Relation

The data presented in the previous section for unconstrained seal is replotted as stress – strain in Figure 25, accounting for the effect of geometry. Yet, the stress-strain curve for rough case is higher than that for the lubricated case, highlighting the effect of friction at the contact surface on the compressive behavior of the seal. The apparent compressive modulus of the annular seal is higher for the rough contact surface than for the lubricated contact surface.

The compressive stress – strain curve was plotted in Figure 26 for constrained condition showing the effect of friction of contact surfaces between the seal and the steel compression plates. The compressive stress varied abruptly from before contact to after contact in the pipe. Similar to the unconstrained condition, the stress for rough contact surface is also higher than the stress for lubricated case in constrained condition.

4.2 Effect of Strain Rates

The non-bonded annular rubber seal was analyzed to characterize the effect of strain rate under the uniaxial compression test in both constrained and unconstrained conditions. Here, the test was performed using two strain rates (0.05 s^{-1} and 0.002645 s^{-1}) for both rough and lubricated contact between the surfaces of the seal and the steel rings. The displacement rates (95 mm/min and 5 mm/min) were used during the tests corresponding to these two strain rates (0.05 s^{-1} and 0.002645 s^{-1}) at a fixed thickness of the seal.

Force-Displacement Relations

The compressive force – displacement curves at 95 mm/min and 5 m / min are compared in Figure 27 (a) and (b) for unconstrained seal with both rough and lubricated contact surfaces. A significant effect of loading rate on the compressive force-displacement curve was observed.

The stiffness of the annular seal in rough contact was higher (2778 N/mm) at 95 mm/min than at 5 mm/min (2339 N/mm). While similar trend was observed in seals with lubricated contact, the stiffness values were lower than those for rough contact; 2084 N/mm at 95 mm/min and 1825 N/mm at 5 mm/min. Hence, the stiffness of the annular rubber seal increased with increasing strain rate.

The rate dependency on the rubber is also observed in the constrained condition. The compressive force - displacement curves at 95 mm/min and 5 mm/min are compared for seals in constrained condition for both rough and lubricated contact surface as shown in Figure 28 and Figure 29, respectively. Similar to the unconstrained case, the force required to achieve a given axial displacement increased with increase in loading rate for both rough and lubricated surfaces.

When the higher stiffened seal resulting from higher strain rate, got contact on the pipe`s inner wall, then, the required compressive force of the seal to compress further increased significantly compare to the required force at lower strain rate for the same axial displacement. Hence, the strain rate applied on the seal during uniaxial compression test constrained in a pipe can affect the pipe stress.

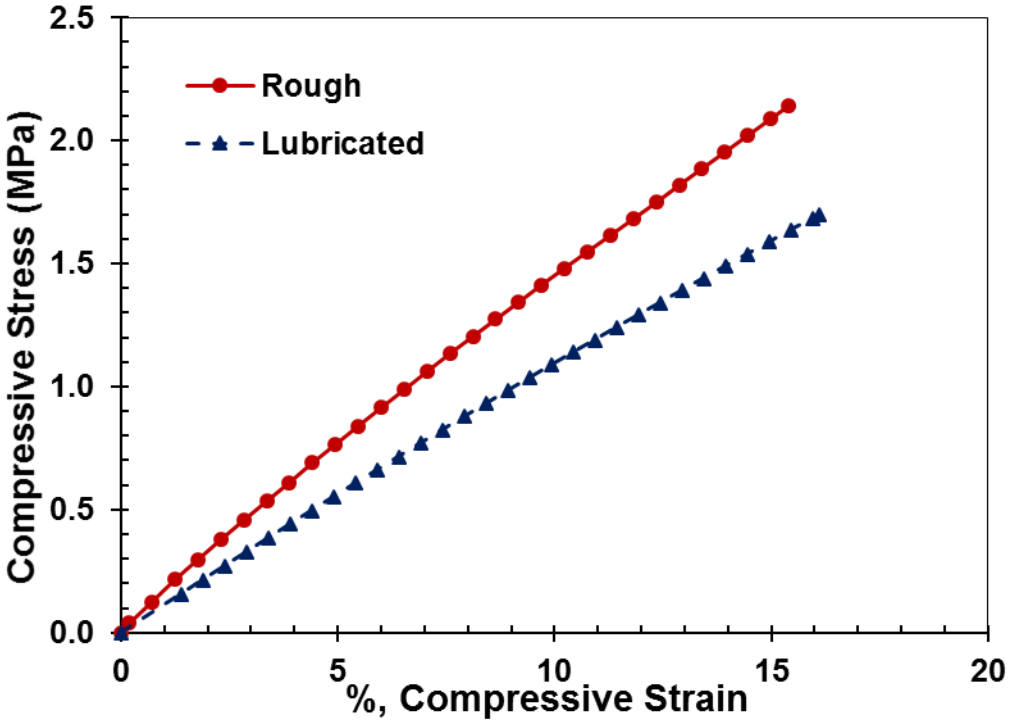

Figure 25: Unconstrained compressive stress-compressive strain curve in both rough and lubricated contact surfaces

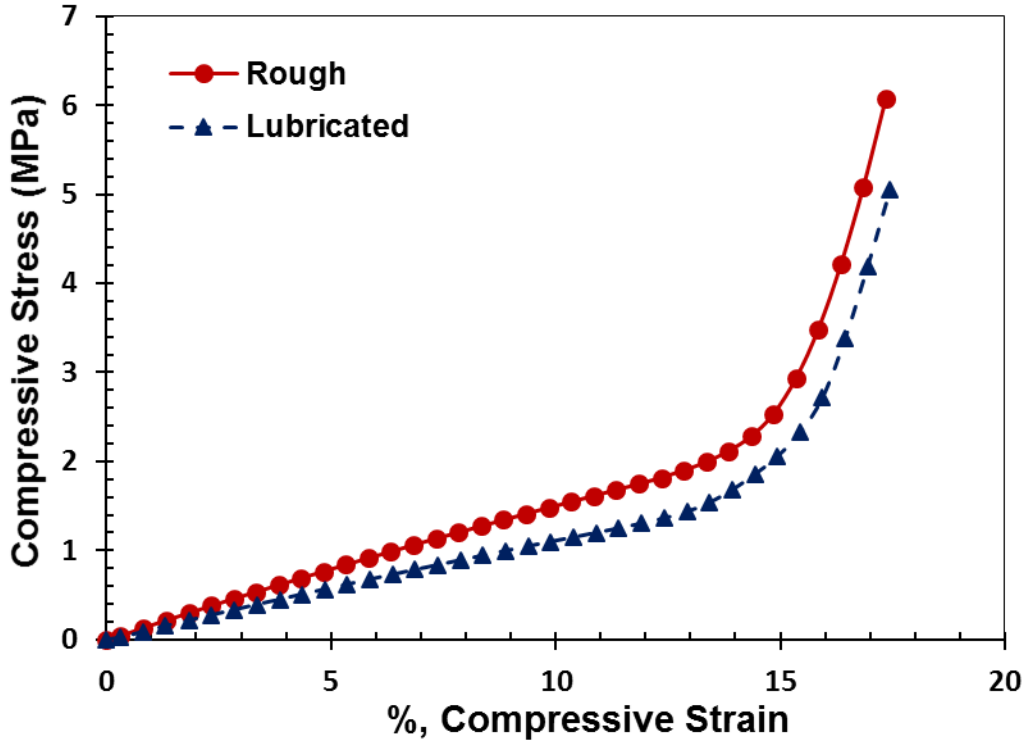

Figure 26: Constrained compressive stress-compressive strain curve in both rough and lubricated contact surfaces

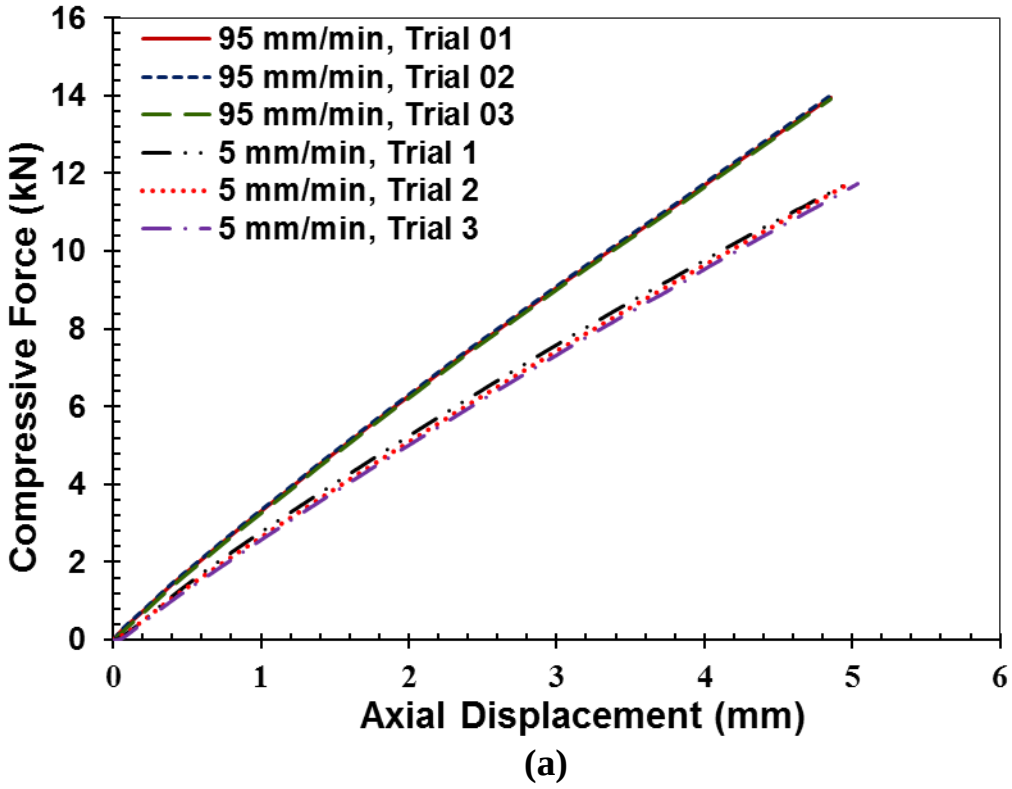

(a)

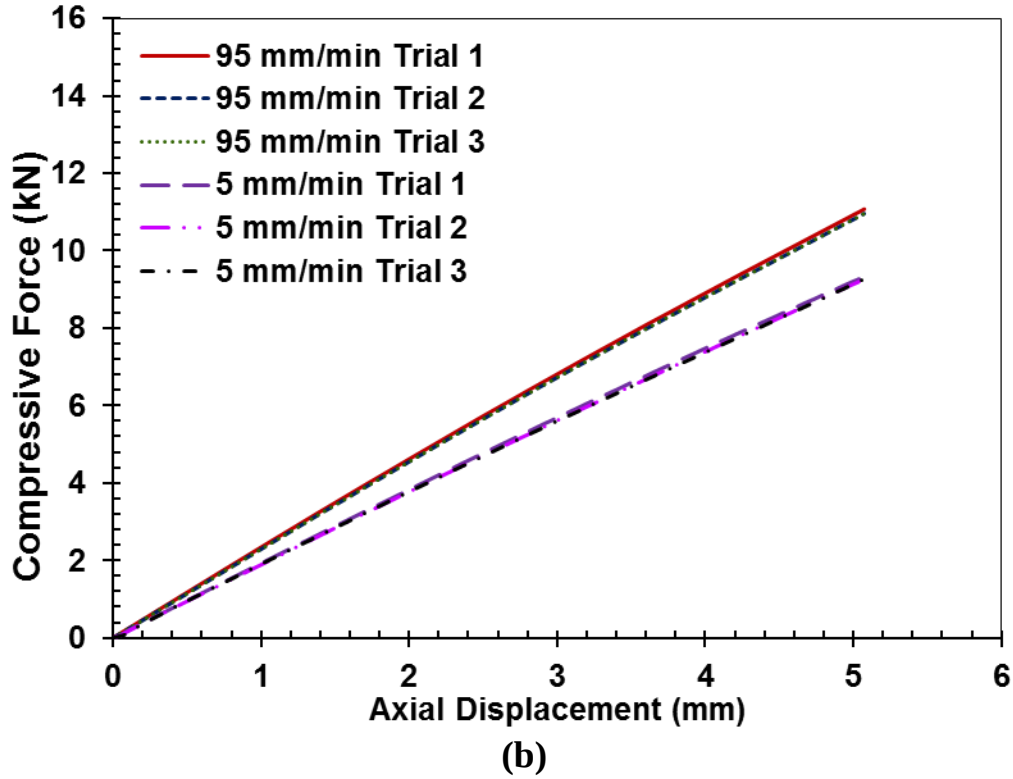

(b)

Figure 27 : Unconstrained compressive force – Displacement curve for (a) rough and (b) lubricated contact surfaces at two strain rates

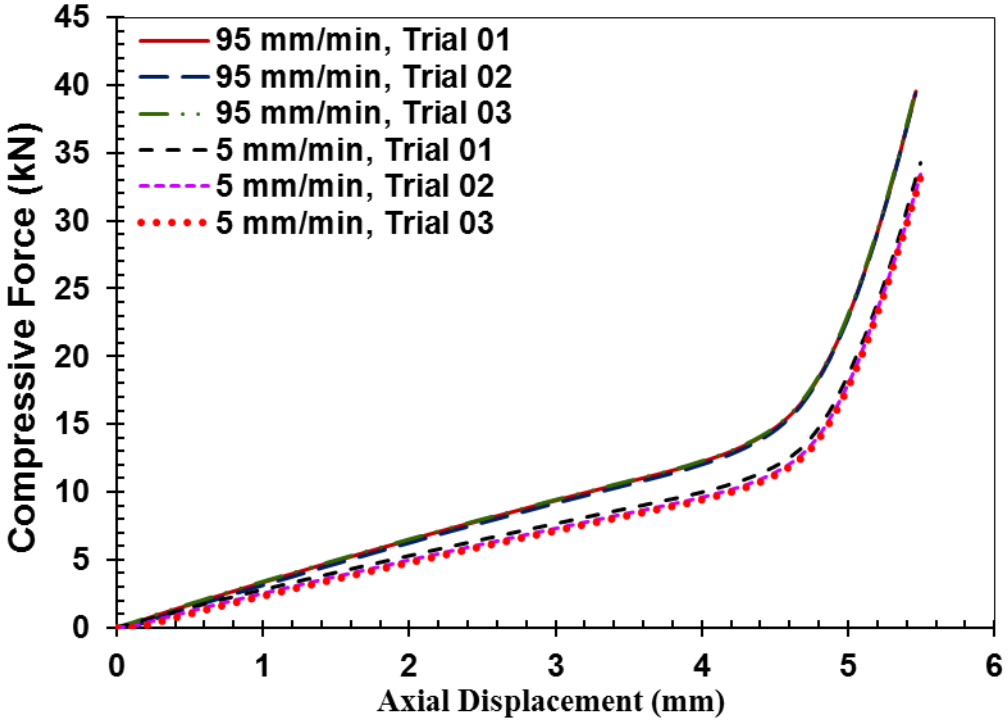

Figure 28: Comparison of Constrained Compressive Force – Displacement curve for two rates in rough contact surfaces

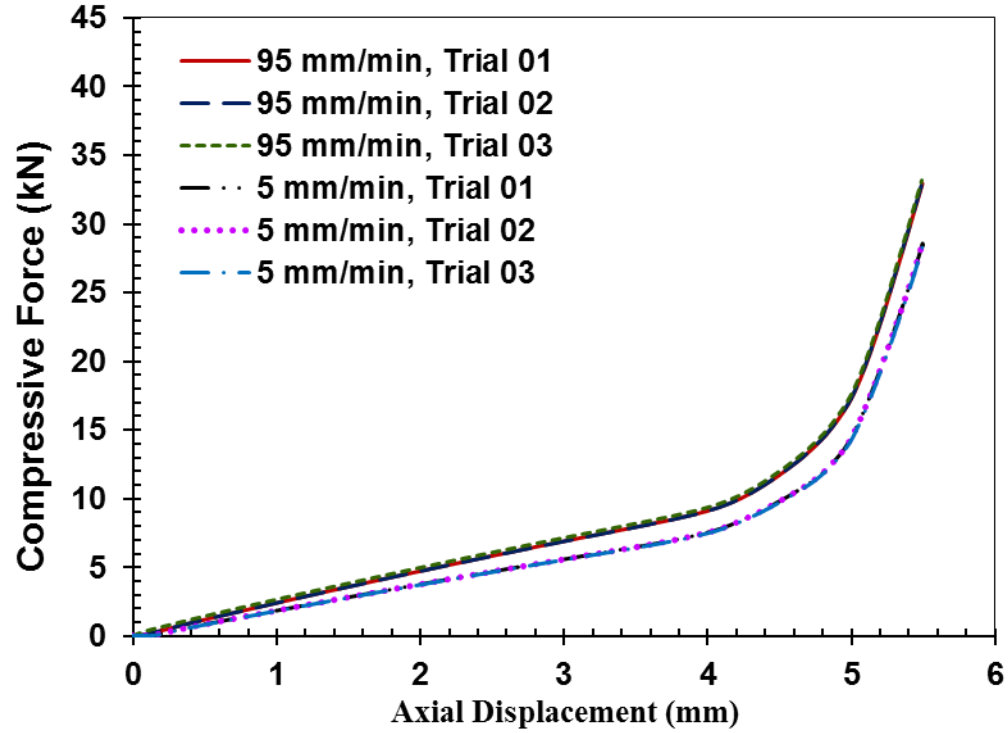

Figure 29: Comparison of Constrained Compressive Force – Displacement curve for two rates in lubricated contact surfaces

4.3 Effect of Shape Factor

Compressive characteristics of the annular seal with varying geometry (defined by the shape factors varying from 0.1 to 0.44) was studied experimentally. Radial deformation, force-displacement relation, and stress-strain relation, and apparent compressive modulus -shape factor relation were determined experimentally and analyzed. Annular seals with different sizes were tested at the same strain and strain rate.

4.3.1 Radial Deformation

The radial deformation was, as defined by the maximum bulge radius, was measured using calipers. The maximum bulge radius, for various shape factor at 15% axial compressive strain and a displacement rate of 5 mm/min, are tabulated in Table 4.for various shape factors of seals with rough contact. The radial deformation increased with increase in shape factor.

The radial displacements for different shape factors of seals with lubricated surface are tabulated Table 5. Similar to rough contact surfaces, the radial displacement is increased with increase in shape factor of the annular seal. It is also observed that the radial displacement of annular seal with lubricated contact was higher than that for the seals with rough contact, for a given shape factor. Due to lower friction in lubricated case, the steel rings would have exhibited less constraint to seal's lateral expansion resulting in higher radial displacement.

.

Table 4: Radial Displacement for different shape factor in seals with rough contact surface

Outer diameter (mm)	Inner diameter (mm)	Thickness (mm)	Shape Factor	Axial Displacement (mm)	Maximum Radial Displacement (mm)
102.5	47	31.5	0.440	5	3.02
96.3	47	31.5	0.3913	5	2.52
73	47	31.5	0.206	5	1.94

Table 5: Radial Displacement for different shape factor in seals with lubricated contact surface

Outer diameter (mm)	Inner diameter (mm)	Thickness (mm)	Shape Factor	Axial Displacement (mm)	Maximum Radial Displacement (mm)
102.5	47	31.5	0.440	5	3.18
96.3	47	31.5	0.3913	5	2.87
73	47	31.5	0.206	5	2.63

4.3.2 Force-Displacement Relations

The compressive force - displacement curves as well as corresponding stress-strain curves shown in Figure 30 and Figure 31 correspond to unconstrained seals rough contact surface as well as same outer diameter (102.5 mm), inner diameter (47 mm), and thickness (31.5 mm). The seals were tested as single, double (by stacking two seals) and triple (by stacking three seals). The shape factor was changed by changing the thicknesses through stacking. The stiffness, given by the slope of these curves, increased with increase in shape factor. Seals procured with unknown history are termed as "Old". A seal with known history (i.e. manufacturing date) was also procured and it is termed as "New". The stiffness of new seal is slightly lower than that for the old seals, specifically at higher displacements, suggesting difference in chemistry / structure between the two batches of seals.

Another way of changing the shape factor is to change the outer diameter without changing the inner diameter and the thickness of the seal. Three seals with outer diameters of 102.5 mm, 96.3 mm and 73 mm but same inner diameter (47 mm) and thickness (31.5 mm) were tested. The compressive force – displacement curves as well as corresponding stress-strain curves, for various seals and stacking, are shown in Figure 32 and Figure 33, respectively, for unconstrained seal with rough surface.

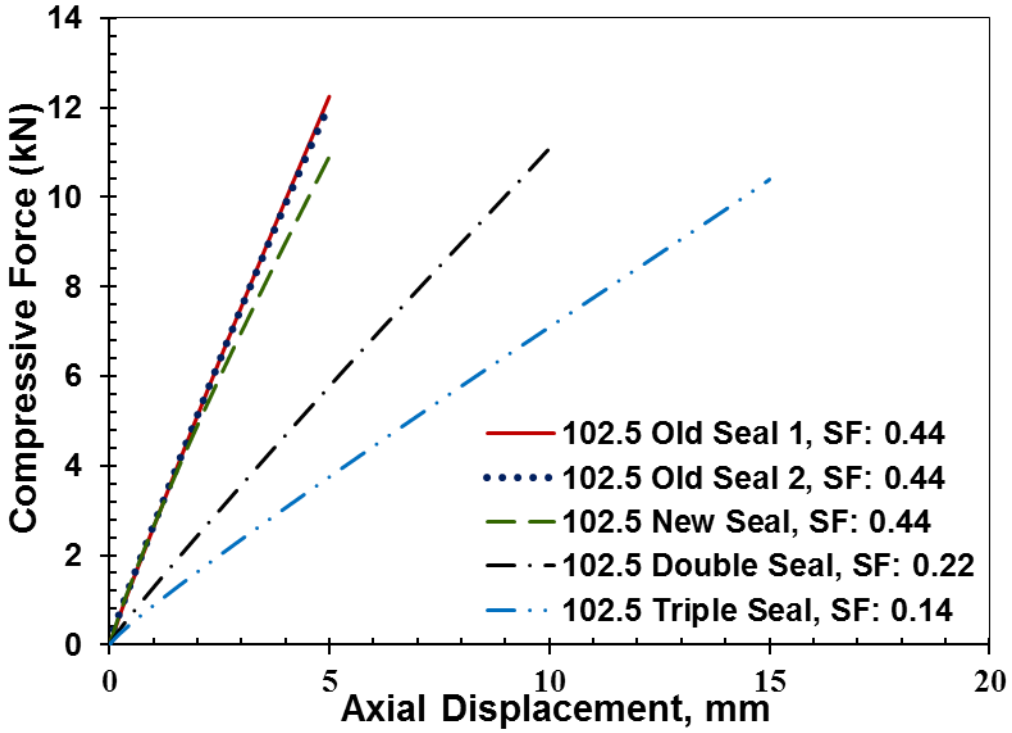

Figure 30: Compressive force - displacement curve for unconstrained seals with rough contact surface, various shape factor, and same outer diameter

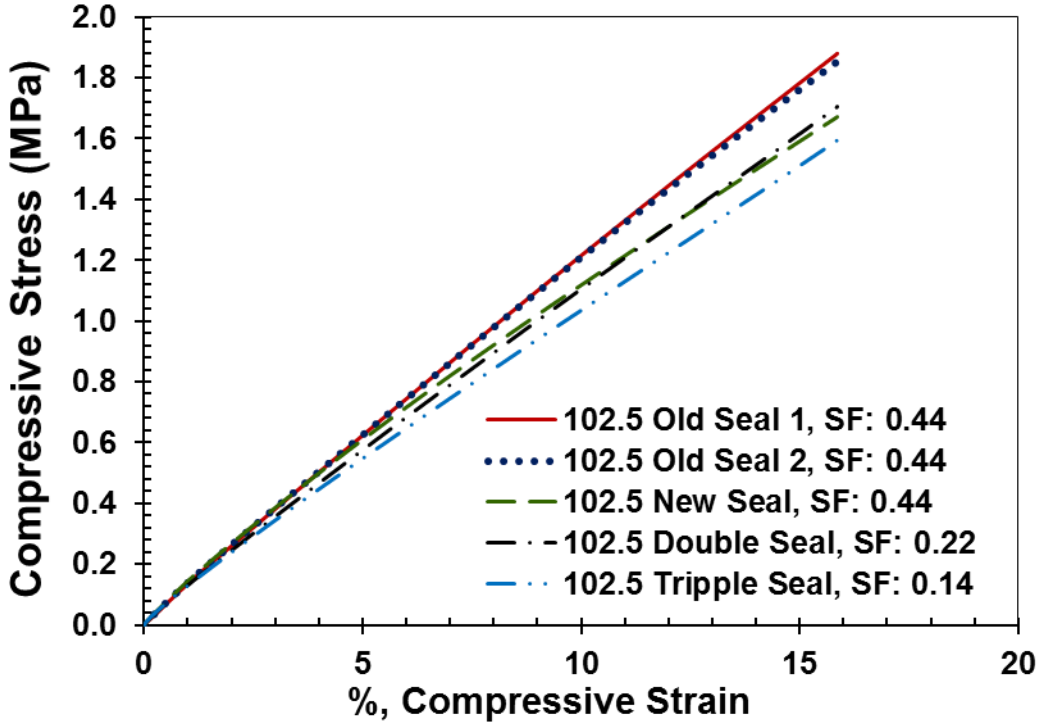

Figure 31: Compressive stress – strain curve for unconstrained seals with rough contact surface, various shape factor, and same outer diameter

The compressive stiffness and the apparent compressive modulus increased with the increase in the shape factor with the exception of the seal with 96.3 mm outer diameter. The stiffness and apparent compressive modulus of the seal with 96.3 mm outer diameter were found higher than that of the seal with 102.5 mm outer diameter although the shape factor for the seal with 96.3 mm outer diameter (0.39) is lower than that (0.44) for the seal with the outer diameter of 102.5 mm. The manufacturing date for these two seals are not known. Hence, batch to batch manufacturing differences as well as different aging histories are believed to be the reasons for the observed anomaly.

The compressive force – displacement relations as shown in Figure 34 were analyzed in constrained condition for the single and stack seal with 102.5 mm outer diameter. At the same axial strain of the seal, the compressive force (46,557 N) is higher for stack seal than the compressive force (22,683 N) for single seal in rough contact surface. Moreover, the required force (~ 12,000N) for the initiation of contact in single seal is higher than the required force (~ 10,000N) for the contact initiation in stack seal. Therefore, the force required for contact initiation is increased with shape factor.

The compressive stress – strain relations were analyzed for large axial strain (30%) in unconstrained condition with two different sizes seals. At large strain, the compressive force-displacement curve showed non-linearity as shown in Figure 35. Moreover, the pattern of the compressive force – displacement curve is varied with different sizes seal.

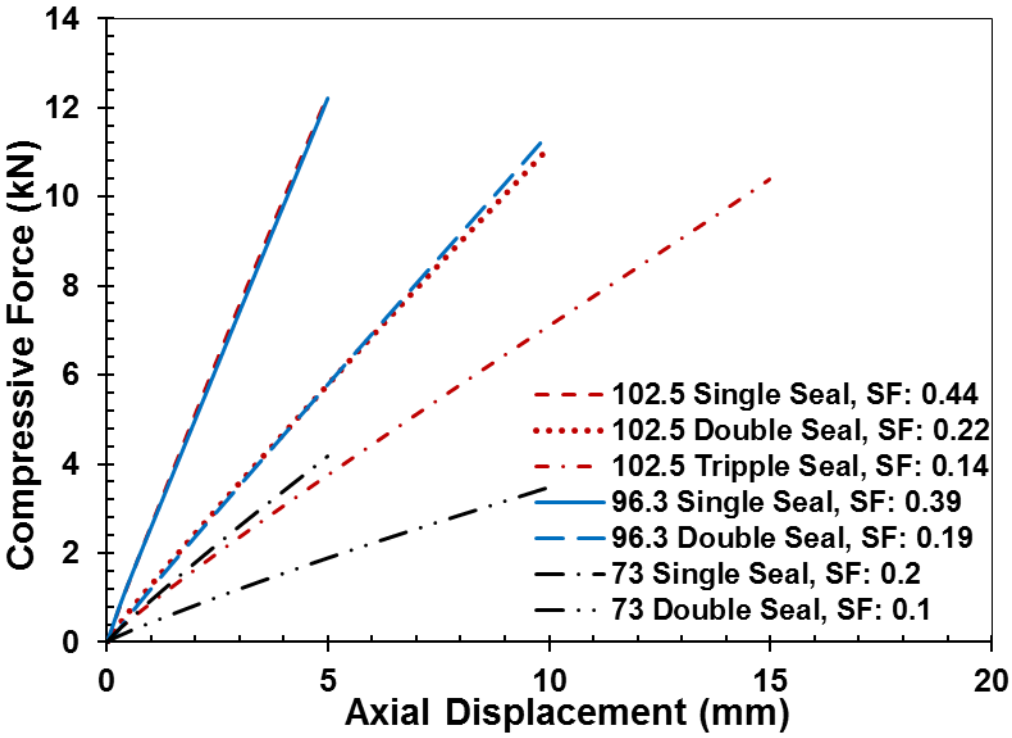

Figure 32: Compressive force - displacement curve for unconstrained seals with rough contact surface, various shape factor, and various outer diameter

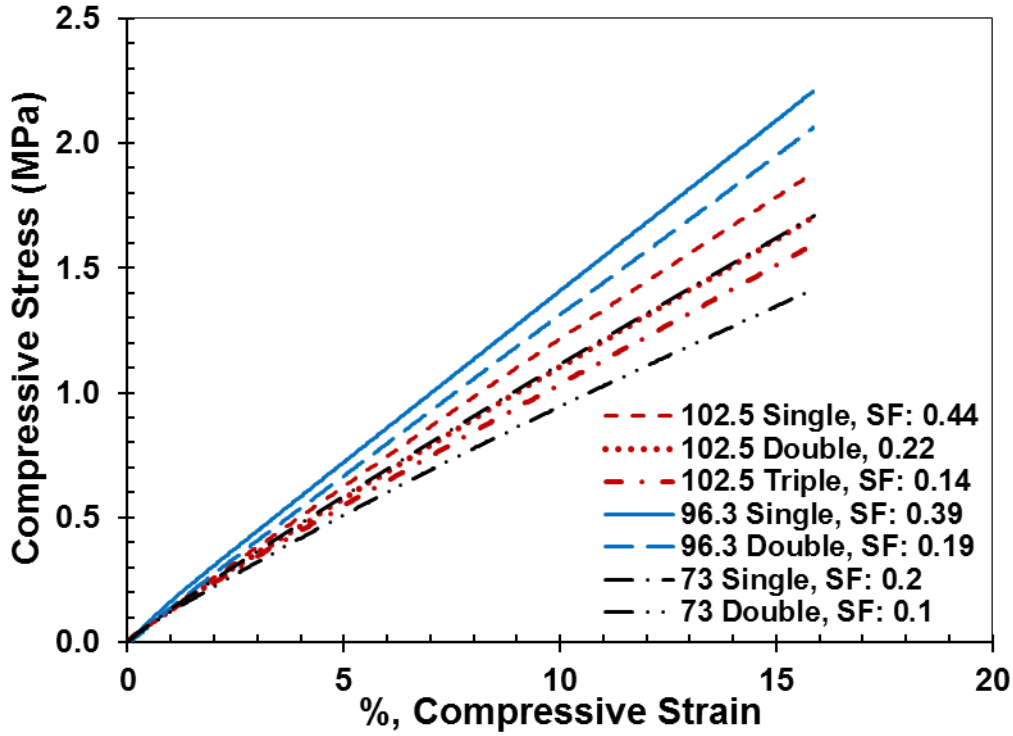

Figure 33: Compressive stress – strain curve for unconstrained seals with rough contact surface, various shape factor, and various outer diameter

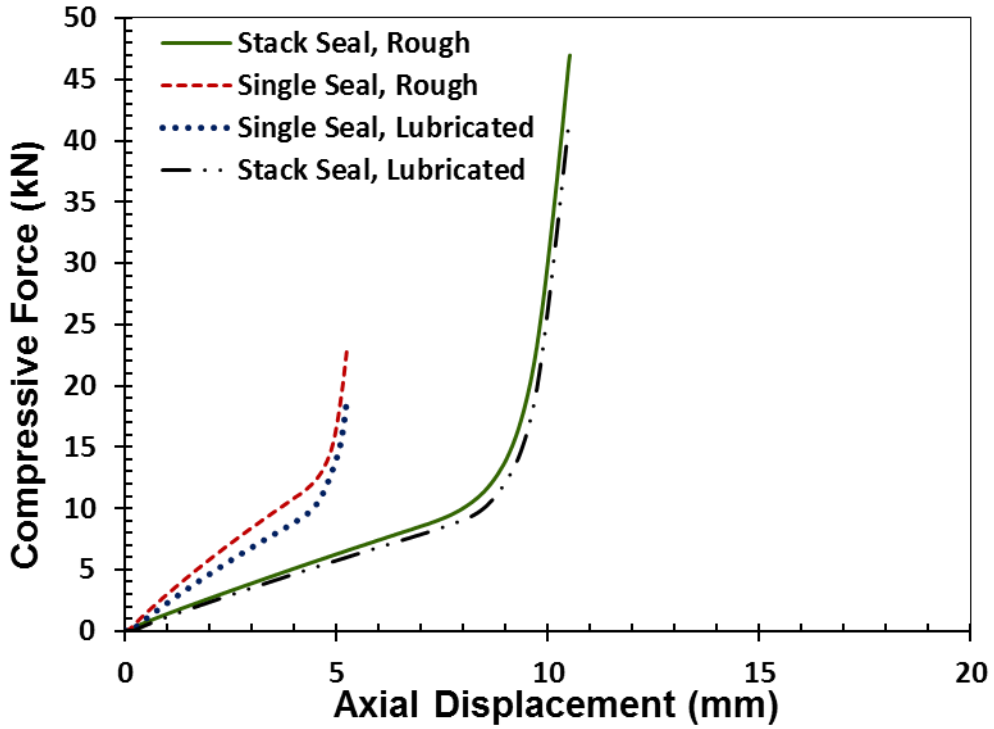

Figure 34: Compressive force- axial Displacement curve for single and stack seal

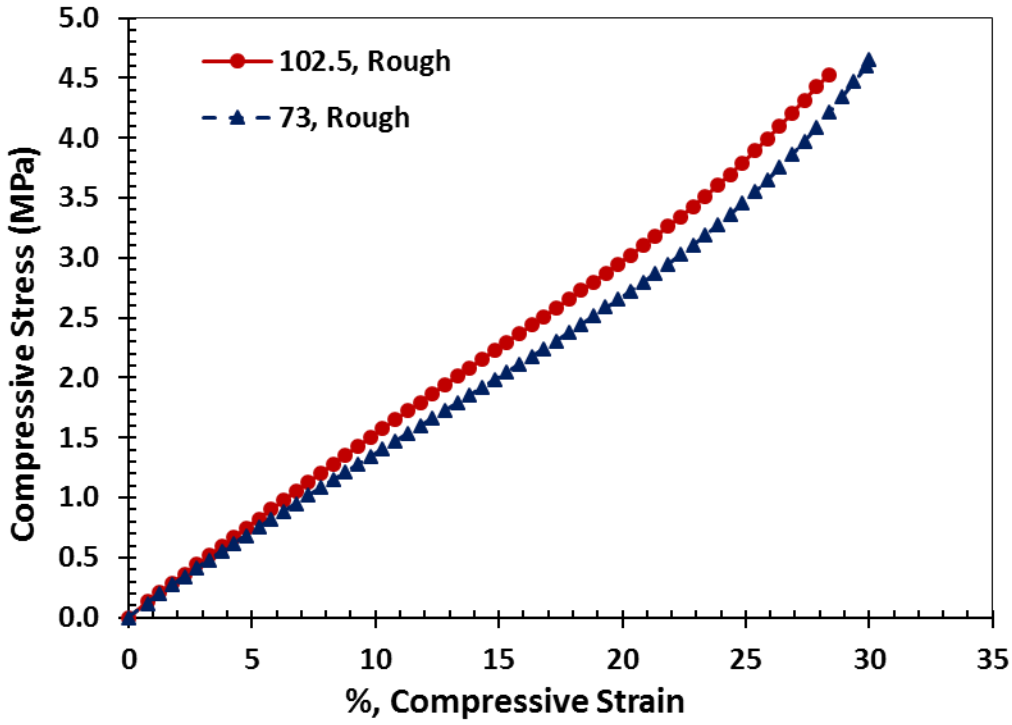

Figure 35: Compressive force- axial Displacement curve at large strain with three different sizes annular seals

4.3.3 Apparent Compressive Modulus

The apparent compressive modulus is plotted as a function of the shape factor in Figure 36 for seals with rough and lubricated contact surfaces. While the apparent compressive modulus of the annular seal with rough contact surface increased with increase in the shape factor, it hardly changed with the shape factor for seals with lubricated contact. This is expected since the changes in apparent modulus is due to changes in constraint imposed by the steel rings to the lateral expansion of the seal and the magnitude of constraint is minimal in seals with lubricated contact surfaces.

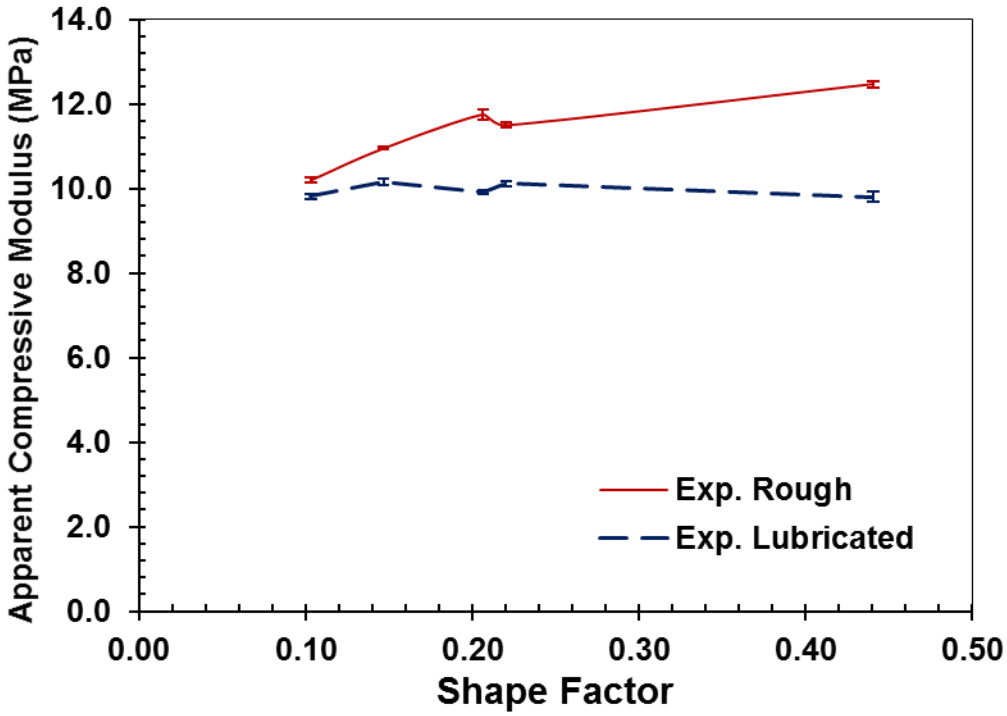

Figure 36: Apparent compressive modulus with shape factor for rough and lubricated contact surfaces

4.4 Contact Pressure Distribution

The pressure exerted by the seal on the inner wall of the pipe over the area of contact (i.e. sealing area) was measured experimentally. The pressure indicating film with varying color density in response to contact pressure is shown in Figure 37 for seals with rough and lubricated contact surfaces between the annular rubber seal and the steel rings. The software supplied by the manufacturer of the film allowed the measurement of contact pressure along a line from the colors formed by the film in response to the contact pressure as shown in Figure 38. The pressure exerted by the seal on the inner wall of the pipe, measured at an axial displacement of 5.5 mm is plotted in Figure 39 as a function of position (corresponding to the position of the strain gauge on the outer wall of the pipe), for seals with rough and lubricated contact surface. Due to the lower precision (±10%) in the measurement of the pressure measuring system, a noisy contact pressure distribution was recorded. Since higher force is required for the seal with rough surface when compared to seal the lubricated case to reach the same axial expansion after making contact with the pipe wall, the higher contact pressure (4.52 MPa) is observed for seal with the rough contact surface than the seal with the lubricated surface (3.31 MPa).

The color gradient formed in the pressure films during loading at two different strain rates are shown in Figure 40 and Figure 41. The contact pressure measured using the software based on the color gradient, for an axial displacement of 5.5 mm, is plotted in Figure 42 as a function of positon on the pipe, for the seal with lubricated contact surface. The higher contact pressure was observed at higher strain rate (3.22 MPa at 95 mm/min versus 2.2 MPa at 5 mm/min) due to higher apparent compression modulus of the seal.

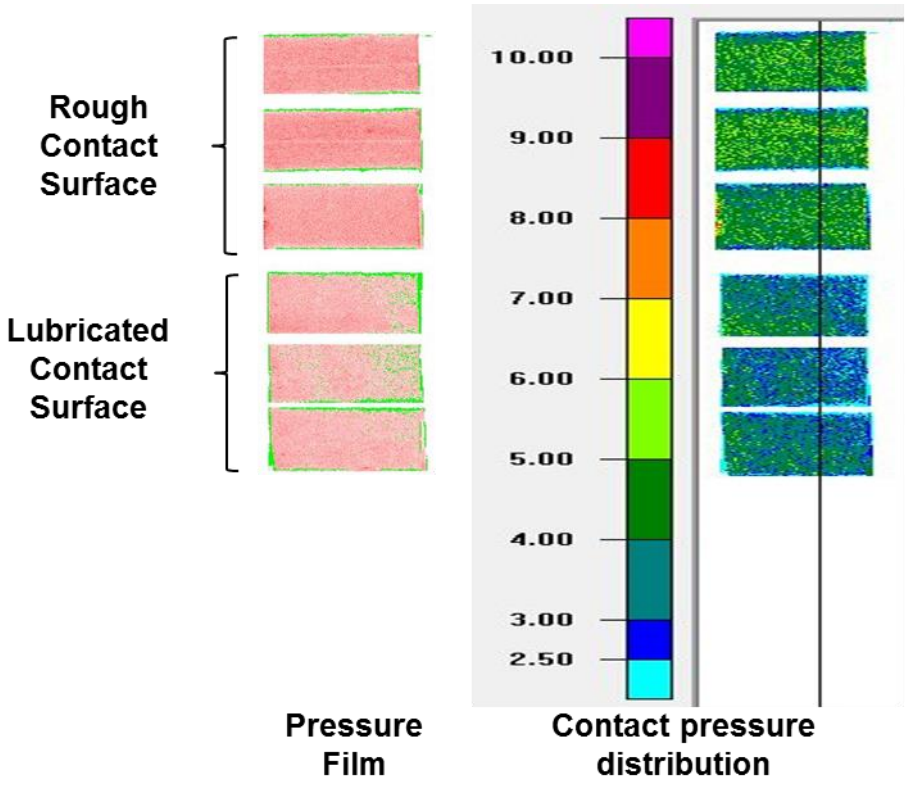

Figure 37: Pressure Indicating Film and Contact Pressure Distribution

Figure 38: Contact Pressure Distribution along the vertical line of the sealing area

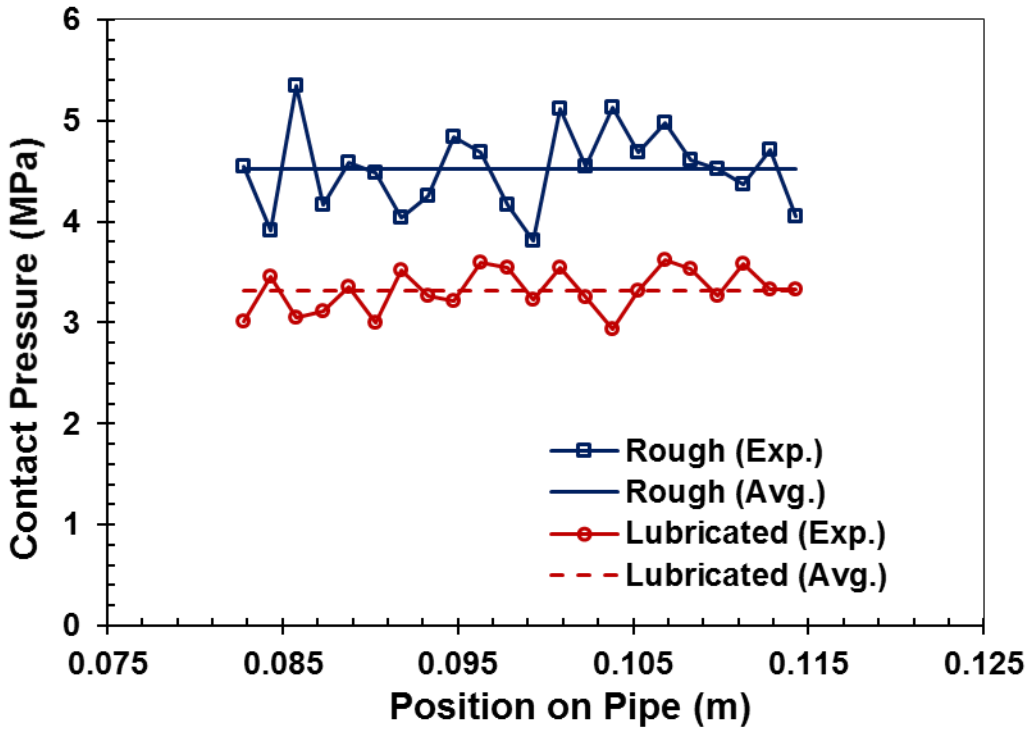

Figure 39: Contact Pressure Distribution for two surface conditions along the position on pipe

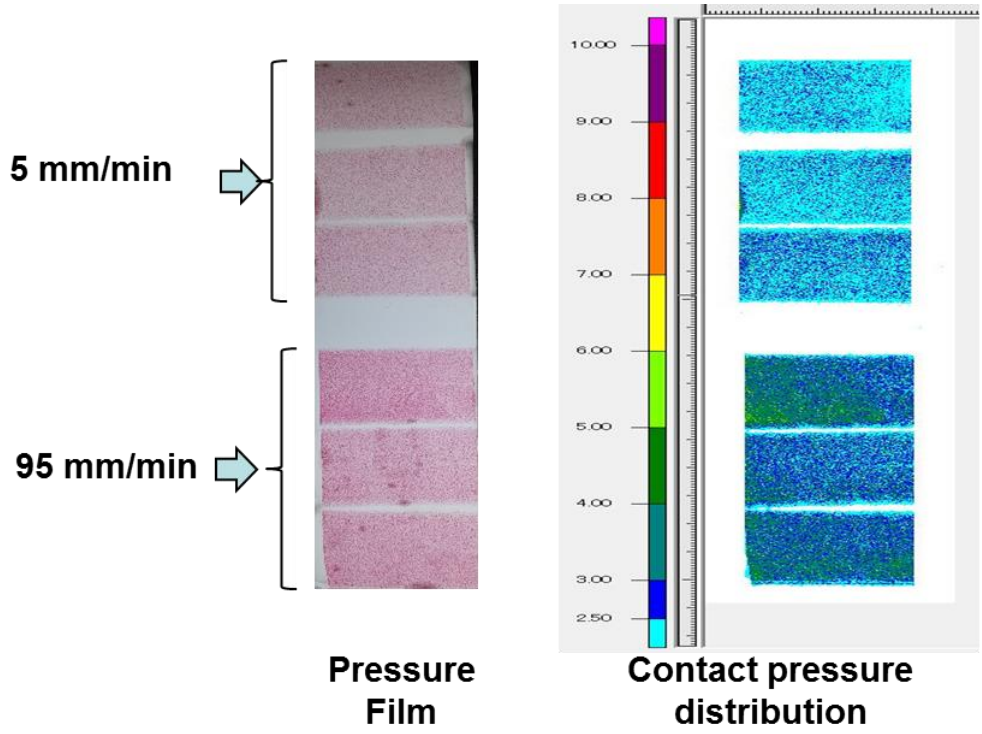

Figure 40: Contact Pressure Distribution at two strain rates

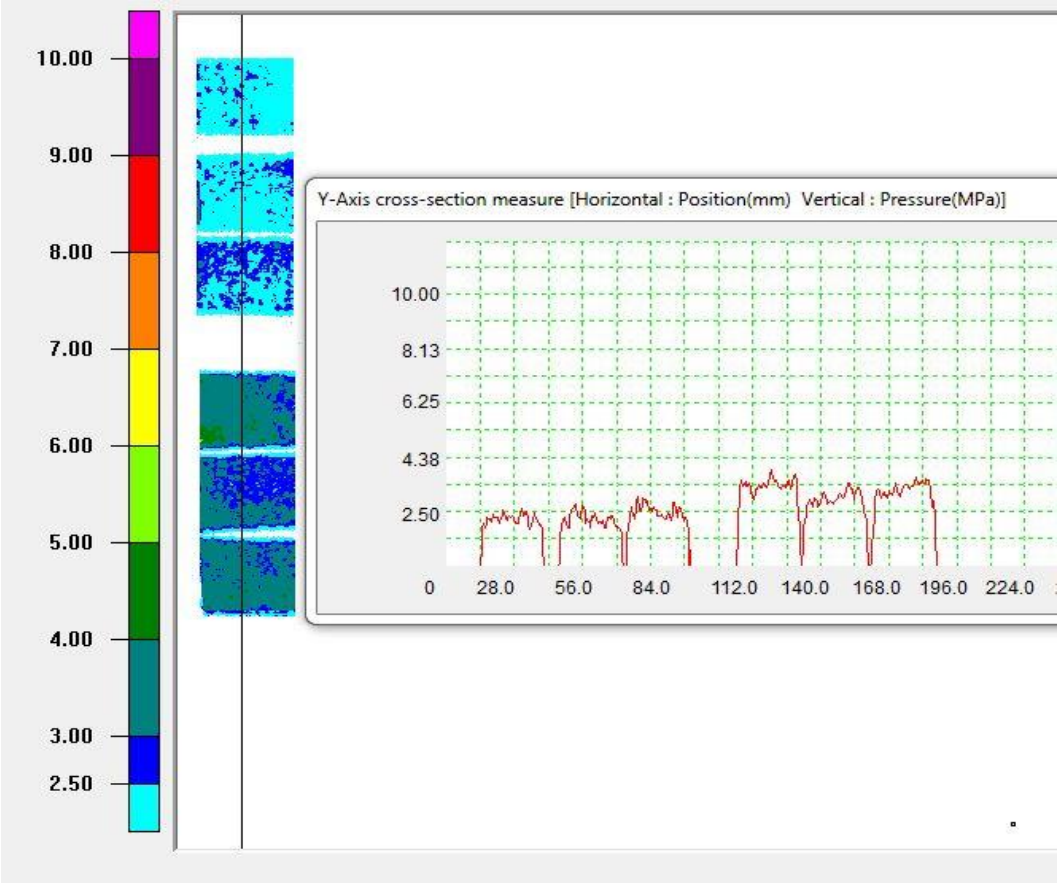

Figure 41: Contact Pressure Distribution for two strain rates

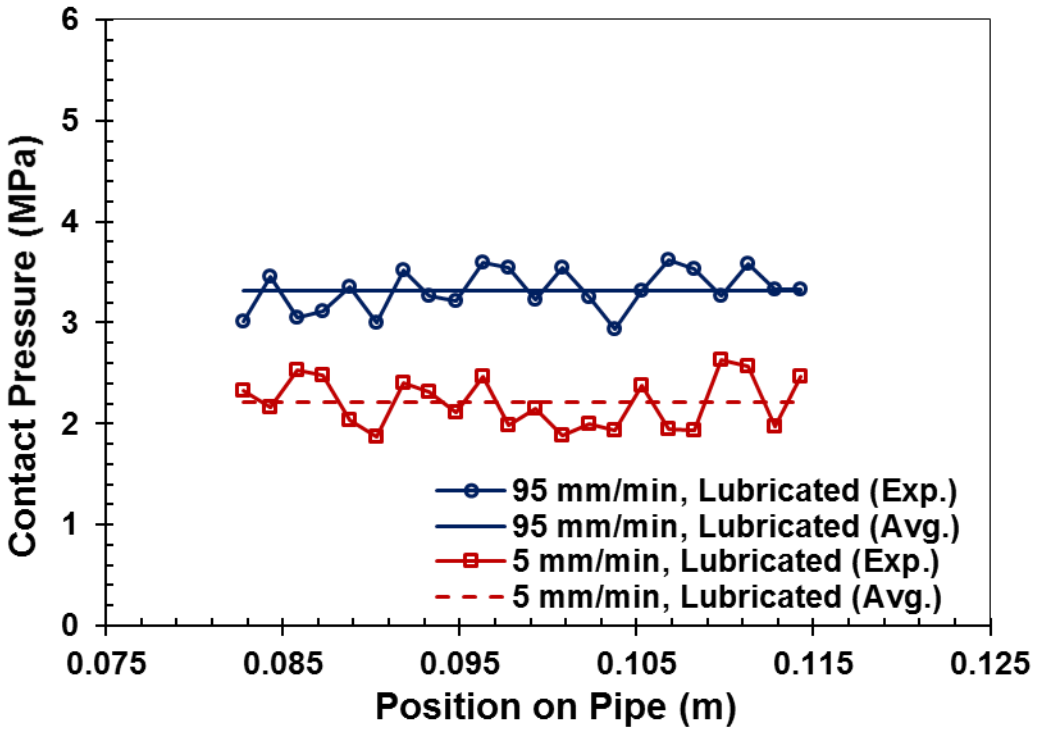

Figure 42: Contact Pressure Distribution for two strain rates along the position on pipe

4.5 Strain Gradients on the Pipe's wall

Seal compression test in constrained condition was performed with different sizes of steel pipe (Thin wall and Intermediate wall). Different sizes seals were used for different sizes pipes. Strain-imposed on the pipe due to sealing actions under uniaxial compression. Uniaxial strain gauges and strain gauge chains were used to measure the hoop strain distribution on the pipe. Each uniaxial strain gauge in the chains was mounted in the hoop direction on the pipe and connected to the data acquisition system's individual channel for recording data during compression test in constrained condition. The hoop strain data was recorded for both rough and lubricated contact surfaces at two strain rates. The strain gradients were recorded and displayed in the data acquisition system as soon as the seal got contact in the pipe's inner wall. The gauges which were mounted in the middle of the sealing area were shown higher strain.

4.5.1 Pipe with Thin Wall Thickness

The uniaxial seal compression test with thin wall pipe was done with single seal and stack seal. The selected seal outer diameter was 102.5 mm for the compression test with thin wall pipe. The radial clearance between the seal and the inner pipe wall was 3.15 mm. The thickness of the pipe wall was 2.75 mm.

The hoop strain gradients for single seal is plotted as a function of position in the sealing area in Figure 43, for seals with rough and lubricated contact surfaces at 95 mm/min displacement rate and at 6 mm axial displacement. The hoop strain exhibited a parabolic variation, which was expected as the deformed shape of the rubber seal was parabolic. Lower strains magnitude was

recorded for lubricated case since the seal required less axial force to reach a certain axial strain after contacting the wall in the case of lubricated surfaces than the case of rough surface.

The maximum hoop strain on the pipe wall was recorded at the position corresponding to the mid-height of the seal since the maximum lateral expansion occurred at that position. The experiment was performed by controlling uniaxial displacement. Force was not controlled for multiaxial displacement after contact. Therefore, higher compressive force was developed due to higher friction of contact surfaces as a consequence it developed higher strain on pipe. As anticipated, the maximum strain and the strain gradient were lower for the lubricated contact surface. A significant effect of strain rate on strain distribution was also observed due to viscoelasticity effect as shown in Figure 44. Higher strain magnitude was observed with higher strain rate.

Hoop strain distributions at three different axial displacements (6.0 mm, 5.5 mm and 5.0 mm) are compared in Figure 45 for the annular seal with rough and lubricated contact surface. The gradient in the hoop strain increased with axial strain. The peak hoop strain on the steel pipe was sensitive to the strain applied to the seal. For example, the peak hoop strain increased by 233% with the increasing of the axial strain by only 3.18% in the rough contact surface.

In other words, the peak hoop strain on the pipe wall linearly increased with the applied axial compressive force on the seal as shown in Figure 46. The data is shown from the initiation of contact with the pipe wall up to 6.0 mm axial displacement for seals with rough and lubricated contact surfaces. Since the seal made earlier contact with the pipe wall in lubricated contact surface than the rough contact surface, less compressive force was required in the lubricated case to reach the same pipe wall strain at the time of contact initiation.

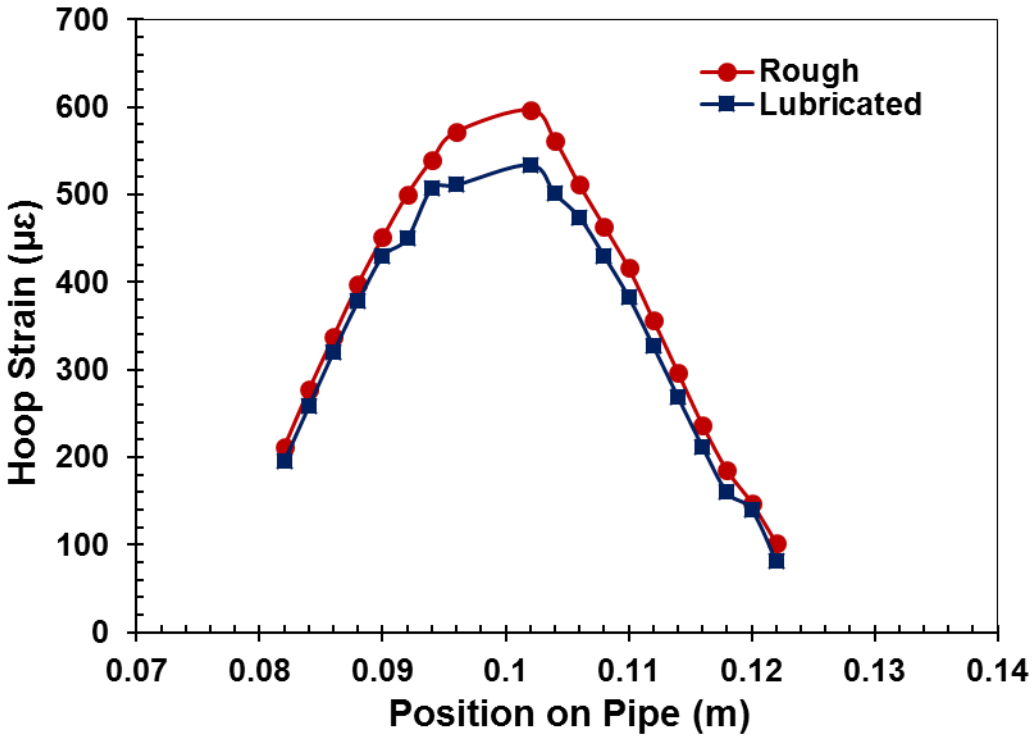

Figure 43: Variation of hoop strain on the pipe wall with position for rough and lubricated contact surfaces between the seal and the steel ring at 6.0 mm axial displacement

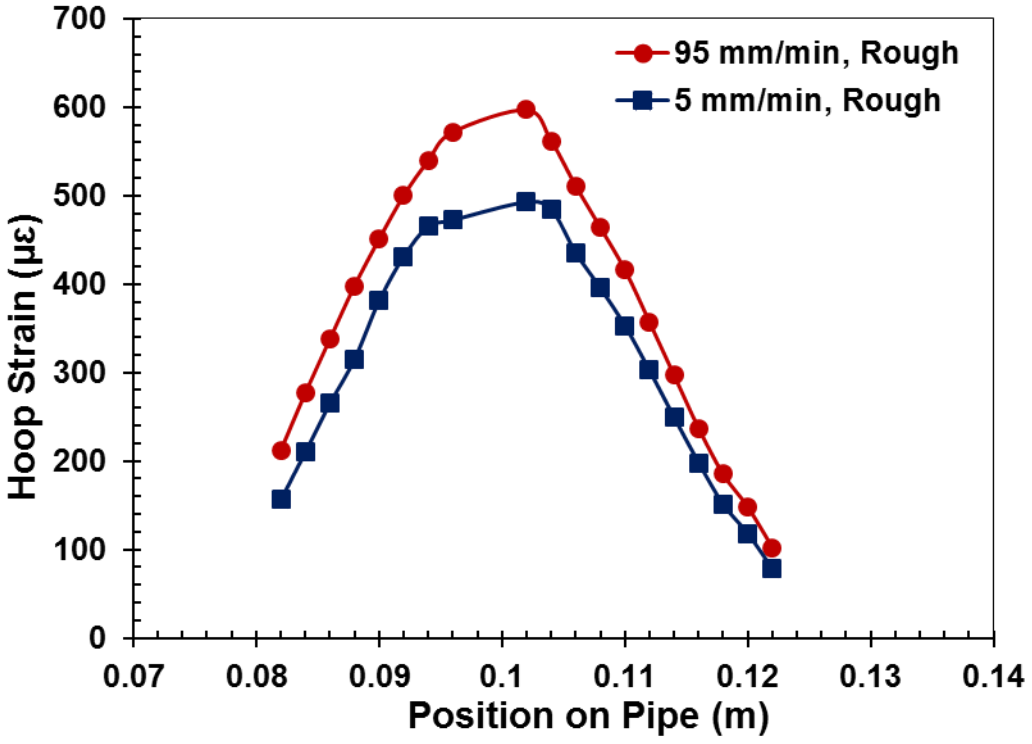

(a)

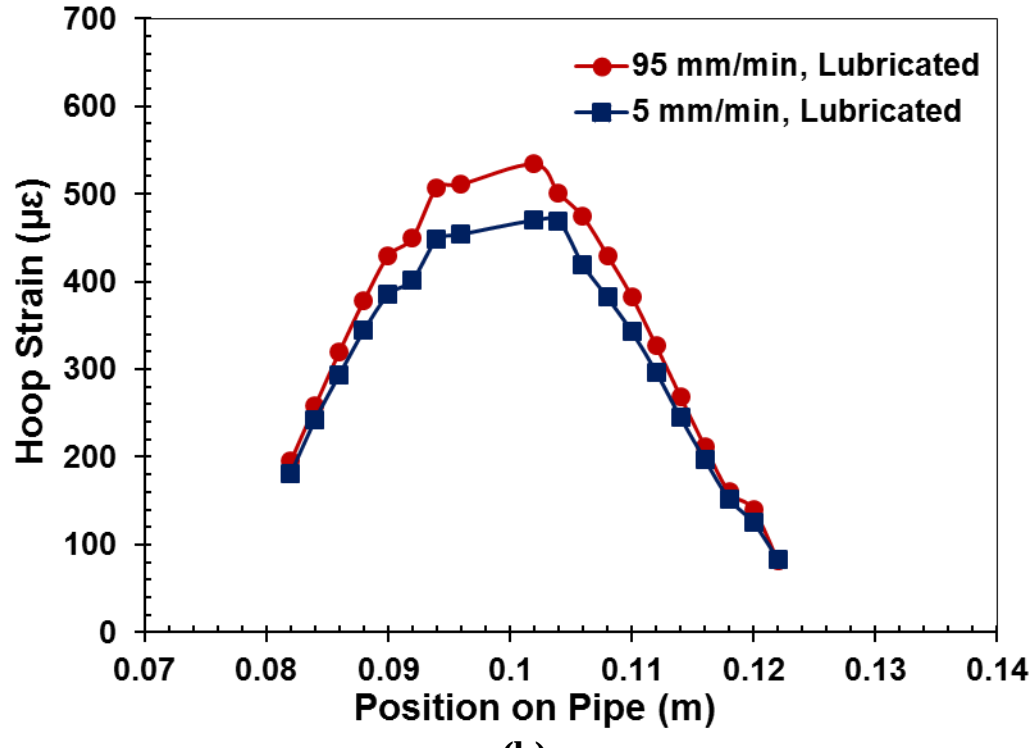

(b)

Figure 44: Comparison of hoop strain distribution on the pipe wall with position on pipe for strain rates at 6.0 mm axial displacement for (a) Rough and (b) Lubricated contact surfaces

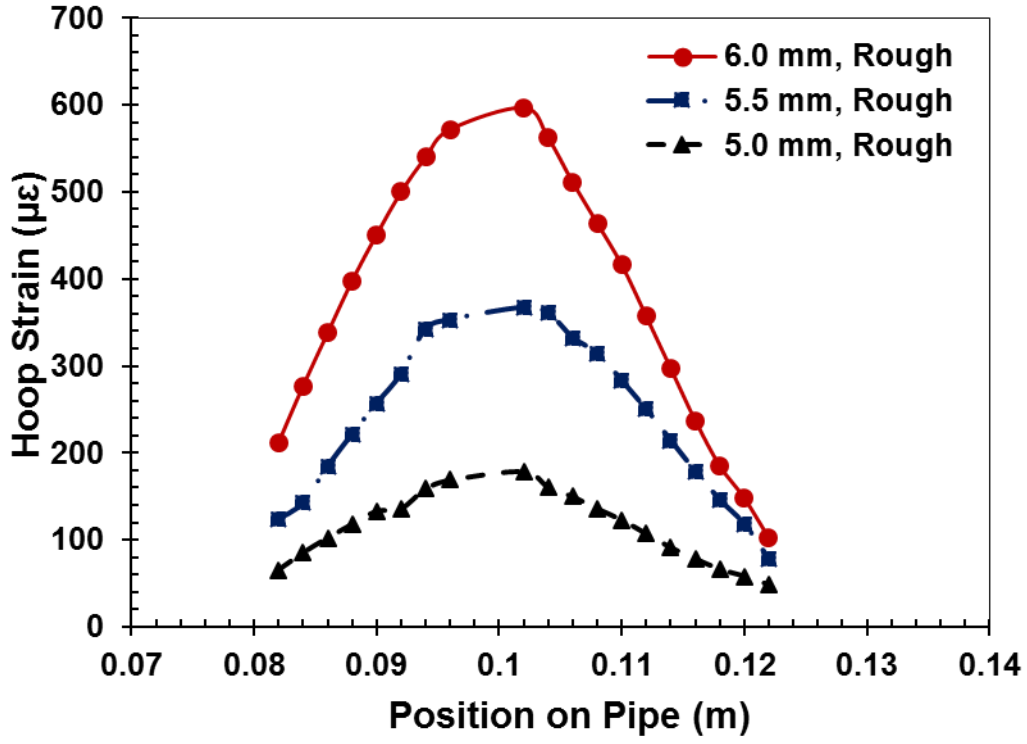

(a)

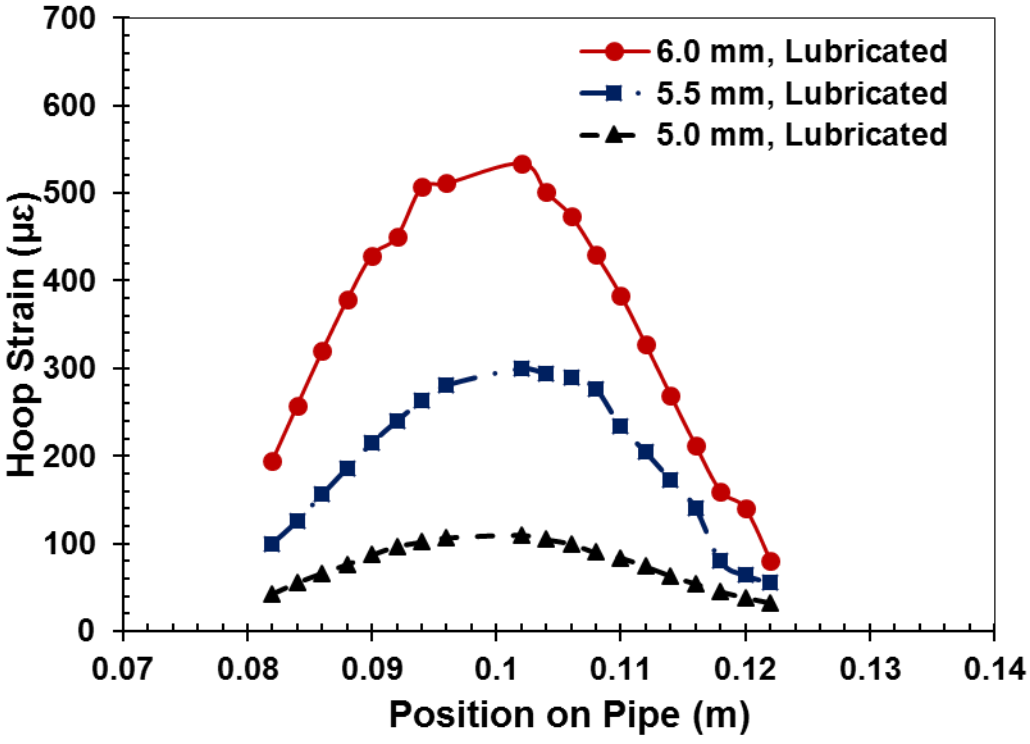

(b)

Figure 45: Comparison of hoop strain distributions for different axial displacement (6.0 mm, 5.5 mm & 5.0 mm) for (a) Rough and (b) Lubricated contact surfaces

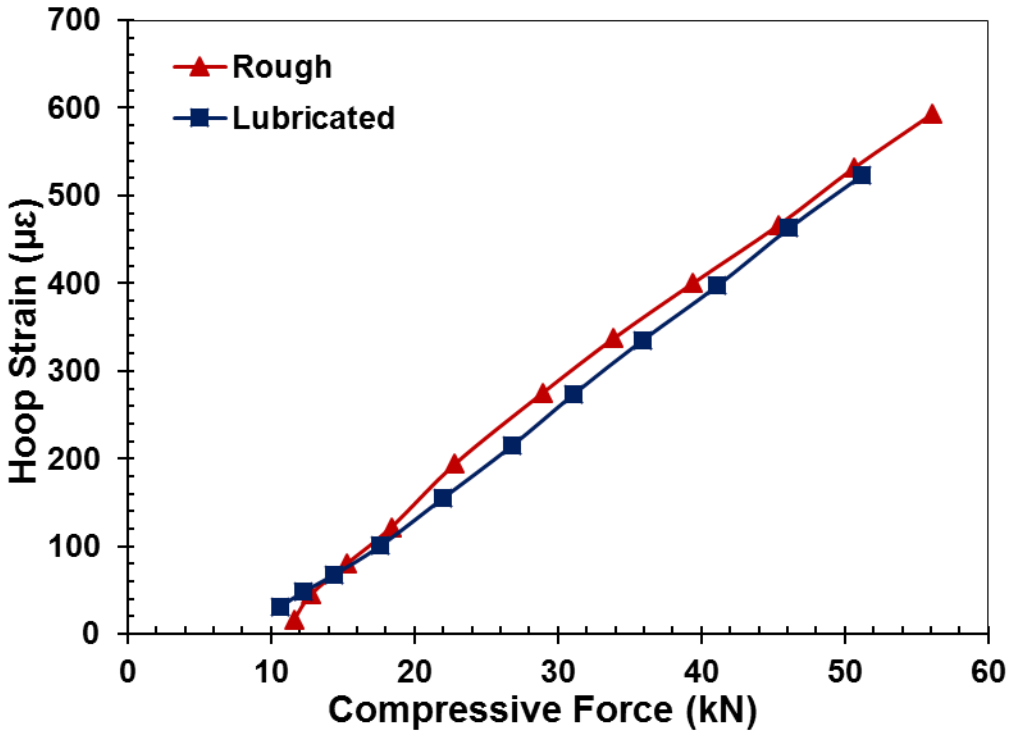

Figure 46: Hoop strain - Compressive force in both rough and lubricated contact surface

Stacked seals were tested in constrained condition upto16.67% of axial strain (at 10.5 mm axial displacement). The outer diameter of the stack seal was 102.5 mm. Single seal with same outer diameter was also tested to compare the strain distributions on the pipe wall at the same axial strain (16.67%) and same radial clearance between the seal and the pipe. It was found that the hoop strain gradient for stack seal was higher than for the single seal as shown in Figure 47. It should be noted that while the strain gauge chain covered the height of one seal, it covered only one half the height of the stacked seal. Hence, the only half of the strain distribution is shown in Figure 47 for the stacked seal.

Shape factor (0.22) of the stacked seal was lower than the shape factor (0.44) of the single seal. Results discussed in the previous sections have established that the apparent compressive modulus of seals increases with the shape factor. Since the test was conducted at the same axial strain, therefore, the axial compressive force was more as shown in Figure 34 for stacked seal than single seal despite lower apparent modulus. Moreover, the required force for initiation of contact with stack seal was lower than the required force for initiation of contact with single seal as shown in Figure 34. Therefore, the additional force for stack seal after contact initiation was more than the additional force for single seal after contact initiation. As a result, higher pipe strain was developed for stacked seal than the strain for single seal.

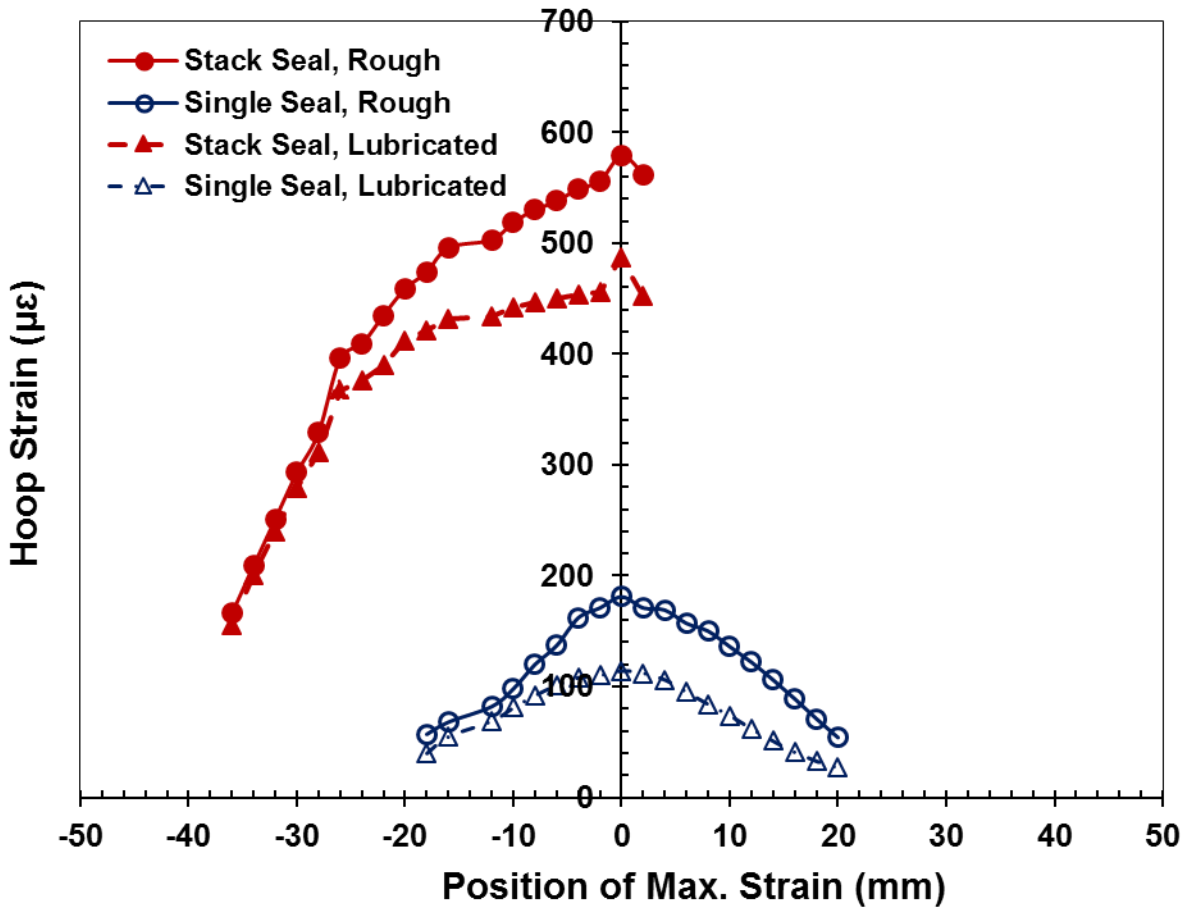

Figure 47: Comparison of hoop strain distribution on the pipe wall with position on pipe with stack and single seal at same axial strain in both Rough and lubricated contact surfaces

4.5.2 Pipe with Intermediate Wall Thickness

Different wall thickness pipes are used in the sealing application. Therefore, the seal compression test was also conducted with intermediate wall thicknesses pipe to observe the strain gradients. The thickness of the intermediate wall pipe was higher than the thickness of thin wall pipe.

The uniaxial compression testing of seals constrained in pipe with intermediate wall thickness (referred as intermediate wall pipe in this section) was performed in single and stacked seal configuration. For intermediate wall pipe, the outer diameter of the seal was selected to be 96.3 mm. The radial clearance was 3.05 mm in between the seal and the pipe in both single and stacked seal compression tests. The thickness of the pipe wall was 5.95 mm.

Instead of strain gauge chain which was used for thin wall pipe, uniaxial strain gauge was used for the intermediate wall pipe which took more space. Due to shortage of strain gauge on the pipe along the sealing area, incomplete parabolic distribution was observed. However, similar to the thin wall pipe, hoop strain distribution on the intermediate wall pipe increased with higher frictional contact surfaces and strain rates. The hoop strain distributions on the intermediate wall pipe are shown in Figure 48 for axial compression of a single seal, with rough and lubricated contact surface conditions. Results obtained at two strain rates are presented in Figure 49. Due to the higher wall thickness of the intermediate wall pipe, maximum strain, and strain distribution was lower for intermediate wall pipe compares to the thin wall pipe at the same axial strain applied to the seal though the radial clearance was lower for intermediate wall pipe.

Stack seal with 96.3 mm outer diameter was tested in constrained condition up to 16.67% of axial strain. Single seal with same outer diameter was also tested to compare the strain distributions on

the pipe wall at the same axial strain (16.67%) and same radial clearance (3.05 mm) in between the seal and the pipe.

Shape factor (0.19) of the stacked seal was lower than the shape factor (0.39) of the single seal for 96.3 mm outer diameter. Similar relation in between the shape factor and pipe strain for thin wall pipe was also observed for intermediate wall pipe. Since the compression test was conducted at the same axial strain (16.67%), then, the axial displacement in case of stacked seal (10.5mm) was twice that for the single seal (5.25 mm) at 16.67% strain and thus, the pipe strain for stacked seal was more than single seal as shown in Figure 50.

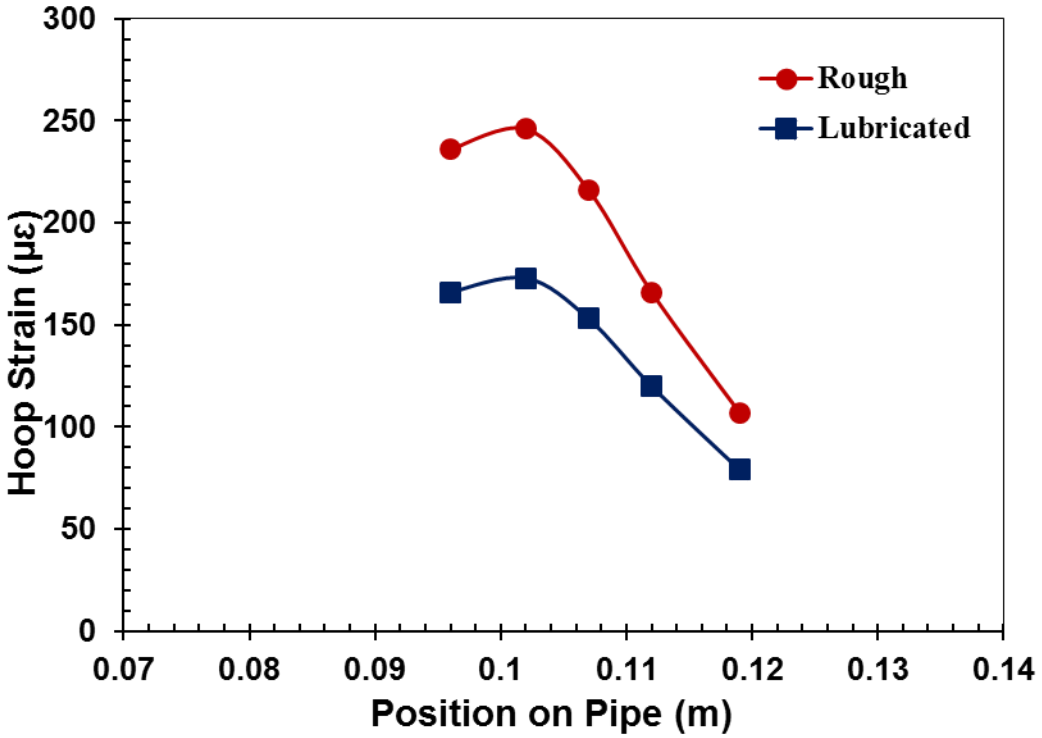

Figure 48: Variation of hoop strain on the pipe wall with position for rough and lubricated contact surfaces between the seal and the steel ring at 6.0 mm axial displacement

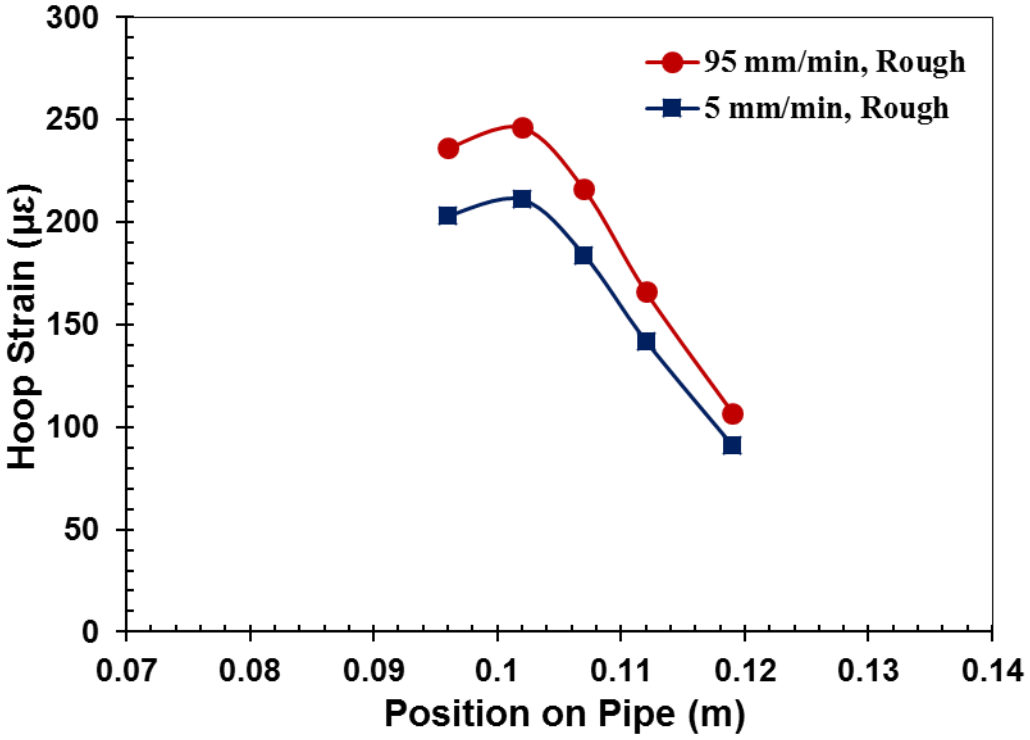

(a)

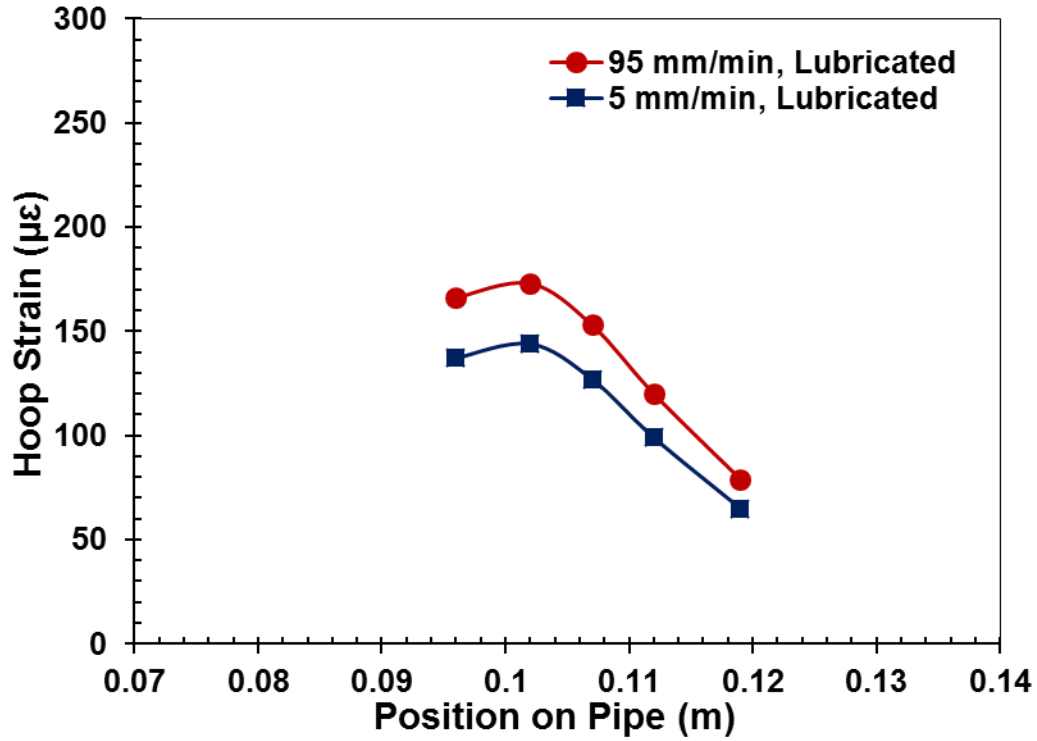

(b)

Figure 49: Comparison of hoop strain distribution on the pipe wall with position on pipe for strain rates at 6.0 mm axial displacement for (a) Rough and (b) lubricated contact surfaces

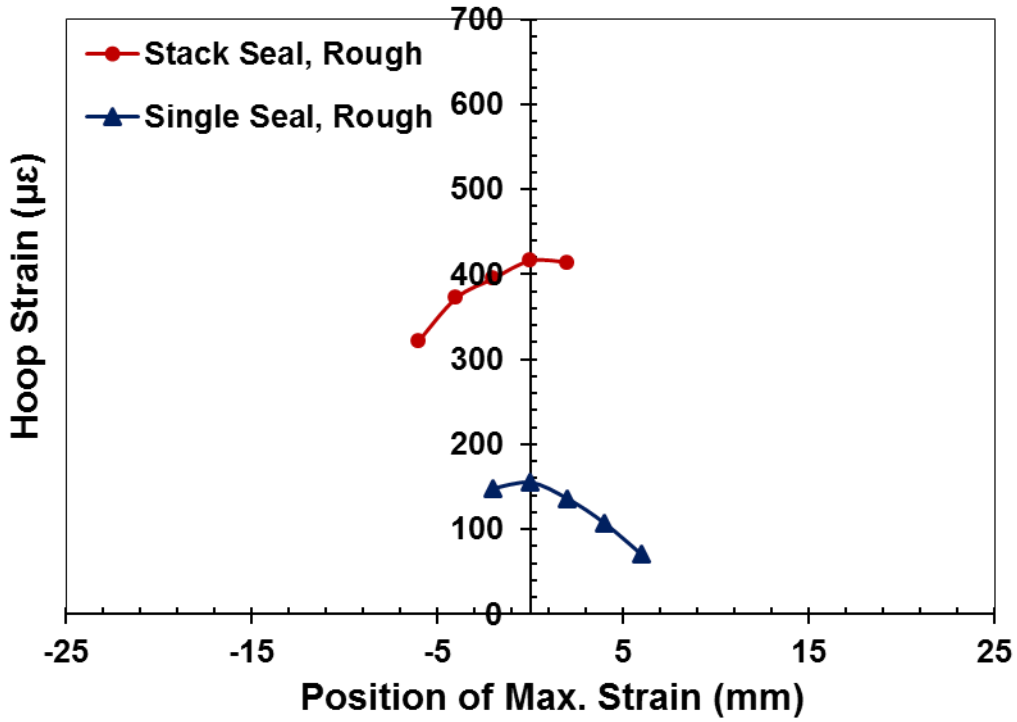

Figure 50: Comparison of hoop strain distribution on the pipe wall with position on pipe with stack and single seal at same axial strain in both Rough contact surfaces

4.5.3 Summary of Experimental Results

Results presented in the previous section indicate that

(a) Lateral expansion of the seals in response to axial compressive load is restricted by the constraint applied through the compression steel rings and the magnitude of this constraint increases with magnitude of friction of the interface between the seal and the compression rings and seal's shape factor.

(b) Due to this, the apparent compressive modulus of the unconstrained seal increases with friction and shape factor.

(c) Due to (a) and (b), the contact pressure and the hoop strain on the pipe wall increase with friction and shape factor, for a given axial displacement and gap between the seal and the pipe wall.

(d) Due to visco-elasticity of the elastomer used in manufacturing the seal, the contact pressure and hoop strain increases with increases with strain rate, when all other parameters are maintained constant.

The effect of shape factor on apparent modulus that controls the lateral expansion has been studied over a very small range due to experimental limitations. In real life, the seals with shape factors beyond this range could be used. Hence, FEM analysis of compressive behavior of unconstrained seal with shape factors beyond the experimental range was studied and presented in 4.6.

4.5.4 Comparison of Experimental Pipe Strain with Prediction

Using the experimental contact pressure, the hoop strain gradients on the pipe wall were predicted using the Roark's empirical equations (12-25), in Chapter 3 [8]. Experimental strain gradients on the pipe's wall compared very well with the theoretical predictions (within 10%) as shown in Figure 51, for two strain rates and surface conditions. Since input of accurate values of contact pressure is key to the success of Roark's formula, further research is required to model the lateral expansion as a function of various factors presented in the previous section.

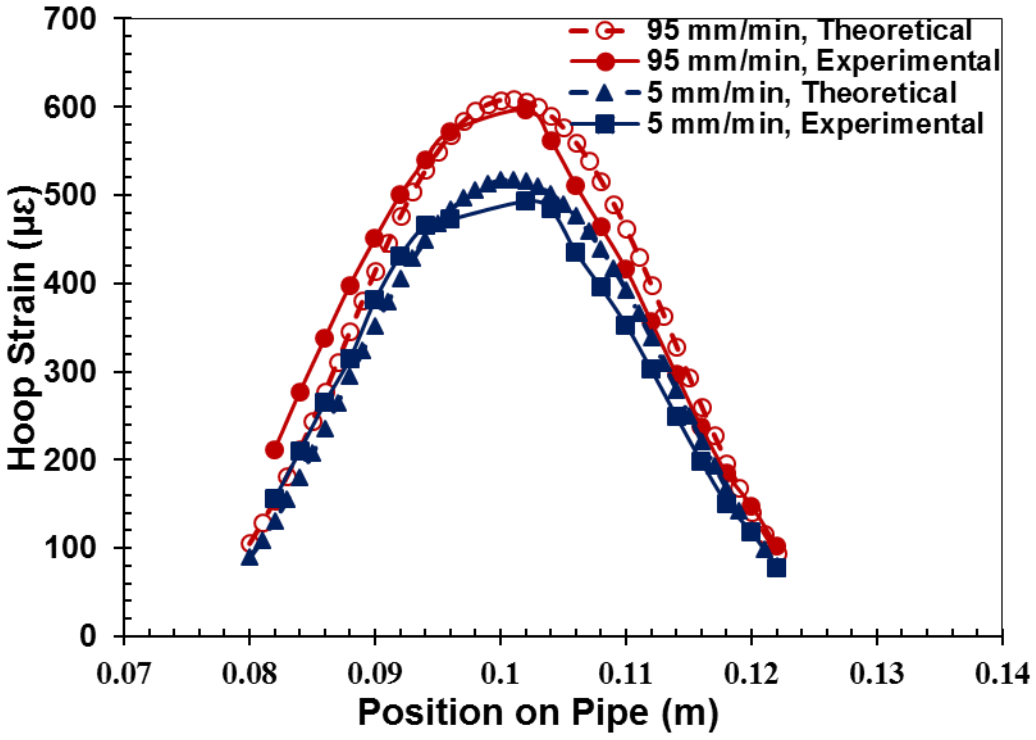

(a)

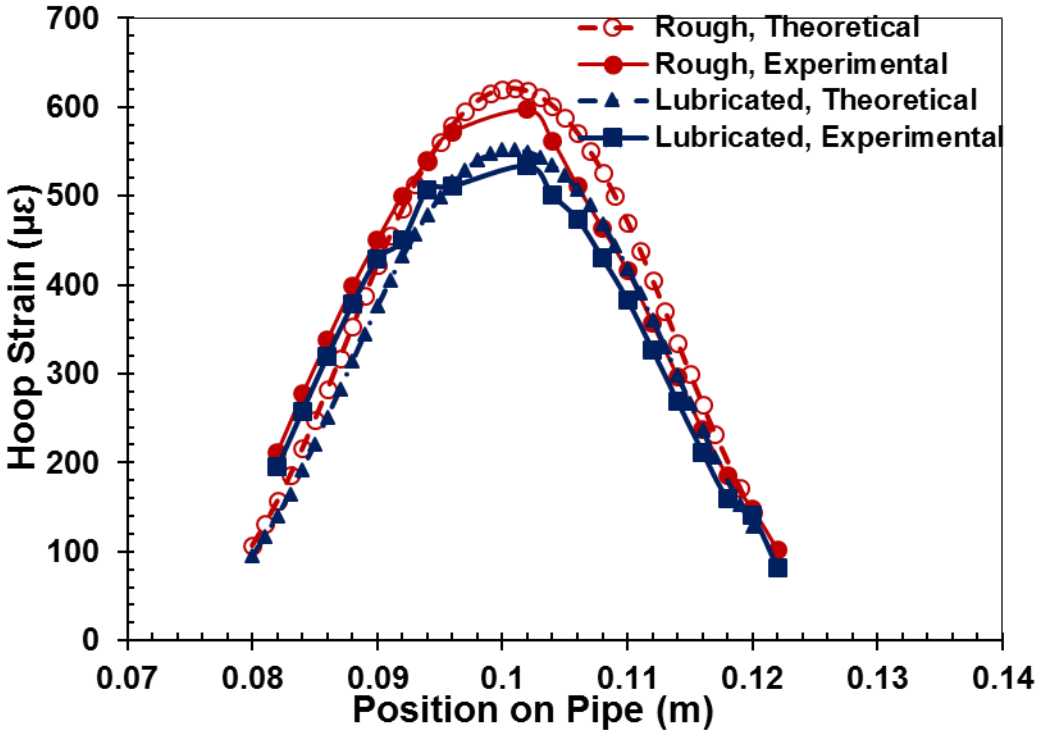

(b)

Figure 51: Comparison of experimental and predicted strain gradients on the pipe wall along the sealing area for (a) surface conditions and (b) strain rates at 6mm axial displacement

4.6 Finite Element Analysis

Knowing the large effect of shape factor or geometry on the pipe strain due to sealing, finite element analysis was conducted for a wide range of shape factors of rubber blocks to explore the effect of shape factors on the apparent compressive modulus for different frictional contact surfaces. The primary intension of this FEM analysis was to explore the effect of shape factors (geometry) on the apparent compressive modulus of the annular rubber seal for different frictional contact surfaces since different sizes seals are used in the industry for sealing applications. Firstly, the parametric study was done for the solid blocks and then it was extended to annular rubber seal for a wide range of shape factors (from 0.1 to 100) in both bonded and rigid frictional contact surfaces.

4.6.1 Solid Rubber Block

The FEM simulation was performed for the solid rubber block with bonded and rigid frictional surfaces and the results are compared with predictions using a model developed by Gent *et al.* [4][5]. The shape factor was changed from 0.1 to 100 by changing the outer diameter of the solid block while the thickness (31.5 mm) was kept constant.

4.6.1.1 Solid Bonded Blocks

The apparent compressive modulus of bonded solid blocks determined using FEA is compared with the values determined using Gent et al.'s model [4] in Figure 52 for a wide range of shape factor (0.1 to 100). FEM predictions compare very well with the predictions using equation (4) in Chapter 3 at low shape factors, however, deviate at higher shape factors. However, this equation does not take into account the bulk compressive deformation of a major portion of the seal at

higher shape factors. Equation (11) in Chapter 3 was developed by Gent *et al.*[4] by extending the equation (4) using bulk modulus. The predicted modulus using this modified empirical equation (11) showed better agreement with the FEA results.

Another assumption used by Gent *et al*. in deriving their theoretical model to derive equation (4) is that the pressure through the thickness of the rubber block under compression is constant. The predictions of pressure using FEM plotted as a function of thickness of the solid block as shown in Figure 53 suggests that this assumption made by Gent *et al.* is not correct.

The radial deformed shape predicted by FEA followed a parabolic shape and compared well with predicted deformed shape of solid bonded blocks according to equation (6) in chapter 3 was developed by gent *et al.*[4] as shown in Figure 54 for lower shape factors. The theoretical predictions for deformed shape deviated from the deformed shape from FEA at higher shape factor. While incompressibility assumption was considered to derive equation (6), the elastomer properties used in FEA is for compressible material. This might be the reason for this discrepancy.

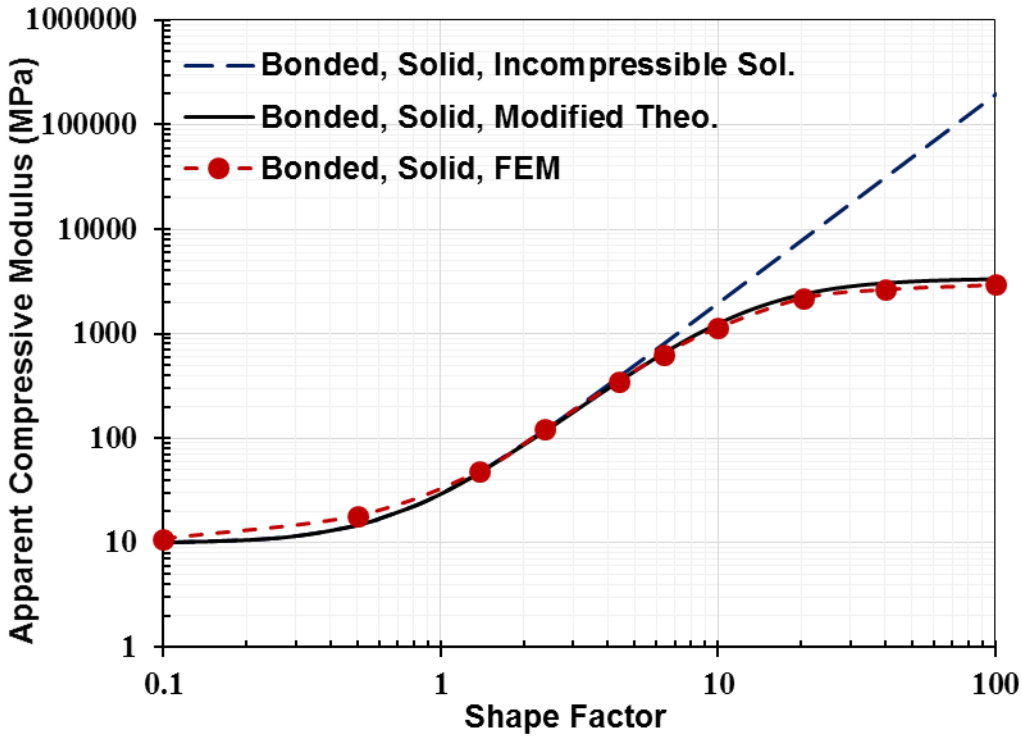

Figure 52: Comparison of theoretical predicted apparent compressive modulus - shape factor curve with FEA results for solid bonded block

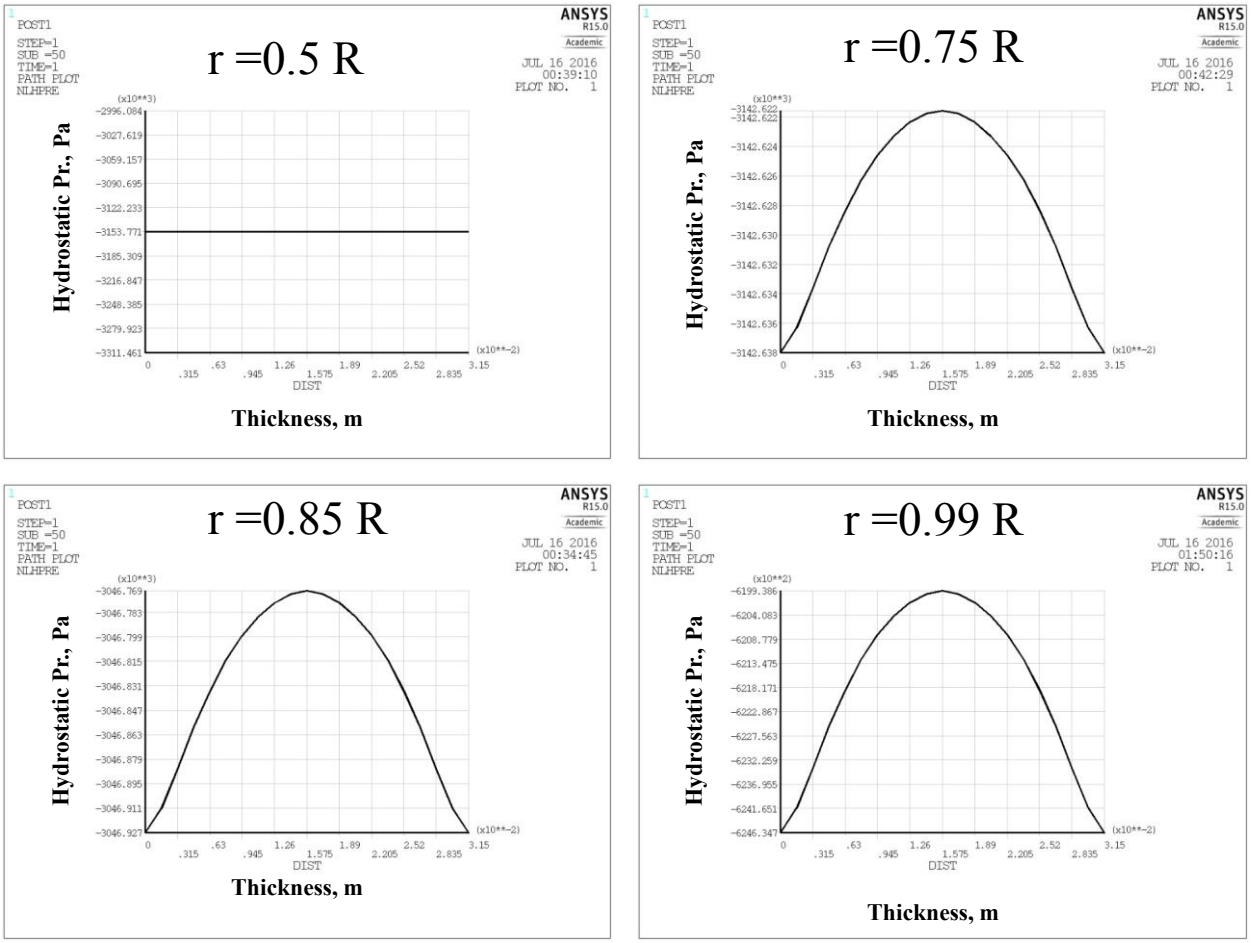

Figure 53: Hydrostatic Pressure along the thickness at different radial distance of the solid rubber block at shape factor (100)

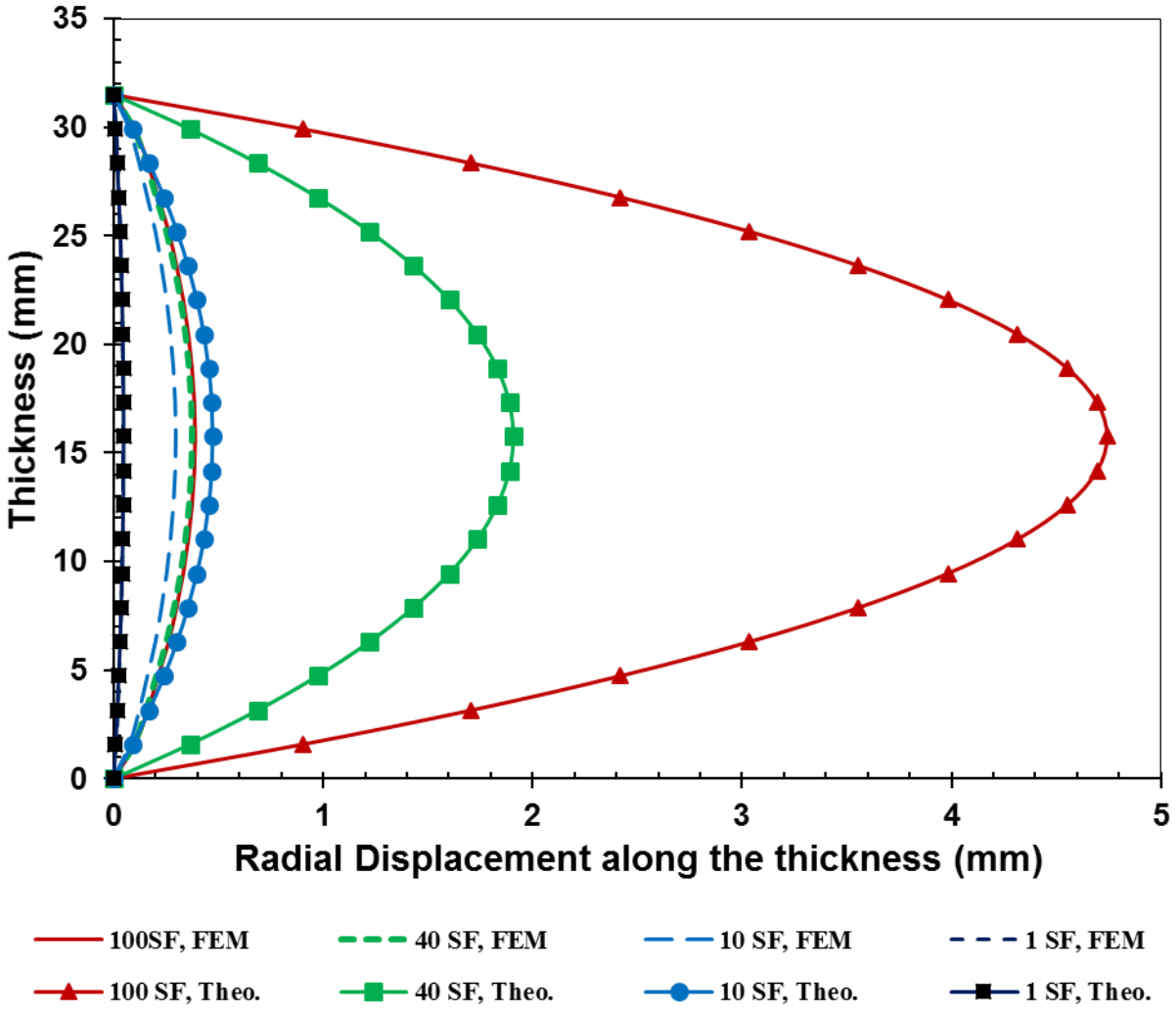

Figure 54: Comparison of theoretical and FEM deformed shape along the thickness of the solid bonded blocks for different shape factors (1, 4, 10, 40 and 100)

4.6.1.2 Solid Block with Rigid Frictional Contact Surfaces

The FEM analysis was then conducted for solid blocks with different rigid frictional contact surfaces.

4.6.1.2.1 Apparent Compressive Modulus

The apparent compressive modulus of solid blocks predicted using FEA is plotted in Figure 55 as a function of shape factor for different frictional coefficients for the interface between the seal and the compression platen. For a given shape factor, the modulus increased with friction coefficient. The effect of friction coefficient was observed significant at intermediate shape factors (1-30).

The apparent compressive modulus of solid blocks predicted by FEA is compared with the theoretical predictions using the equations (8-10) in chapter 3 developed by Gent *et al.* [5].as shown in Figure 56. The FEA results compare reasonably well with theoretical predictions for shape factors less than 10. The possible reasons for this discrepancy at higher shape factors are the assumptions made by Gent *et al*. [4]while developing the equations.

According to the FEM results as shown in Figure 55, when the friction coefficient is between 0.05 and 0.8, the apparent compressive modulus increased in a different way with the shape factor in three ranges. At lower range of shape factors ($0.1 \leq SF \leq 1$), the apparent compressive modulus increased gradually. On the other hand, the variation of apparent compressive modulus at an intermediate range of shape factors ($1 \leq SF \leq 30$) was increased abruptly compare to the apparent compressive modulus at the lower range of shape factors. However, at the higher range of shape factor ($30 \leq SF \leq 100$), the apparent modulus reached a plateau value with small increments.

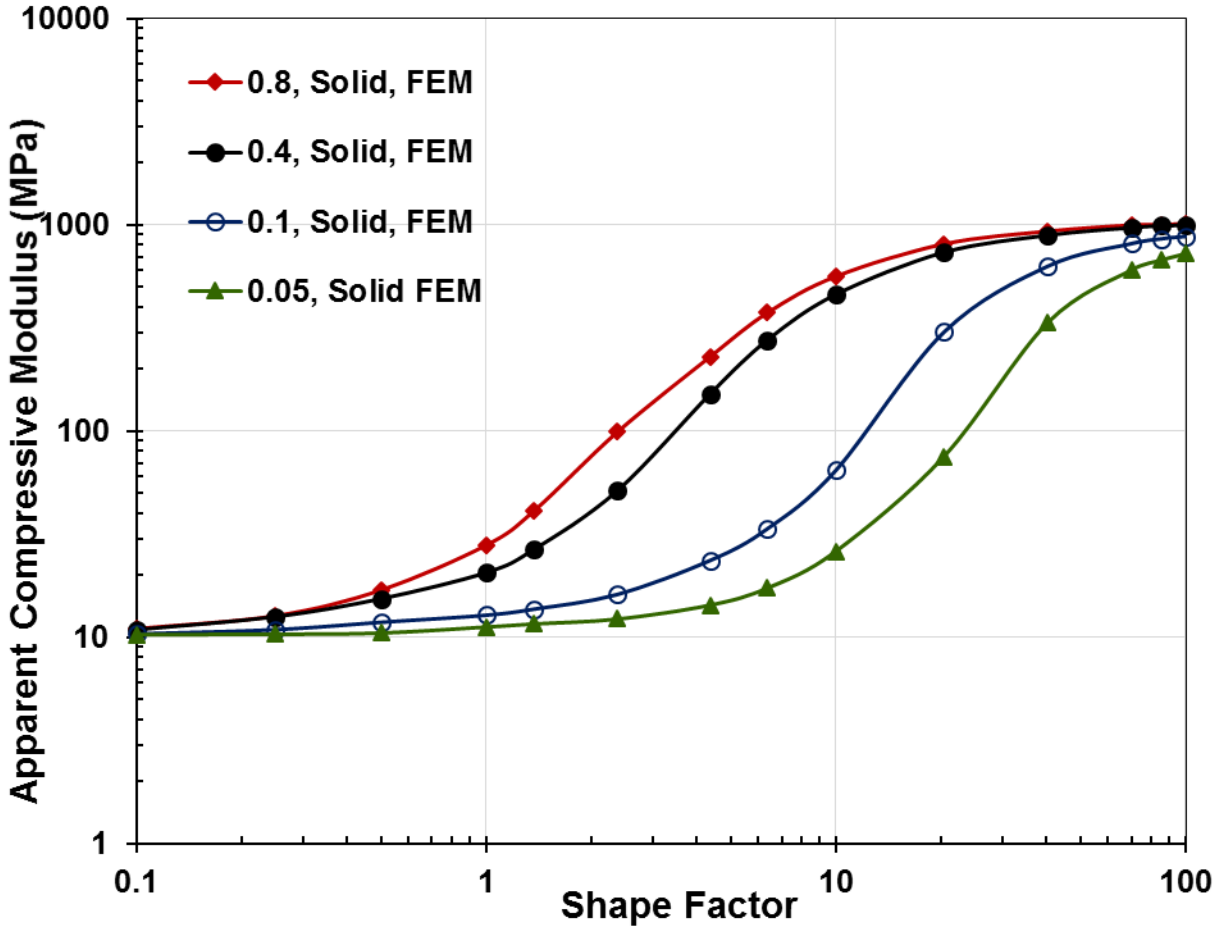

Figure 55: Apparent compressive modulus - shape factor for solid block with rigid frictional surfaces

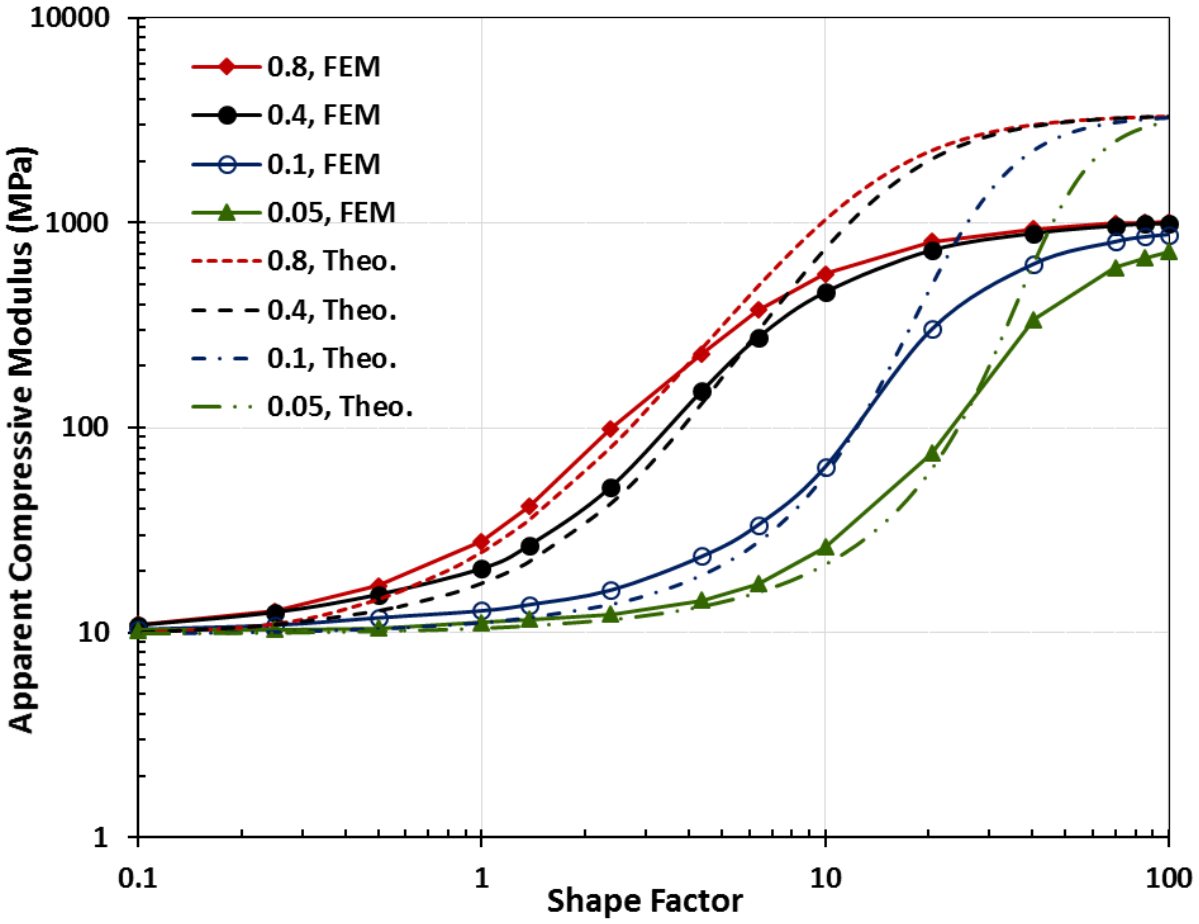

Figure 56: Comparison of theoretical predicted apparent compressive modulus - shape factor curve with FEA results for solid block with rigid frictional surfaces

4.6.1.2.2 Contact Status

Here, the contact status of the solid rubber block was analyzed to understand the reason for the shape of the curves in Figure 55. Contact status means the amount of sticking and sliding areas on the rubber block under compression. The size of the non-slip or sticking zone for solid block with a shape factor of 10, is shown in Figure 57 and Figure 58 for friction coefficients of 0.8 and 0.05, respectively. Here, the sliding area was minimum for 0.8 and maximum for 0.05 Thus, significant differences in the sticking volume due to variation in friction coefficients is the reason for rapid increase in apparent compressive modulus for shape factors in the range of 1-30.

The sliding and sticking zone, for seals with a shape factor of 100 is plotted in Figure 59 and Figure 60 for friction coefficients of 0.8 and 0.05, respectively. The amount of sticking zone for lower (0.05) and higher (0.8) friction coefficients did not vary significantly and is believed to be the reason for least difference in modulus for various friction coefficients

On the other hand for small shape factor (0.5), the sticking area varied significantly from lower (0.05) to higher (0.8) friction coefficients as shown in Figure 61 and Figure 62 respectively. For smaller shape factors of the solid rubber block, the apparent compressive modulus changes at a lower rate with respect to a change in friction coefficient (i.e. it is less sensitive). The proportionality between the area of sticking and sliding zones do not greatly affect the change in the apparent compressive modulus as compared to the converse behavior at larger shape factors.

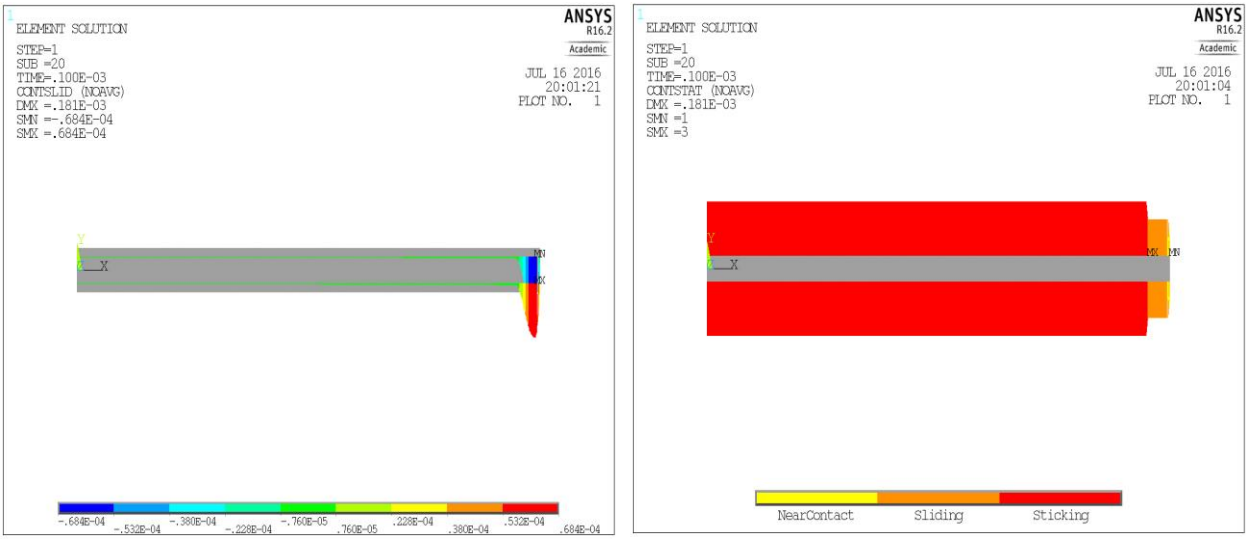

(a) (b)

Figure 57: (a) Contact Sliding Distance (b) Sticking and sliding zone at 0.8 friction coefficient for intermediate shape factor (10)

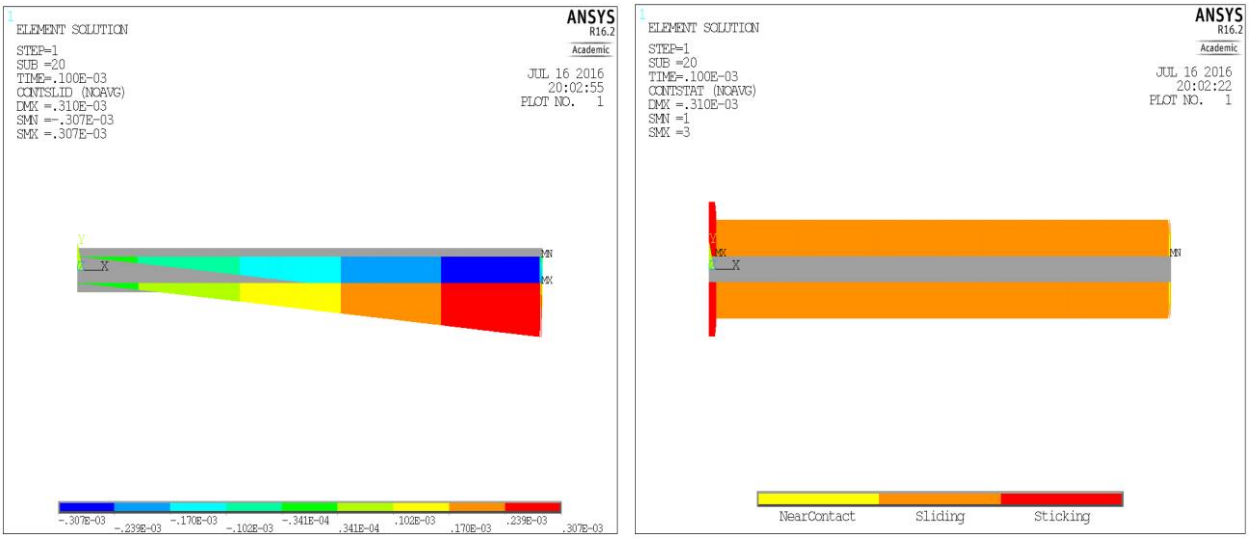

(a) (b)

Figure 58: (a) Contact Sliding Distance (b) Sticking and sliding zone at 0.05 friction coefficient for intermediate shape factor (10)

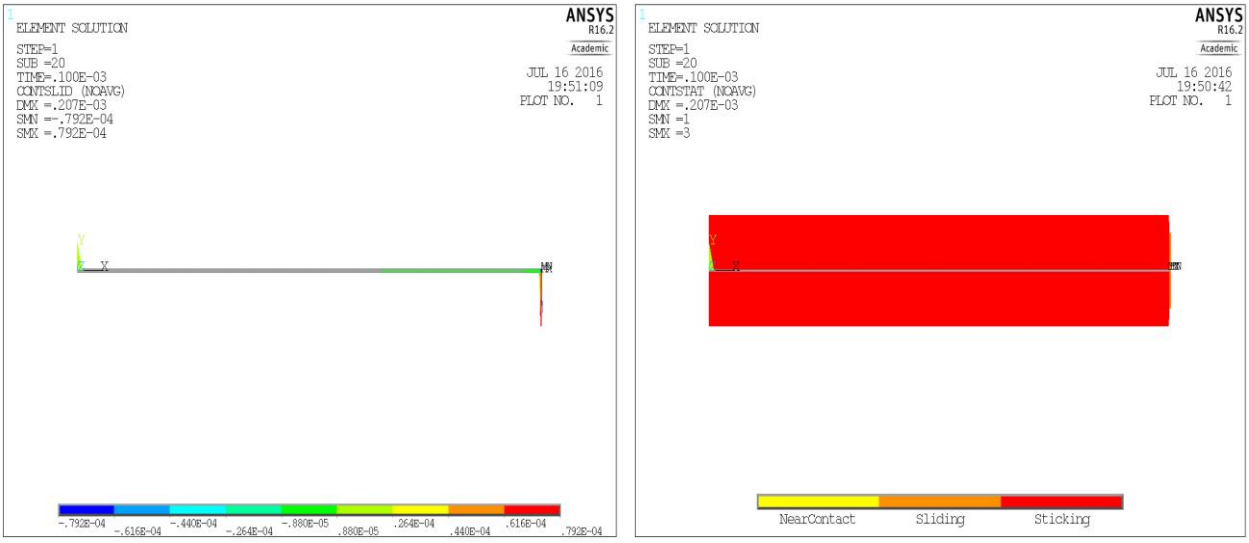

(a) (b)

Figure 59: (a) Contact Sliding Distance (b) Sticking and sliding zone at 0.8 friction coefficient for higher shape factor (100)

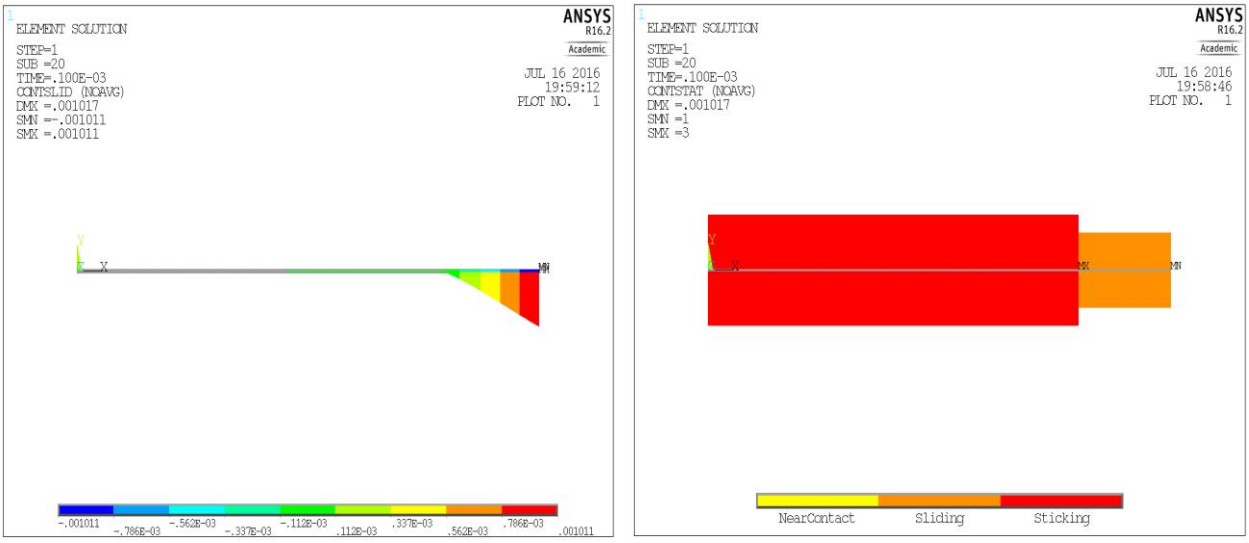

(a) (b)

Figure 60: (a) Contact Sliding Distance (b) Sticking and sliding zone at 0.05 friction coefficient for higher shape factor (100)

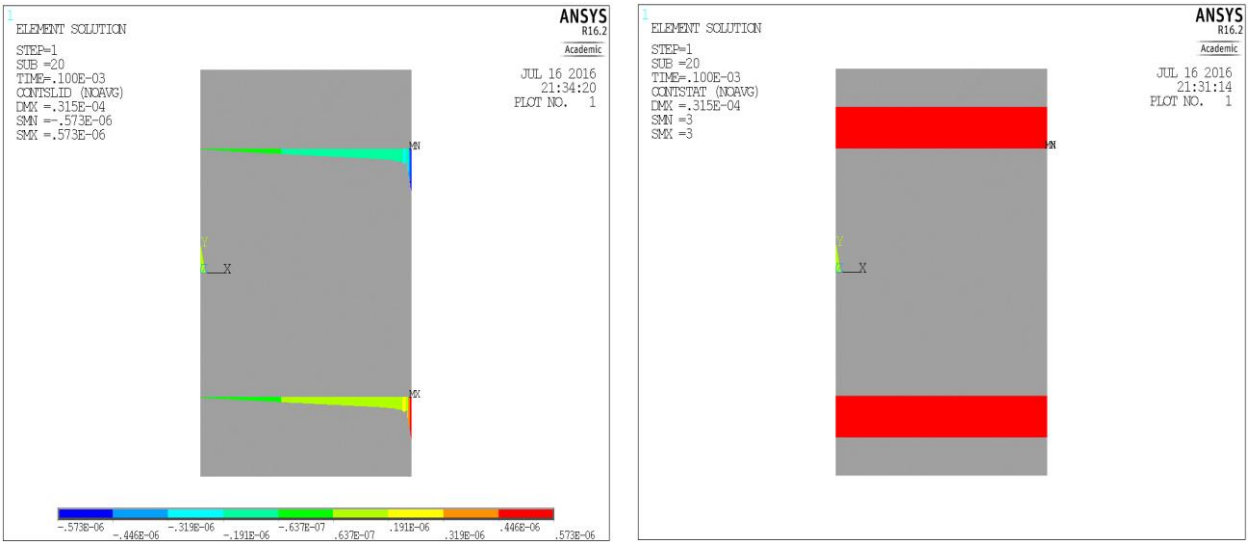

(a) (b)

Figure 61: (a) Contact Sliding Distance (b) Sticking and sliding zone at 0.8 friction coefficient for lower shape factor (0.5)

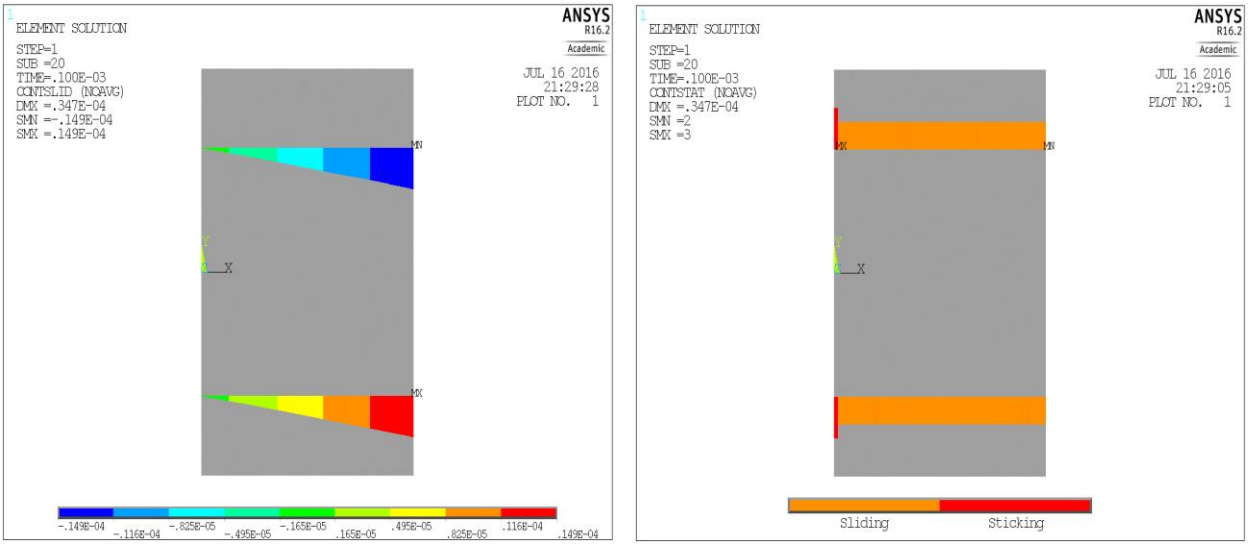

(a) (b)

Figure 62: (a) Contact Sliding Distance (b) Sticking and sliding zone at 0.05 friction coefficient for lower shape factor (0.5)

The apparent compressive modulus is plotted as function of - percentage of the sticking/non-slip zone in Figure 63 for different shape factors and frictional coefficients of solid blocks. Each line in this Figure is for one shape factor and four different frictional coefficients (0.05, 0.1, 0.4 and 0.8). The apparent modulus increased linearly with the percentage of the non-slip zone for each shape factor. It is observed that at higher friction (0.8), the apparent compressive modulus varied significantly with shape factor although the percentage of non-slip zone varied from approx. 80 to 100%.

In Figure 55, it is observed that the apparent compressive modulus increased significantly for intermediate values of shape factor (1 to 30) when the friction coefficient was increased from 0.05 to 0.8. The reason behind of this is the amount of sticking volume during uniaxial compression. For example, the percentage of sticking or non-slip zone, for a shape factor of 10, increased from 0.25% to 90.7% when the friction coefficient was increased from 0.05 to 0.8.as a result, the sticking volume also increased significantly.

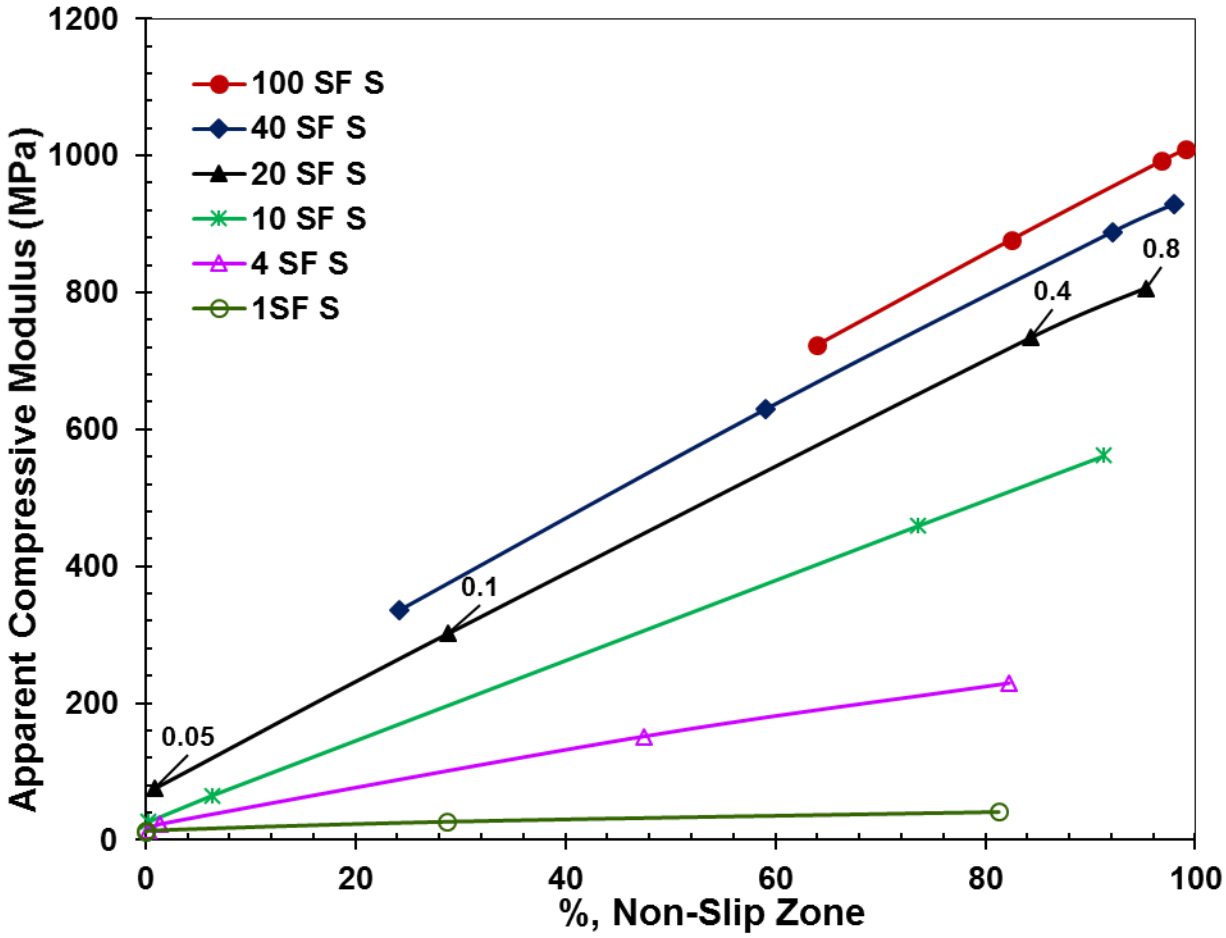

Figure 63: Apparent compressive modulus - % non-slip zone for various shape factor and frictional coefficients (0.05, 0.1, 0.4, and 0.8) of solid blocks

4.6.1.2.3 Deformed shape

The deformed shapes of the solid rubber blocks shown in Figure 64 were more parabolic at higher (0.8) friction coefficient whereas the deformed shape was uniform rather than parabolic for lower friction coefficient (0.1). Similar to the experimentally deformed shape in rough and lubricated frictional surfaces, the simulation results was more parabolic in rough contact surface than in lubricated contact surface. It was also observed that the deformed shape of the bonded annular block was more parabolic than that of the other rigid frictional surfaces. According to the radial displacement curve along the thickness, it is observed that the maximum radial displacement increased with increasing shape factor.

Elastic layer behavior along the thickness in bonded case is different than that of in the frictional case. In the deformed shape for different frictional coefficients and bonded case, the lateral displacement from the top/bottom side of the thickness to the mid-height of the thickness is high in bonded case comparing to other frictional cases. Moreover, the displacement of the block at the corner along the thickness was higher with lower friction constraints since more sliding was occurred at lower friction.

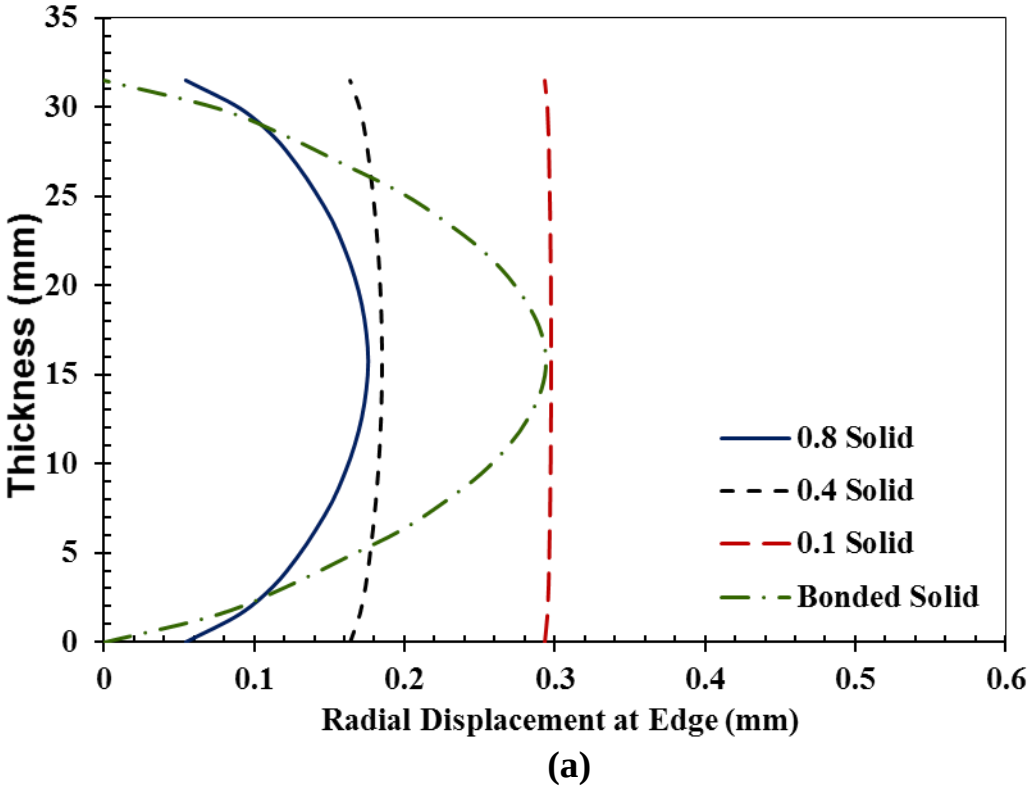

Figure 64: Radial displacement at edge along the thickness of the solid block at (a) shape factor (10) and (b) shape factor (100).

4.6.2 Annular Rubber Seal

After analyzing the compressive behavior of the solid rubber block, the finite element analysis was performed for the annular rubber seal in both bonded and frictional contact surfaces.

At first, the simulation results for annular rubber seal in both rough and lubricated contact surfaces were measured and compared with the experimental results. Later, the finite element analysis was extended to a wide range of shape factors with different friction coefficients to explore the effect of seal's shape factor on the apparent compressive modulus. The shape factor was changed from 0.1 to 100 by changing the outer diameter of the annular seal while the inner diameter (47 mm) and thickness (31.5 mm) were kept at fixed value.

The experimental compressive stress - strain curve was compared with the finite element compressive stress - strain curve as shown in Figure 65 for both rough and lubricated contact surfaces. Since the finite element model was developed from the same material properties of new annular seal material (OD: 102.5mm), therefore the experimental results matched well with the simulation results. On the other hand, the simulation results varied from the experimental results for another size seal (OD:73mm) is shown in Figure 66 as the material properties of this old seal were different due to aging or different chemical composition.

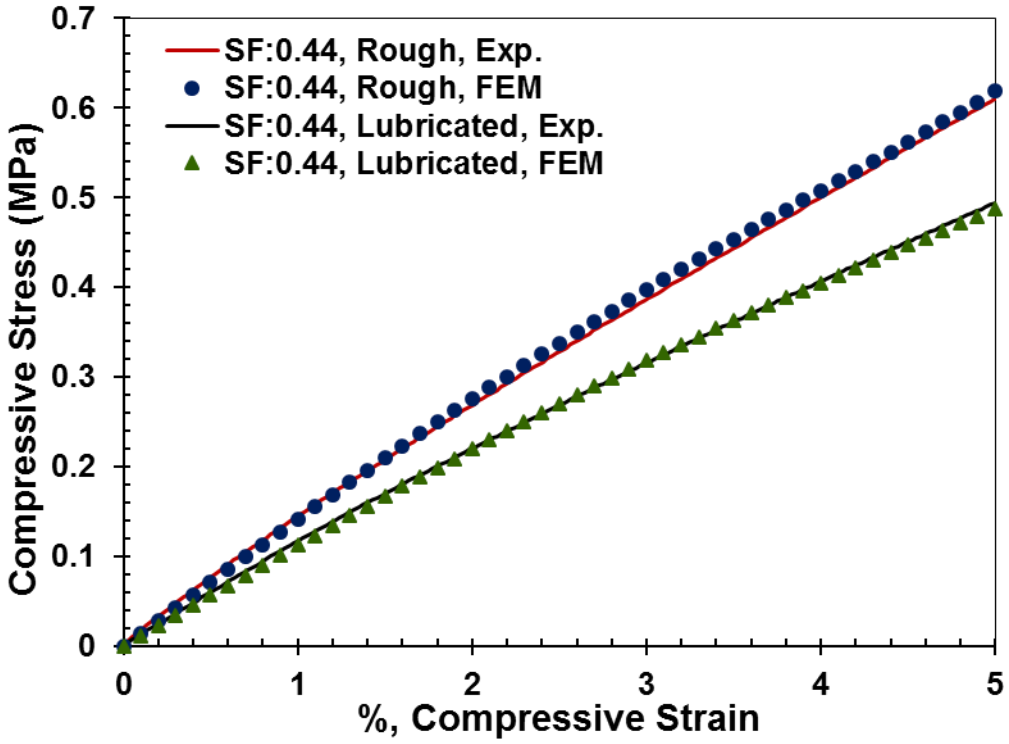

Figure 65: Comparison of experimental compressive stress - compressive strain curve with finite element compressive stress - compressive strain curve

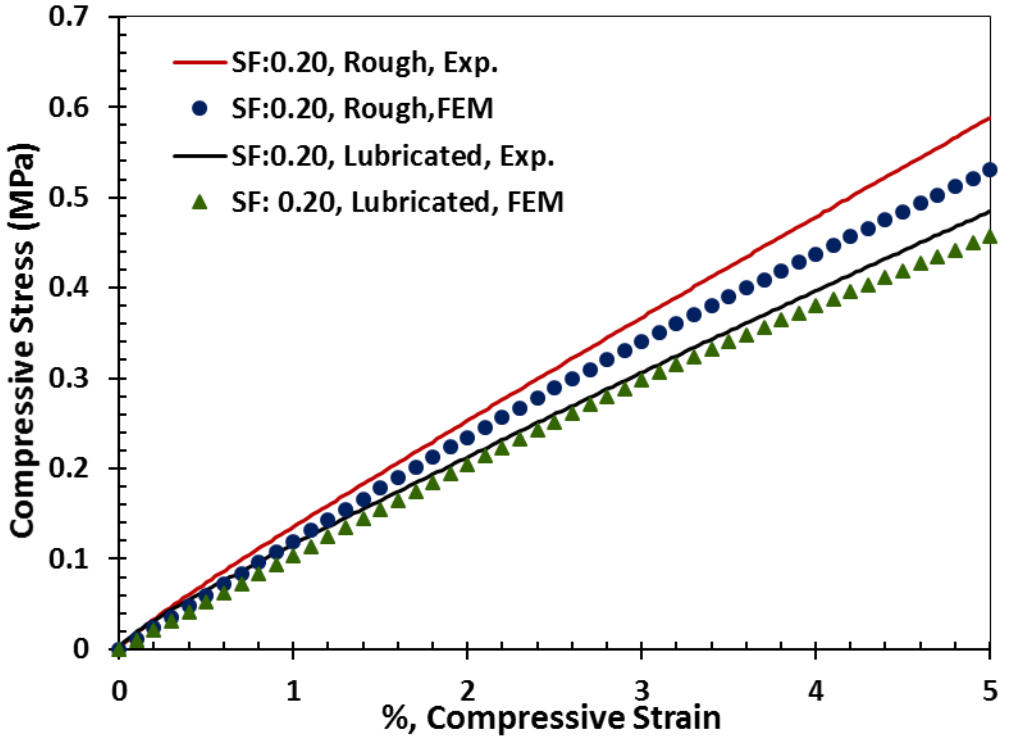

Figure 66: Comparison of experimental compressive stress - compressive strain curve with finite element compressive stress - compressive strain curve

4.6.2.1 Apparent Compressive Modulus

The experimental apparent compressive modulus for lower shape factor was compared as shown in Figure 67 with simulated apparent compressive modulus for various shape factor. The experimental apparent compressive modulus for old seals showed a higher value than the simulated apparent compressive modulus as the old seal showed higher stiffness as well as apparent compressive modulus than a new seal. However, the simulated apparent compressive modulus of the annular rubber seal matched well with the experimental apparent compressive modulus for the new annular rubber seal.

The finite element analysis was then extended to a wide range of shape factor (0.1 to 100) of the annular seal with four different friction coefficients (0.05, 0.1, 0.4, and 0.8) and bonded condition.

The simulation results of the annular seal with bonded condition were compared with the theoretical predictions as shown in Figure 68. Similar to the results of solid blocks, it was found that the incompressible assumptions for predicting the apparent modulus according to equation (7) grossly overestimates the finite element results at high shape factor. However, the modified empirical corrections considering the bulk compressibility according to the equation (11) brought the prediction into better agreement with the FEA results.

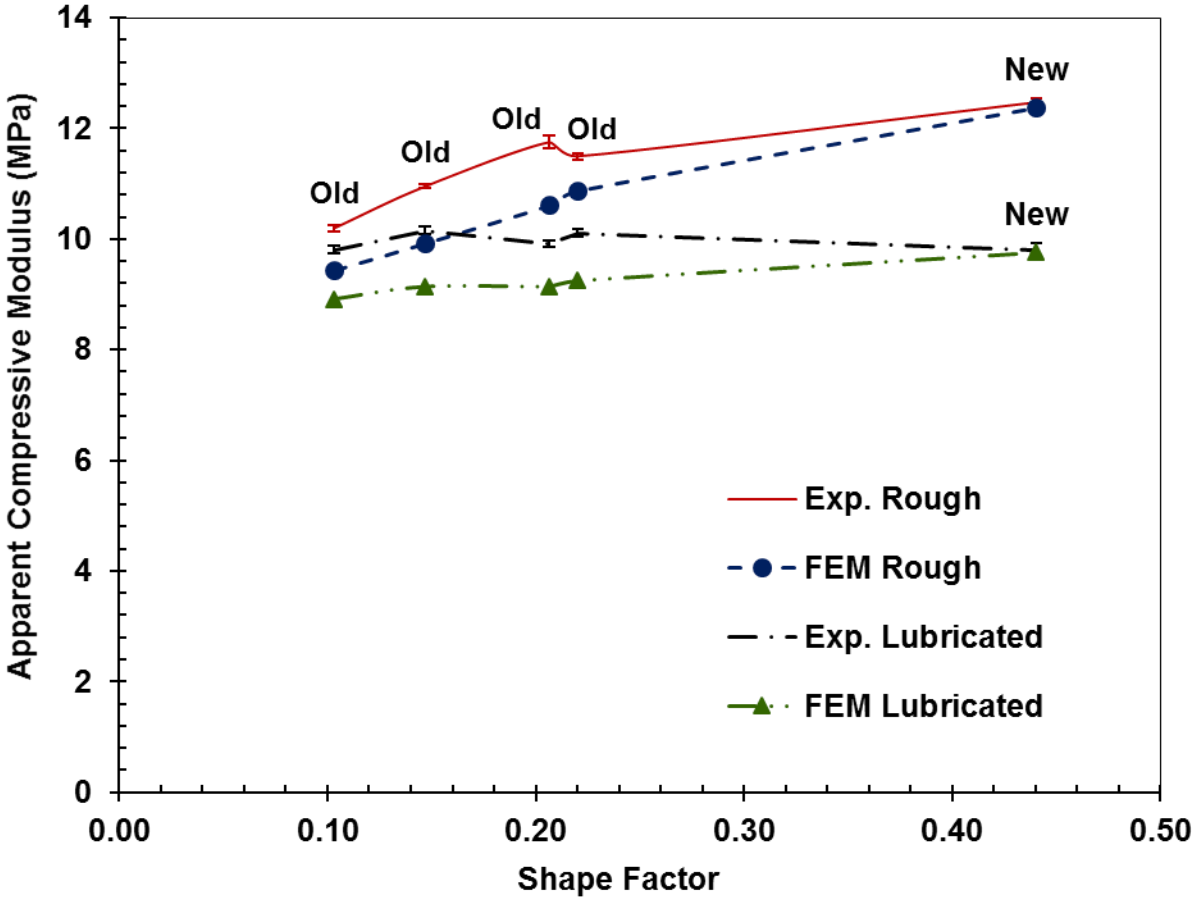

Figure 67: Comparison of Experimental Apparent Compressive Modulus - Shape factor with simulated apparent compressive modulus - shape factor

The comparison of apparent compressive modulus-shape factor curve for solid blocks and annular blocks is shown in Figure 69. The trend of the apparent modulus – shape factor curve for the annular block was same as the solid block, however, the values of the apparent modulus were lower for an annular block in bonded conditions.

Confirming the finite element model by comparing the experimental and theoretical predictions, the simulation was extended for a wide range of shape factors (0.1 to 100) of annular seal for various frictional surfaces (0.05, 0.1, 0.4, and 0.8). The apparent compressive modulus with the shape factor for annular seal with rigid frictional surfaces is shown in Figure 70.

The apparent compressive modulus for the annular seal is compared as shown in Figure 71 with the apparent compressive modulus for solid blocks for different frictional contact surfaces in between the seal and the steel rings. Similar to the bonded conditions, the trend of the apparent modulus – shape factor curve as shown in Figure 71 for the annular block was same as the solid block but the values of the apparent modulus were lower for an annular block in rigid frictional surfaces due to the additional sliding and deformation in the center hole.

4.6.2.2 Deformed Shape

The deformed shapes of the annular rubber seal were compared with the deformed shapes of the solid block as shown in Figure 72 in both bonded and frictional contact surfaces. Similar to the solid blocks, the deformed shapes of the annular blocks were more parabolic at higher (0.8) friction coefficient whereas the deformed shape was uniform rather than parabolic for lower friction coefficient (0.1). The deformed shapes of the solid and annular rubber seals are almost similar in both bonded and frictional cases.

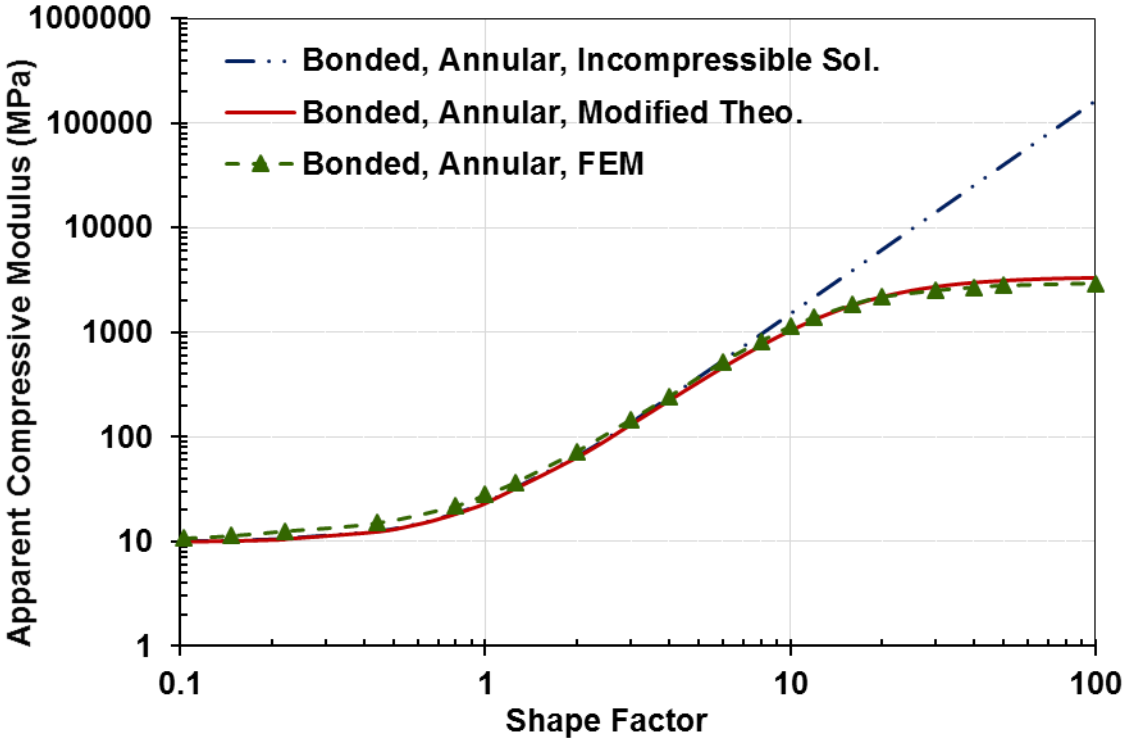

Figure 68: Apparent compressive modulus - shape factor for annular bonded block

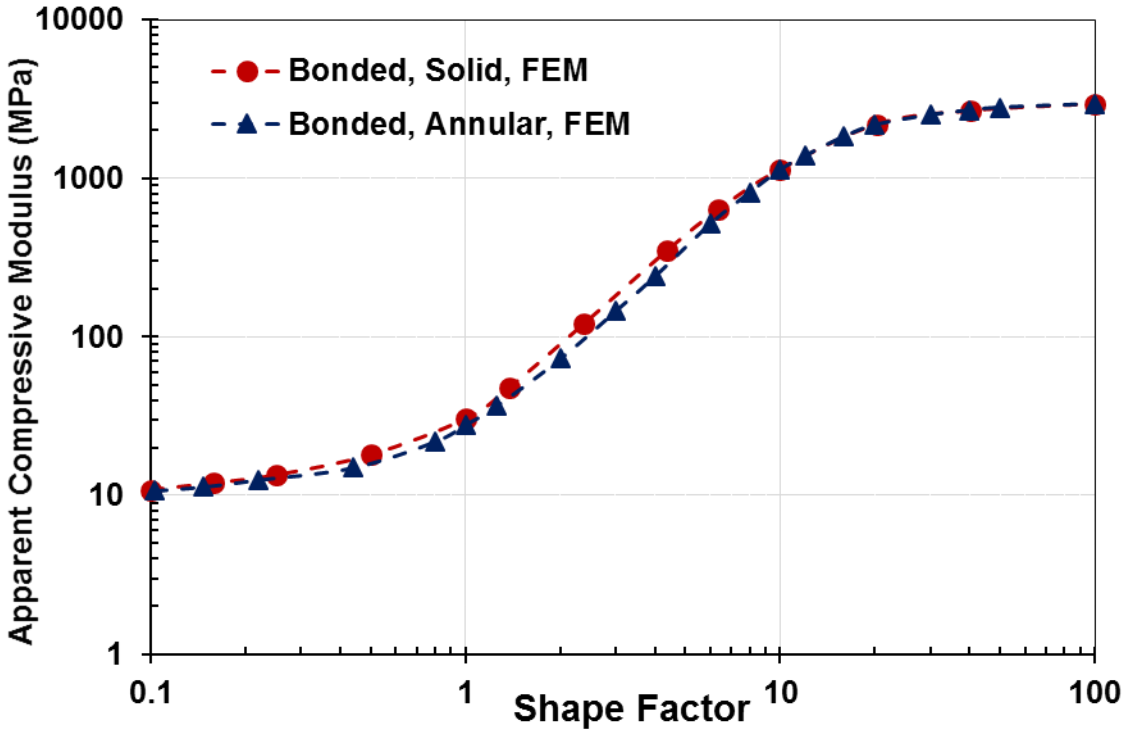

Figure 69: Comparison of apparent compressive modulus-shape factor curve for solid blocks and annular blocks.

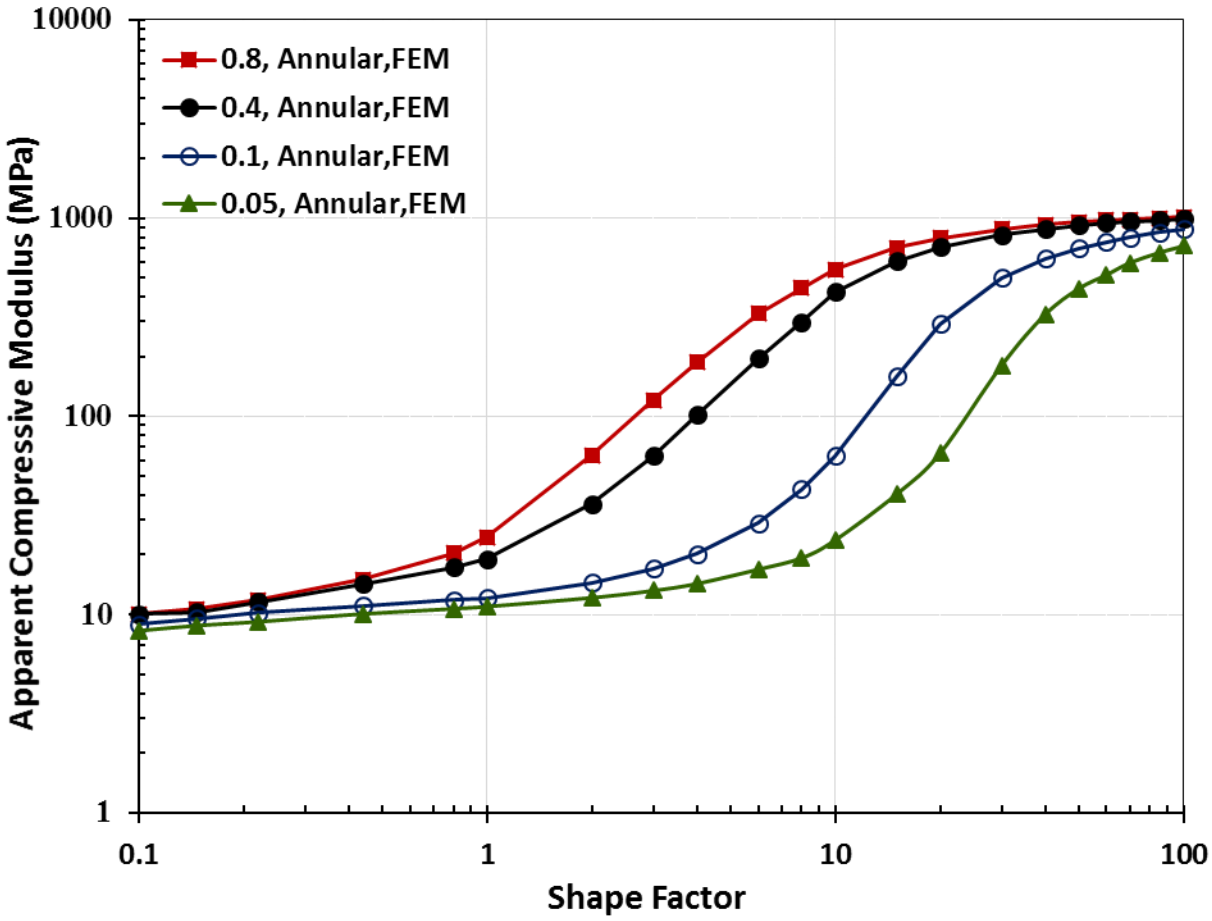

Figure 70: Apparent compressive modulus - shape factor for annular block with rigid frictional surfaces

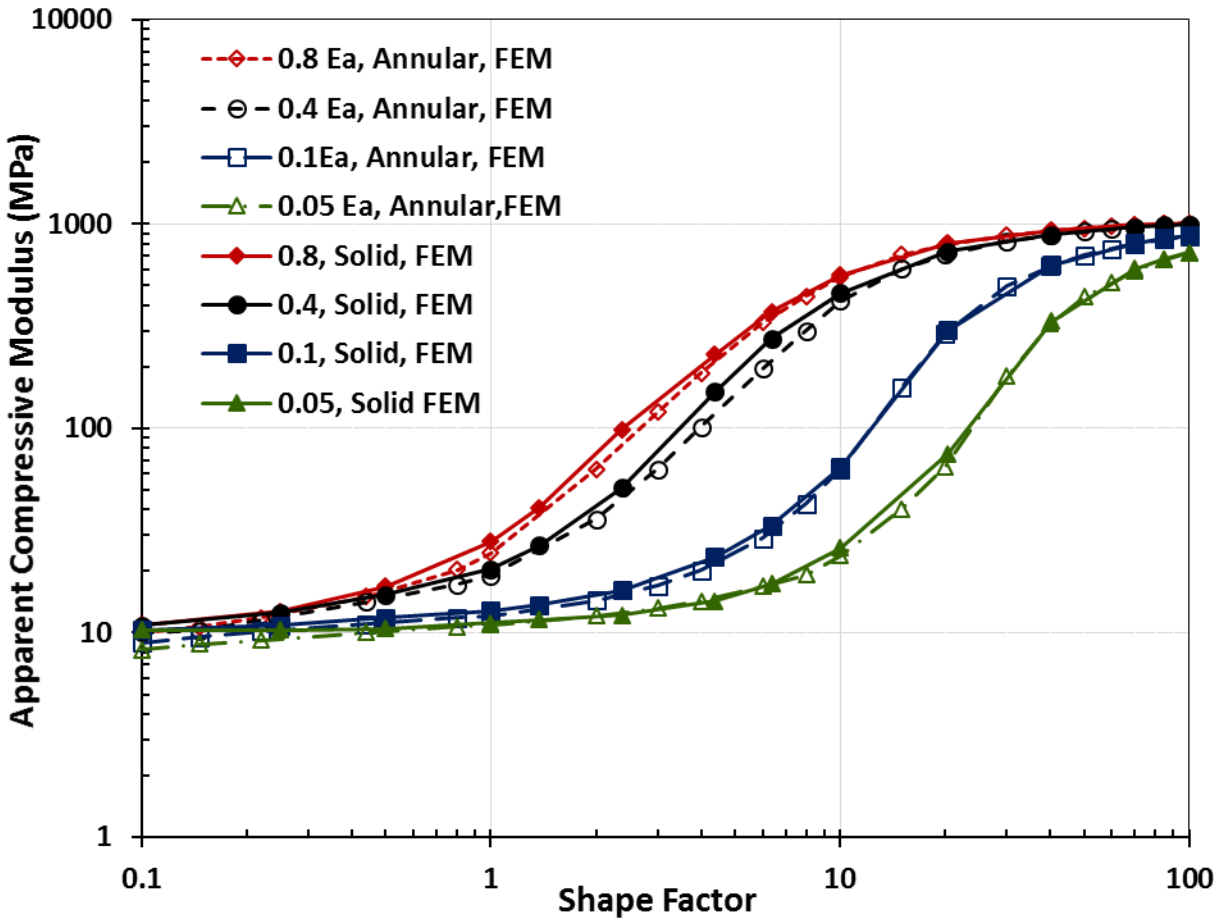

Figure 71: Comparison of apparent compressive modulus - shape factor curve from FEA results for solid block and annular seal for different frictional surfaces

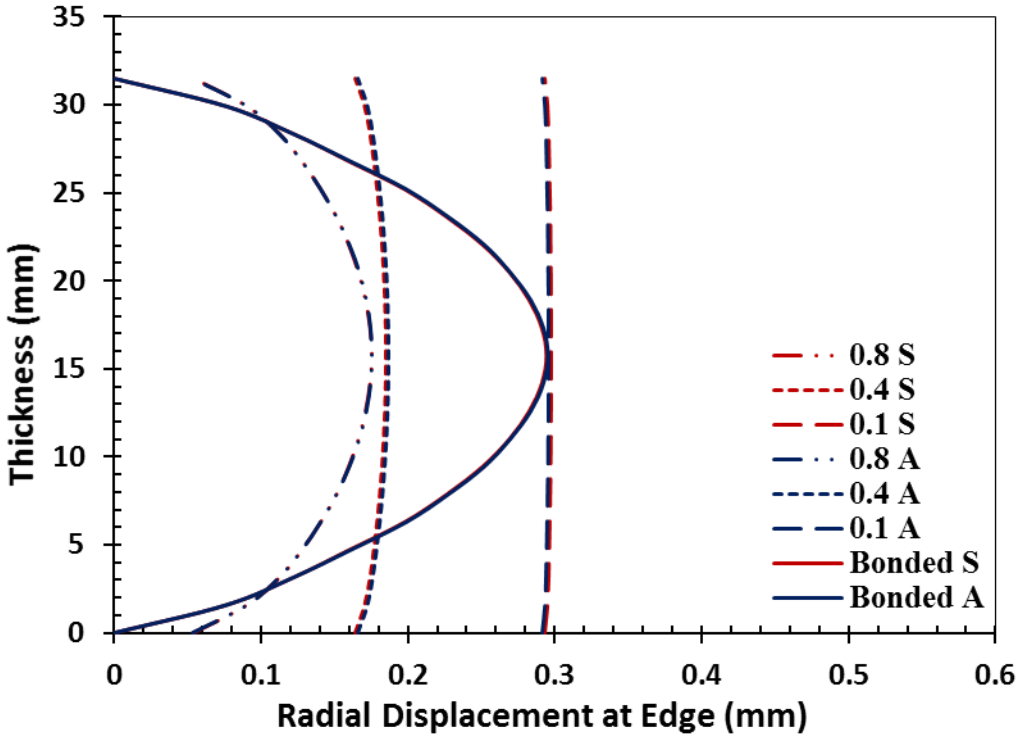

(a)

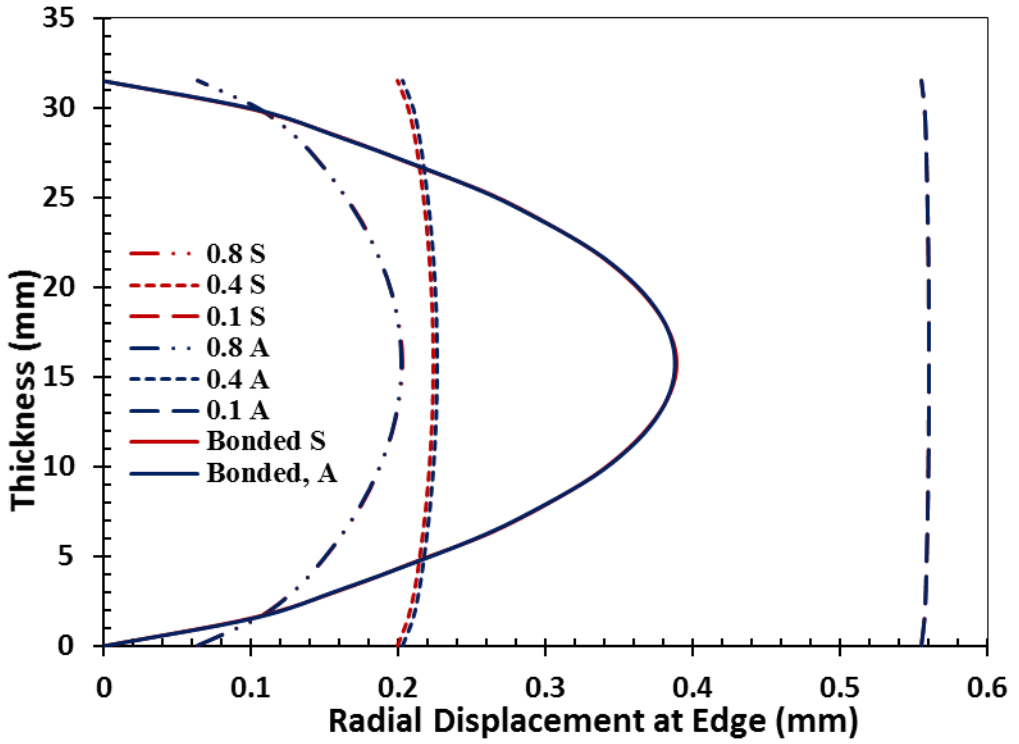

(b)

Figure 72: Comparison of radial displacement at edge along the thickness of the solid block and annular seal at (a) shape factor (10) and (b) shape factor (100). (A: Annular & S: Solid)

4.6.2.3 Contact Status

The amount of non-slip or sticking zone for three different shape factors (100, 10 and 0.5) with the 2D-axisymmetry plot for annular seal with the friction coefficients of 0.8 and 0.05 is shown from Figure 73 to Figure 78. Due to the central hole of the annular seal, it slides in both center and edge side. Similar to the solid blocks, it was showing analogous contact status for different shape factors with different friction coefficients except sliding on the center side.

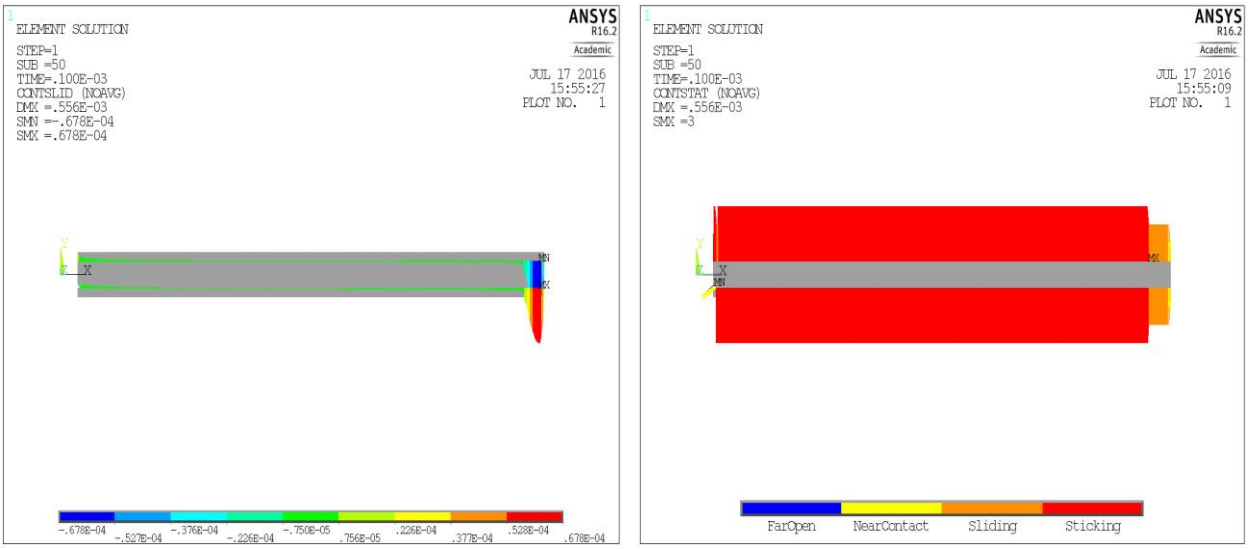

(a) (b)

Figure 73: (a) Contact Sliding Distance (b) Contact Status at 0.8 friction coefficient with annular block for intermediate shape factor (10).

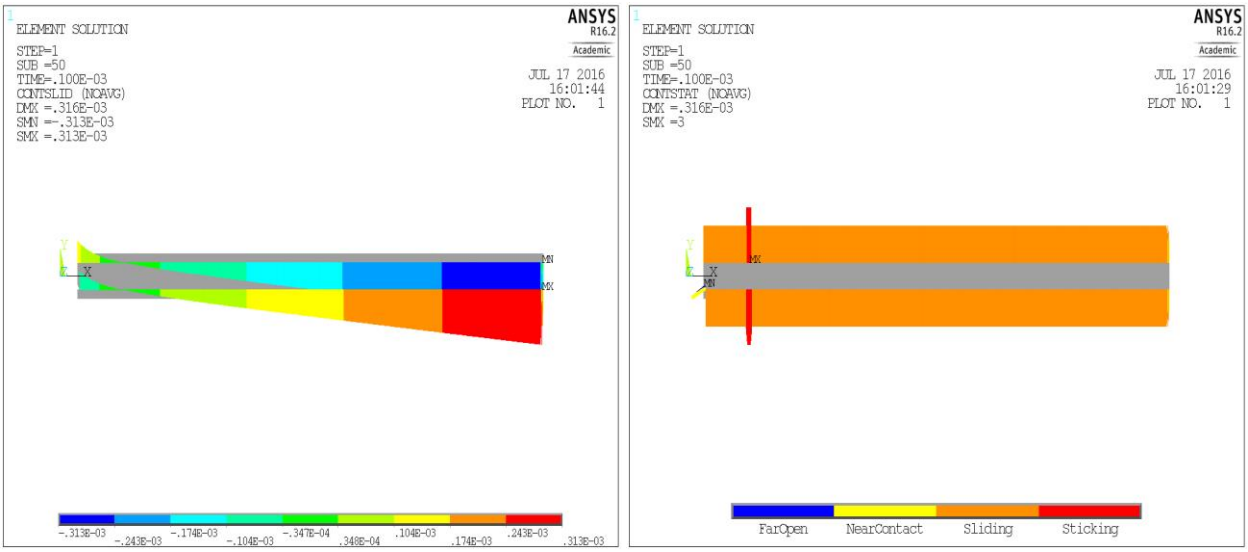

(a) (b)

Figure 74: (a) Contact Sliding Distance (b) Contact Status at 0.05 friction coefficient with annular block for intermediate shape factor (10).

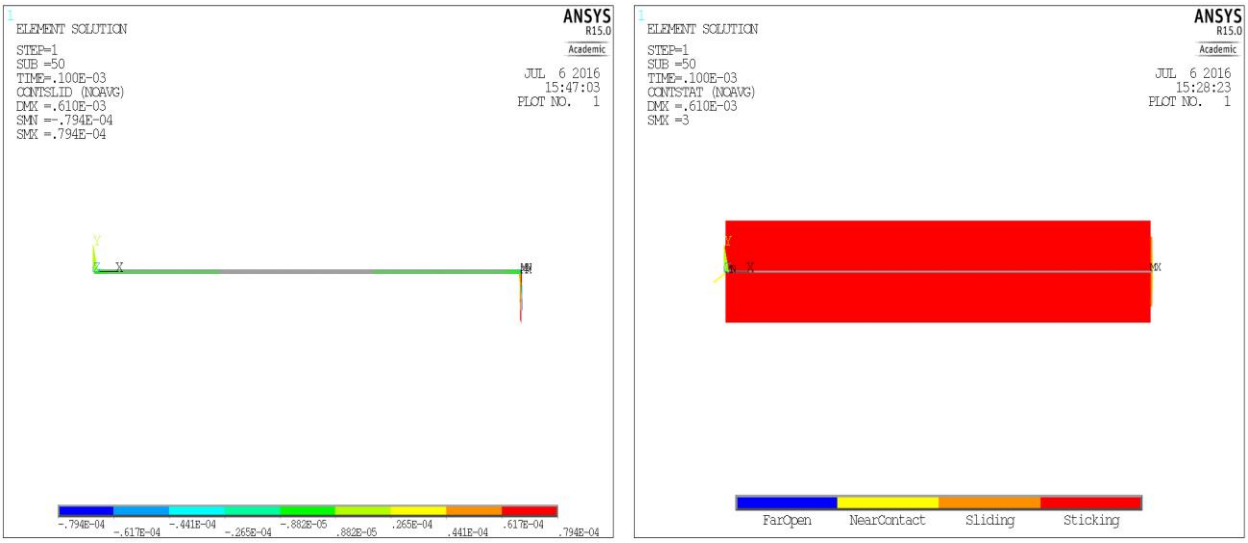

(a) (b)

Figure 75: (a) Contact Sliding Distance (b) Contact Status at 0.8 friction coefficient with annular block for intermediate shape factor (100).

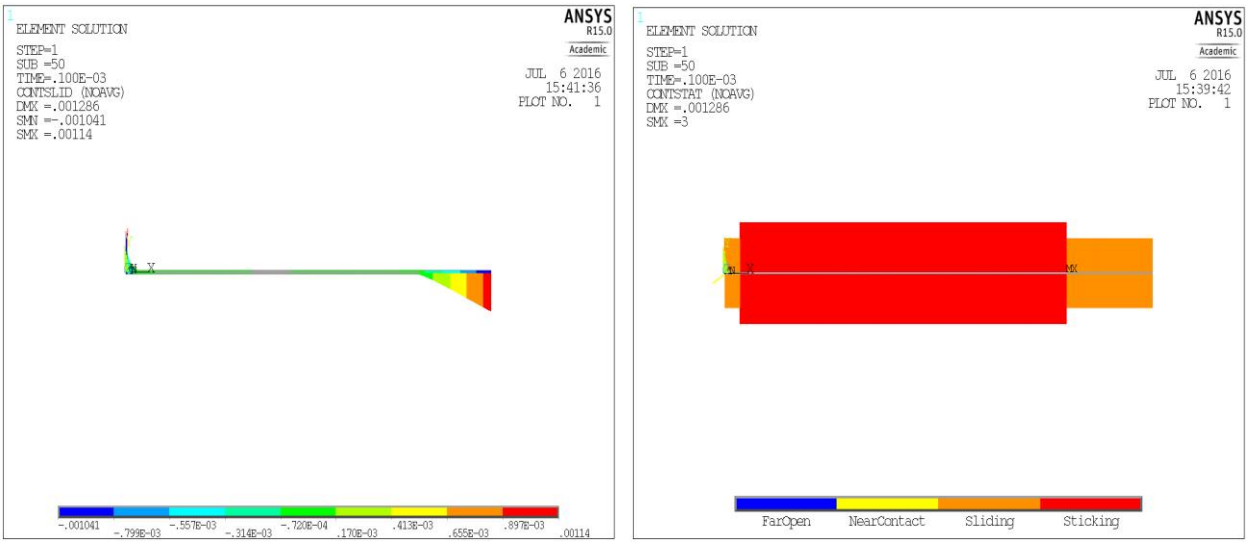

(a) (b)

Figure 76: (a) Contact Sliding Distance (b) Contact Status at 0.05 friction coefficient with annular block for intermediate shape factor (100).

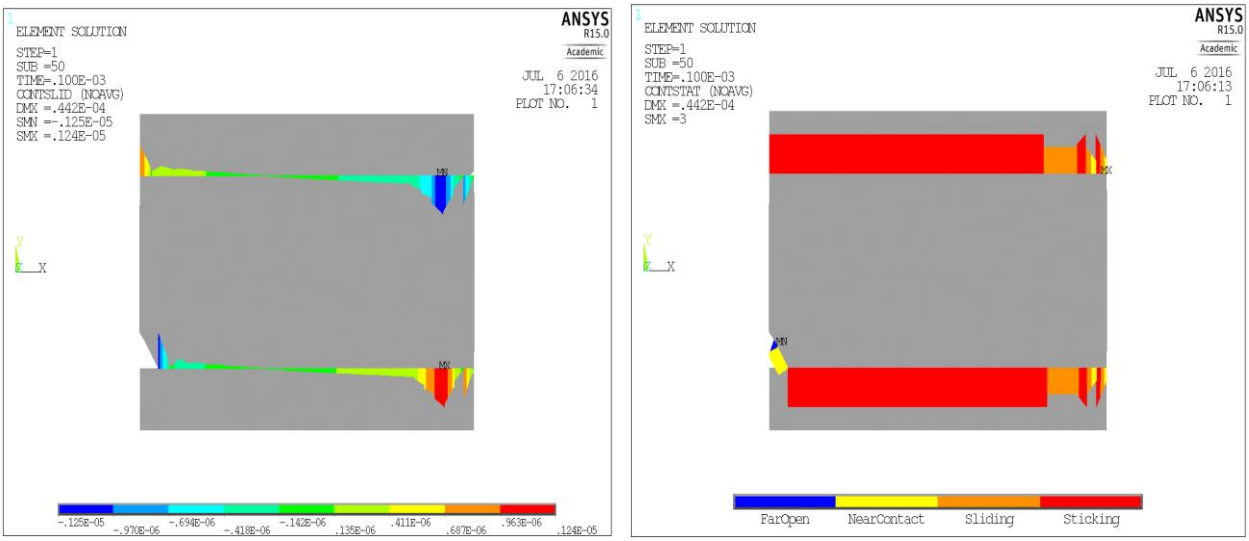

(a) (b)

Figure 77: (a) Contact Sliding Distance (b) Contact Status at 0.8 friction coefficient with annular block for intermediate shape factor (1).

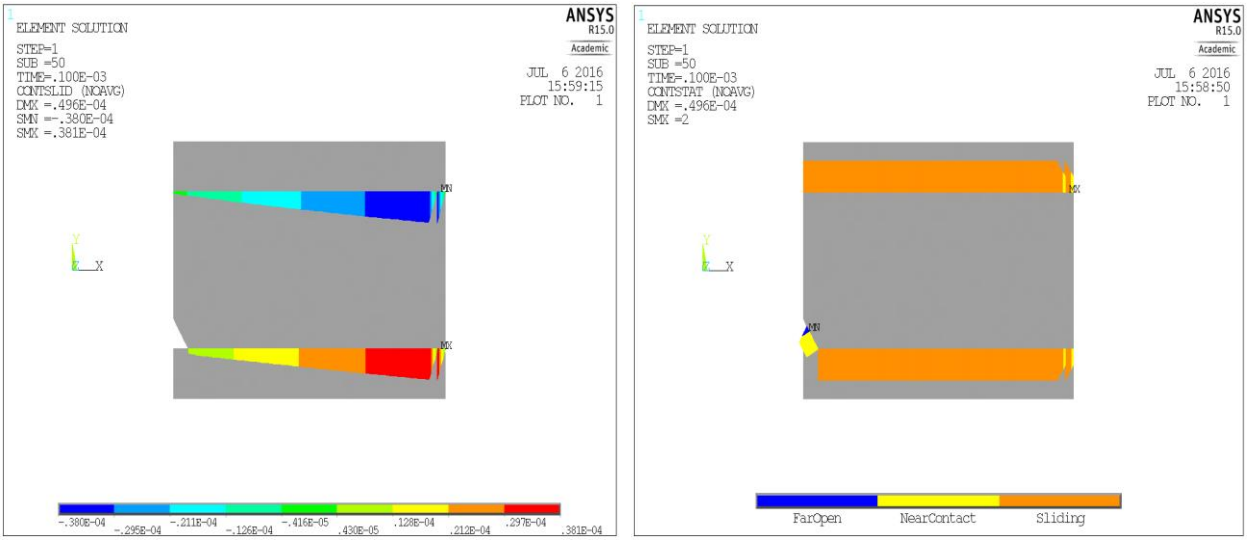

(a) (b)

Figure 78: (a) Contact Sliding Distance (b) Contact Status at 0.05 friction coefficient with annular block for intermediate shape factor (0.5).

4.7 Summary of Results

Here, the results of the compressive behavior of the annular rubber seal in constrained and unconstrained conditions are summarized below:

- Surface Conditions
    - The deformed shape of the seal is more parabolic in rough contact surface than in lubricated contact surface.
    - The stiffness (2778 N/mm) of the seal with rough contact surface was higher than the stiffness (2084 N/mm) of the seal with the lubricated contact surface at the same axial displacement. Therefore, seal stiffness increased by 33.3 % with the increasing of friction (from lubricated to rough) in between the seal and the steel rings under uniaxial compression.
    - In constrained condition, the compressive force of the seal for rough contact surface increased sharply from 12,000 N (approx.) to 39,588 N after the initiation of contact on the pipe's inner wall for 1mm (from 4.5mm to 5.5mm) axial displacement. Therefore, a rapid increase in the compressive force was observed for constrained conditions (with pipe) due to the constraint applied by the pipe's inner wall on the radial expansion of the seal.
    - The compressive force (~12,000 N) for rough contact surface was higher than the compressive force (~9000N) for lubricated contact surface at the time of contact initiation on the pipe wall. Higher compressive force and axial displacement were required in higher frictional contact surfaces than the lower frictional contact surfaces between the seal and the steel plates to reach the same radial expansion.

- Strain Rates
    - The seal stiffness (2778 N/mm) for higher strain rate was found higher than the seal stiffness (2339 N/mm) for lower strain rate. The seal stiffness increased from lower to higher strain rate is about 18.8 %.
- Shape Factor
    - Since the maximum radial displacement (3.02 mm) for the seal of 102.5 mm dia. was more than the maximum radial displacement (1.94 mm) for the seal of 73 mm dia., therefore, the maximum radial displacement increased with the increasing of the shape factor.
    - Apparent compressive modulus of the seal increased gradually (from 10.2 MPa to 12.7 MPa) with the increasing of shape factor in rough contact surface for a lower range of shape factor (from 0.1 to 0.44). On the other hand, the apparent compressive modulus of the annular seal with lubricated contact surface is increased slightly compare to the rough contact surface.
    - The apparent compressive modulus (12.7 MPa) of old seal showed higher value than that (12.19 MPa) of the new seal for the same shape factor (0.44) or geometry due to aging effect or different chemical composition.
- Contact Pressure Distribution
    - The contact pressure (4.526 MPa) between the seal and the pipe wall was found high for the rough contact surface than the contact pressure (3.313 MPa) for the lubricated contact surfaces. Therefore, the friction of contact surfaces influences the contact pressure between the seal and pipe.

- The higher contact pressure (3.313 MPa) was observed for higher rate (95mm/min) than the contact pressure (2.20 MPa) at lower rate (5 mm/min).

- Hoop Strain Gradient
  - The hoop strain on the pipe's outer membrane exhibited a parabolic distribution along the sealing area.
  - The maximum hoop strain was located at the position of the pipe corresponding to the mid-height of the seal since the maximum lateral expansion occurred at that position.
  - The maximum strain (367 με) on the pipe wall for rough contact surfaces was higher compare to the maximum strain (300 με) for lubricated contact surfaces during the compression test at the same axial compressive strain of the seal.
  - In case of strain rate, the Strain on the pipe wall increased with the increasing of the applied strain rate of the seal during compression.
  - The peak hoop strain (597 με) on the pipe at 6.0 mm axial displacement of the seal was significantly high compare to the peak hoop strain (179 με) at 5.0 mm axial displacement.
  - Stacked seal exhibited higher pipe strain (579 με) compare to the strain (171 με) for the single seal during the compression test at the same axial compressive strain.
  - The experimental strain gradients were in good agreement with the predicted strain gradients within 10% deviation in both surface conditions and strain rates.

- Finite Element Analysis
  - The apparent compressive modulus of solid and annular rubber block from FEA increased with increasing of the shape factor.

- The predicted apparent modulus considering the incompressible assumption grossly overestimates the finite element results at higher shape factor. However, modified empirical prediction considering the bulk compressibility brought the prediction into better agreement with the FEA results.
- The deformed shape of the seal through the thickness showed parabolic at higher friction coefficient (0.8) whereas the deformed shape is uniform at lower friction coefficient (0.05).
- The apparent compressive modulus of solid and annular rubber block changed in three different way with the shape factor when the friction co-efficient is between 0.05 and 0.8. At lower range of shape factors ($0.1 \leq SF \leq 1$), the apparent compressive modulus increased gradually. On the other hands, at an intermediate range of shape factors ($1 \leq SF \leq 30$), the apparent compressive modulus increased abruptly compare to the apparent compressive modulus at the lower range of shape factors. However, at the higher range of shape factor ($30 \leq SF \leq 100$), the apparent modulus reached a plateau value with small increments.
- The amount of non-slip zone or sticking zone changes with the friction coefficients in between the annular seal and the steel rings and the shape factors (geometries). Since the sticking zone and sticking volume changed with friction coefficients and shape factors, therefore the apparent compressive modulus changed with friction coefficients and shape factors.
- The apparent compressive modulus of annular rubber seal is lower than the apparent compressive modulus of solid rubber block in both bonded and rigid frictional surfaces.

5 CONCLUSIONS AND FUTURE WORK

The main objective of this thesis was to experimentally study the compressive behavior of a seal constrained in a pipe and the strains introduced in the pipe wall. The objective of this research was successfully accomplished through different tasks which are summarized as follows.

- An experimental methodology was developed to carry out the uniaxial compression test of an annular rubber seal in both constrained and unconstrained states to explore the compressive behavior using three input operational parameters: strain rates, surface conditions, and shape factors. The output parameters in the unconstrained state were: radial deformed shape, force-displacement relations, stiffness and apparent compressive modulus. For the constrained condition, force-displacement relations, the contact pressure distribution between the seal and pipe wall, and the hoop strain distribution on pipe's outer membrane were analyzed.
- The hoop strain gradient on the outer pipe wall was predicted by using Roark's formula [8] inputting the seal contact pressure to compare with the experimental hoop strain gradient. The apparent compressive modulus was predicted by using the Gent's equation[3]–[5].
- A parametric study was performed using the FE model for a wide range of shape factors (from 0.1 to 100) with different friction coefficients (0.05, 0.1, 0.4 and 0.8) in order to determine their effect on the apparent compressive modulus of the seals. The radial deformed shape, hydrostatic pressure of the seal, contact status (sticking and sliding zone) between the seal and the steel rings were analyzed to support this parametric study.

The results of this research works are summarized below:

- Since the maximum compressive force of seal, contact pressure and pipe strain are increased by 19.4%, 36.6% and 22.33%, respectively, from lubricated to rough contact surface at 17.5% axial compressive strain of the seal. Therefore, the increase in the friction of the contact area between the seal and steel rings increases the pressure exerted by the seal on the pipe and consequently the magnitude of the pipe strain.
- The pipe strain increased with the increasing of the seal stiffness and apparent compressive modulus caused by the increase in friction and strain rate.
- The hoop strain introduced in the pipe wall originated from the constraint imposed by the pipe on the lateral expansion of the seal, varies parabolically with a maximum value at the mid-height of the seal.
- Maximum strain on the pipe is extremely sensitive with the applied strain on the seal after contact due to incompressibility. For instance, the maximum hoop strain increased sharply from 179 με to 597 με for the increasing of the axial displacement from 5.0 mm to 6.0 mm for rough contact surfaces.
- Stacked seal exhibited higher pipe strain (579 με) compare to the strain (171 με) for the single seal during the compression test at the same axial compressive strain of the seal.
- The maximum pipe strain increased with the shape factor for a constant axial displacement and gap between the seal and the pipe wall.
- Predicted hoop strain distribution from the theoretical analysis compared well with the experimental hoop strain distribution with a maximum deviation of 10%.

- The apparent compressive modulus varied non-linear proportionally with the shape factor for different frictional coefficients. According to the parametric study using the FEA, when friction coefficient is between 0.05 and 0.8, shape factor of the seal influences the apparent compressive modulus in such a way that:
    a. At lower range of shape factors ($0.1 \leq SF \leq 1$), the apparent compressive modulus increased gradually. This was confirmed by the experimental results.
    b. Whereas, at an intermediate range of shape factors ($1 \leq SF \leq 30$), the apparent compressive modulus increased abruptly.
    c. For a higher range of shape factors ($30 \leq SF \leq 100$), the apparent compressive modulus reached a plateau or consistent value (with small increments) as it reached close to the modulus of bulk compression.

The objective of this research was successfully achieved by exploring the compressive behavior of the annular rubber seal in unconstrained and constrained states and developing a relation with the friction of contact surface, strain rate and seal's shape factor to the pipe strain in the application of pipeline sealing. The behavior of the annular rubber seal constrained in a pipe and the interaction between the pipe and the seal has not been studied clearly in the past. The significance of this research was to clearly understand the compressive behavior of the annular rubber seal and to establish a relation between the annular rubber seal and the steel pipe for sealing applications. Hence, the knowledge provided by this research can provide a suitable guideline to perform the sealing of pipeline efficiently in a pressurized environment by avoiding the pipe yield.

Future studies for the continuation of this research work are recommended as follows:

- The experimental study can be performed for a wide range of shape factors of the annular rubber seal.
- Experimentally determine the effect of higher ranges of shape factors on the apparent compressive modulus for different frictional surfaces.
- Develop a theoretical approximation to predict the apparent compressive modulus of the annular rubber seal with rigid frictional surfaces.
- Compressive behavior of the seal can be explored subjected to temperature, age and chemical contamination.

REFERENCES

[1] T. Grelle, D. Wolff, and M. Jaunich, "Temperature-dependent leak tightness of elastomer seals after partial and rapid release of compression," *Polym. Test.*, vol. 48, pp. 44–49, 2015.

[2] M. Jaunich, K. von der Ehe, D. Wolff, H. Voelzke, and W. Stark, "Understanding low temperature properties of elastomer seals," *Packag. Transp. Storage Secur. Radioact. Mater.*, vol. 22, no. 2, pp. 83–88, 2011.

[3] A. N. Gent and P. B. Lindley, "The Compression of Bonded Rubber Blocks," *Proc. Inst. Mech. Eng.* , vol. 173 , no. 1 , pp. 111–122, Jun. 1959.

[4] A. N. Gent, "Compression of Rubber Blocks," *Rubber Chem. Technol.*, vol. 67, no. 3, pp. 549–558, 1994.

[5] A. N. Gent, F. M. Discenzo, and J. B. Suh, "Compression of Rubber Disks Between Frictional Surfaces," *Rubber Chem. Technol.*, vol. 82, no. 1, pp. 1–17, 2009.

[6] D. Bartel, Alix; Wu, Christine; Krokosz, "Experimental Stress Analysis of an Axially Compressed Hyper-Elastic Annular Seal in a Pressurized Environment," in *CSME International Congress 2014*, 2014.

[7] D. Zhao, D; Wu, C; Krokosz, "Analysis of Contact Stresses and Strains For Pipe with a Rubber Seal," in *The Canadian Society for Mechanical Engineering International Congress 2014*, 2014.

[8] R. Young,Warren; Budynas, *Roark's Formulas for Stress and Strain*, 7th Editio. New York: McGraw-Hill Education, 2002.

[9] J.Gough, "No Title," *Proc. Lit. Phil. Soc. Manchester*, vol. 1, no. 2nd Ser., p. 288, 1805.

[10] A. N. Gent and K. W. Scott, "Dynamic Mechanical Properties," in *Engineering with Rubber*, Carl Hanser Verlag GmbH & Co. KG, 2011, pp. 89–118.

[11] A. Stevenson and R. Campion, “Durability,” in *Engineering with Rubber*, Carl Hanser Verlag GmbH & Co. KG, 2011, pp. 205–257.

[12] P. H. Mott and C. M. Roland, “Uniaxial Deformation of Rubber Cylinders,” *Rubber Chem. Technol.*, vol. 68, no. 5, pp. 739–745, 1995.

[13] S. Pinarbasi, Y. Mengi, and U. Akyuz, “Compression of solid and annular circular discs bonded to rigid surfaces,” *Int. J. Solids Struct.*, vol. 45, no. 16, pp. 4543–4561, 2008.

[14] A. N. Gent and E. A. Meinecke, “Compression, bending, and shear of bonded rubber blocks,” *Polym. Eng. Sci.*, vol. 10, no. 1, pp. 48–53, 1970.

[15] B. P. Holownia, “Effect of Poisson’s ratio on bonded rubber blocks,” *J. Strain Anal. Eng. Des.* , vol. 7 , no. 3 , pp. 236–242, Jul. 1972.

[16] P. B. Lindley, “Compression moduli for blocks of soft elastic material bonded to rigid end plates,” *J. Strain Anal. Eng. Des.* , vol. 14 , no. 1 , pp. 11–16, Jan. 1979.

[17] M. S. Chalhoub and J. M. Kelly, “Effect of bulk compressibility on the stiffness of cylindrical base isolation bearings,” *Int. J. Solids Struct.*, vol. 26, no. 7, pp. 743–760, 1990.

[18] C. G. Koh and J. M. Kelly, “Compression stiffness of bonded square layers of nearly incompressible material,” *Eng. Struct.*, vol. 11, no. 1, pp. 9–15, 1989.

[19] C. G. Koh and H. L. Lim, “Analytical solution for compression stiffness of bonded rectangular layers,” *Int. J. Solids Struct.*, vol. 38, no. 3, pp. 445–455, 2001.

[20] J. M. Horton, G. E. Tupholme, and M. J. C. Gover, “Axial Loading of Bonded Rubber Blocks,” *J. Appl. Mech.*, vol. 69, no. 6, pp. 836–843, Oct. 2002.

[21] O. H. Yeoh, G. A. Pinter, and H. T. Banks, “Compression of Bonded Rubber Blocks,” *Rubber Chem. Technol.*, vol. 75, no. 3, pp. 549–562, 2002.

[22] H.-C. Tsai and C.-C. Lee, “Compressive stiffness of elastic layers bonded between rigid

plates," *Int. J. Solids Struct.*, vol. 35, no. 23, pp. 3053–3069, 1998.

[23] S. Pinarbasi, U. Akyuz, and Y. Mengi, "A new formulation for the analysis of elastic layers bonded to rigid surfaces," *Int. J. Solids Struct.*, vol. 43, no. 14–15, pp. 4271–4296, 2006.

[24] S. L. Burtscher and A. Dorfmann, "Compression and shear tests of anisotropic high damping rubber bearings," *Eng. Struct.*, vol. 26, no. 13, pp. 1979–1991, 2004.

[25] M. C. Constantinou, A. Kartoum, and J. M. Kelly, "Analysis of compression of hollow circular elastomeric bearings," *Eng. Struct.*, vol. 14, no. 2, pp. 103–111, 1992.

[26] J. M. Horton, G. E. Tupholme, and M. J. C. Gover, "Axial Loading of Annular Bonded Rubber Blocks," *Rubber Chem. Technol.*, vol. 76, no. 5, pp. 1194–1211, 2003.

[27] K. J. Patenaude, Z. Tao, J. L. Mead, R. G. Stacer, and G. Rodriguez, "Response of Elastomeric Blocks During Large Compression Strains," *Rubber Chem. Technol.*, vol. 78, no. 2, pp. 188–198, 2005.

[28] R. Sridharan, K; Sivaramakrishnan, "COMPRESSIVE AND SHEAR ANALYSIS OF RUBBER BLOCK UNDER LARGE STRAIN," *Am. J. Appl. Sci.*, vol. 10, no. 7, pp. 681–687, 2013.

[29] K. Sridharan and R. Sivaramakrishnan, "Compression and Deformation of Cylindrical Rubber Blocks," *MAPAN*, vol. 29, no. 2, pp. 107–114, 2014.

[30] J. S. Bergström and M. C. Boyce, "Constitutive modeling of the large strain time-dependent behavior of elastomers," *J. Mech. Phys. Solids*, vol. 46, no. 5, pp. 931–954, 1998.

[31] M. Hossain, D. K. Vu, and P. Steinmann, "Experimental study and numerical modelling of VHB 4910 polymer," *Comput. Mater. Sci.*, vol. 59, pp. 65–74, 2012.

[32] R. K. Sahu and K. Patra, "Rate-dependent mechanical behavior of VHB 4910 elastomer," *Mech. Adv. Mater. Struct.*, vol. 23, no. 2, pp. 170–179, 2016.

[33] J. de Vicente, J. R. Stokes, and H. A. Spikes, “Rolling and sliding friction in compliant, lubricated contact,” *Proc. Inst. Mech. Eng. Part J J. Eng. Tribol.* , vol. 220 , no. 2 , pp. 55–63, Feb. 2006.

[34] M. Mofidi, E. Kassfeldt, and B. Prakash, “Tribological behaviour of an elastomer aged in different oils,” *Tribol. Int.*, vol. 41, no. 9–10, pp. 860–866, 2008.

[35] B. N. J. Persson, U. Tartaglino, O. Albohr, and E. Tosatti, “Rubber friction on wet and dry road surfaces: The sealing effect,” *Phys. Rev. B*, vol. 71, no. 3, p. 35428, Jan. 2005.

[36] B. N. J. Persson, U. Tartaglino, O. Albohr, and E. Tosatti, “Sealing is at the origin of rubber slipping on wet roads,” *Nat Mater*, vol. 3, no. 12, pp. 882–885, Dec. 2004.

[37] Y. Ling, P. Engel, and W. Brodsky, “Compression of Bonded Annular Rubber Blocks,” *J. Eng. Mech.*, vol. 121, no. 6, pp. 661–666, Jun. 1995.

[38] R. J. and D. K. A. Bartel, C. Wu, “Numerical Study of an Axially Compressed Hyper-Elastic Annular Seal in a Pipe,” in *CSME International Congress 2016*, 2016.

[39] “Honning Tool,” *Harbor Freight Tools*. [Online]. Available: http://www.harborfreight.com/4-inch-engine-cylinder-hone-97164.html.

[40] I. Axel Products, “Testing Brief: Compression or Biaxial Extension?” [Online]. Available: http://www.axelproducts.com/downloads/CompressionOrBiax.pdf. [Accessed: 17-May-2016].

[41] I. Tekscan, “Pressure Indicating Film.” [Online]. Available: https://www.tekscan.com/products-solutions/pressure-sensing-film/pressure-indicating-film?tab=configuration.